Dispersal and mixing of stormwater run-off plumes in the Port of Tauranga, New Zealand

A thesis submitted in partial fulfilment

of the requirements for the degree

of

Masters of Science

in Earth Sciences

at

The University of Waikato

by

Nadine Ramona Brunschwiler

The University of Waikato

2015

THE UNIVERSITY OF
WAIKATO
Te Whare Wānanga o Waikato

Abstract

Buoyancy differences between two water bodies can often dominate flows such as stormwater discharge or river plumes in the coastal environment. The buoyancy difference usually arises due to differences in salinity, temperature and suspended solids. These flows form plumes or 'gravity currents', which can also transport pollutants and nutrients around in the receiving water body. The plume consists of a bulbous head, a mixing region on the tail, and billows behind the head. The form of the head and the plume water properties dictate what kinds of instabilities develop, which in turn influence the degree and manner of mixing that occurs. Additionally, the mixing depends on the local hydrodynamics of the receiving water body.

I report observations of the dynamics of a stormwater run-off plume in a strongly tidal estuary, with particular emphasis on investigation of dispersion and dilution processes. The field site for my thesis research is the barrier-enclosed basin of Tauranga Harbour adjacent to the Port of Tauranga wharf in Mount Maunganui. The Port of Tauranga is the largest timber export port in New Zealand. The area has about 20 storm water runoff pipes that discharge into the main tidal channel of the estuary. The log handling produces bark leachates and resin acids, which get discharged during and after rain events. The leachate is responsible for a serious discolouration of the water.

Several surveys were undertaken during rain events to measure plume characteristics and these are compared with a similar undertaken during dry conditions. Based on these measurements and visual observations, the plume was estimated to disperse within around four hours as the freshwater was dispersed into a relatively strong tidal flow (maximum speeds of 0.7 m/s). Acoustic Doppler Current Profiler data and conductivity-temperature-depth data indicated that the maximum across-channel extent of the plume was around 120 m and the maximum along channel extent was around 200 m (for the conditions observed). The plume stability decreases with distance from the source. The plume can be classified as a free buoyant jet or upstream intruding plume.

This study will provide inputs into the toxicity assessment of the storm runoff, which will be investigated in a separate project using caged arrays of filter-

feeding bivalves to determine the cumulative effects of resin acids and leachates on mussels.

Acknowledgements

I dedicate this work to my Grandfather.

I thank Justin Walker for his support. I would not have survived these last few months/the last year without you.

I want to express my thanks to all the field work helpers, drawn from the ranks of staff and students here at the University of Waikato, Department of Earth and Ocean Sciences. Julia Mullarney, David Culliford, Dirk Immenga, Chris Morcom, Beth, ….and others. A thank you goes to Dean Sandwell for the support in the laboratory and field work. Steve Hunt was a great help for deployed instrument set up instructions.

I would like to thank Sydney Wright, Earth Sciences secretary, for her help and assistance over the years.

Many thanks go to the Port of Tauranga who provided me with this great project and part scholarship which enable me to do a Masters here in New Zealand.

A big thank you goes to my fellow students and friends who made this experience extraordinary, Justin Walker, Martin Poot, Olivia Jordan, Megan Saunders, Melissa Kleyburg, Emma Bagley, Billy Bodger, …

Last but not least I want to thank my family who always supported me in pursuing my dreams even when they brought me half way around the world…

Table of Contents

List of Figures

List of Tables

Chapter One

Introduction

1.1 Background

The Port of Tauranga has a large timber export area. This timber export produces a strongly discoloured discharge plume into the harbour during rain events. To comply with resource consent the Port has to monitor the discharge. As the discharge is known to contain resin acids a toxicology study and a dispersion study had to be committed to investigate whether the discharge is toxic to the marine environment and where it ends up. This study investigates the discharge plume behaviour and dynamics.

1.2 Pollution

Pollution can be defined as a deviation from the natural state, which means the presence of matter or energy in a place where it is not common or is unintended (Yapp & Yapp, 1972). This kind of pollution is a widespread problem, especially in coastal areas, which are increasingly stressed by growing populations and anthropogenic activities. Such contamination in the marine environment is therefore of growing concern (Matranga & Yokota, 2008).

With the development of new techniques in assessing chemicals, new contaminants are found regularly. These contaminants often have unknown effects on marine life. In New Zealand estuaries pollution can pose a significant health risk for gathering seafood. Pollution can be subjective; we note that the assessment of what is perceived by the public as pollution might actually be natural variation. An example of natural variation is ‘red tides’. ‘Red tides’ are naturally occurring algal blooms that make the water appear red or brown. The other extreme is also possible; a water body can be extremely polluted without appearing so to the naked eye. Pollution is not always obvious which makes it necessary to analyse the environment carefully. In order to assess pollutant levels a threshold has to be established to determine the baseline and range of variability.

In water research this means water samples have to be collected and analysed (Miller & Spoolman, 2011).

In water bodies the presence of suspended particles can affect the transfer and sequestration of contaminants. Transfer usually depends on size distribution and settling velocity of the particles while sequestration draws mainly on the physiochemical and biological processes that affect the suspended particles which in turn affect settling velocity and distribution. These physiochemical and biological processes are re-suspension, coagulation, deposition, fragmentation, mineralization, repackaging, and production. Coagulation might play an important role as it impacts on particle size directly and on settling velocity indirectly by increasing volume concentration (Ahn, 2012; Miller & Spoolman, 2011).

1.3 Plumes

Buoyancy differences between two water bodies can often dominate flows such as stormwater discharge or river plumes in the coastal environment. The buoyancy difference usually arises due to differences in salinity, temperature and suspended solids (Jones *et al.*, 2007). These flows form plumes or 'gravity currents' which can also transport pollutants and nutrients around in the receiving water body. The plume consists of a bulbous head, a mixing region on the tail, and billows behind the head. The form of the head and the plume water properties dictate what kind of instabilities develop, which in turn influence the degree and manner of mixing that occurs. Additionally, the mixing depends on the local hydrodynamics of the receiving water body (Simpson, 1997). Cross-sectional and plan views of a typical plume are given in Figure 1.1. Jones *et al.* (2007); Nash and Jirka (1996) describe the structure of a buoyant surface discharge into steady ambient conditions by kinematic buoyancy fluxes J_0, momentum fluxes M_0, into a steady receiving environment with a water depth H and velocity u_a. With these parameters length scales L_M (transition distance) and time scales T_M (development time) can be calculated. Additionally, L_M provides a maximum jet h_{max} depth which can be used to determine if bottom interaction takes place. To measure deflection of the jet, L_m, or the jet-to-cross-flow length scale can be calculated.

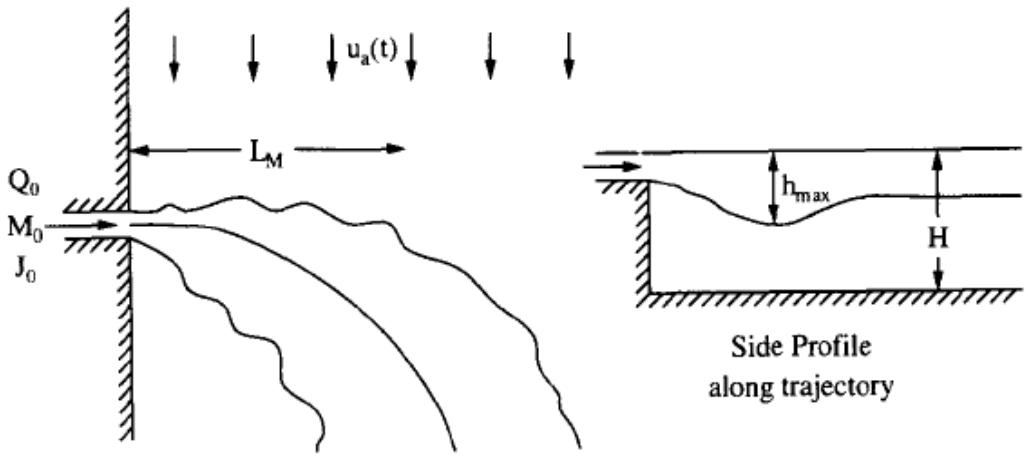

Figure 1.1: Schematic view (plan and cross-sectional) of a buoyant discharge into a steady ambient conditions. Source:(Nash & Jirka, 1996).

In the coastal environment the ambient conditions are hardly ever steady due to tides. Therefore the model had to be adapted to different rates of flow reversal, $du_a(t)/dt$ which results in new length and time scales L_u and T_u. The relationships between the different parameters show that for most of the tidal cycle the ambient velocity is negligible for the buoyancy discharge. At slack tide however the tidal velocities become the dominant influence on the length scale (Nash & Jirka, 1996).

According to Jones *et al.* (2007) plumes can be categorized into four main flow regimes (Figure 1.2). These categories are free jet, shoreline-attached jet, wall jet, and upstream intruding plume. These jets can be characterized by several parameters such as discharge fluxes for volume Q_0, buoyancy J_0, momentum M_0, discharge velocity U_0, and density difference $\Delta\rho_0$. The receiving water body has a water depth H and ambient flow velocity u_a. With these parameters discharge length scale L_Q, jet-to-plume length scale L_M, jet-to-cross-flow length scale L_m, and plume-to-cross-flow length scale L_b can be defined. L_Q describes the region where the flow is established and has a significant role in surface jets. L_M describes the region in which the plume spreading is controlled by momentum. L_m gives the point at which the flow becomes strongly influenced by the ambient cross-flow. L_b determines the distance a strongly buoyant jet may intrude an ambient current.

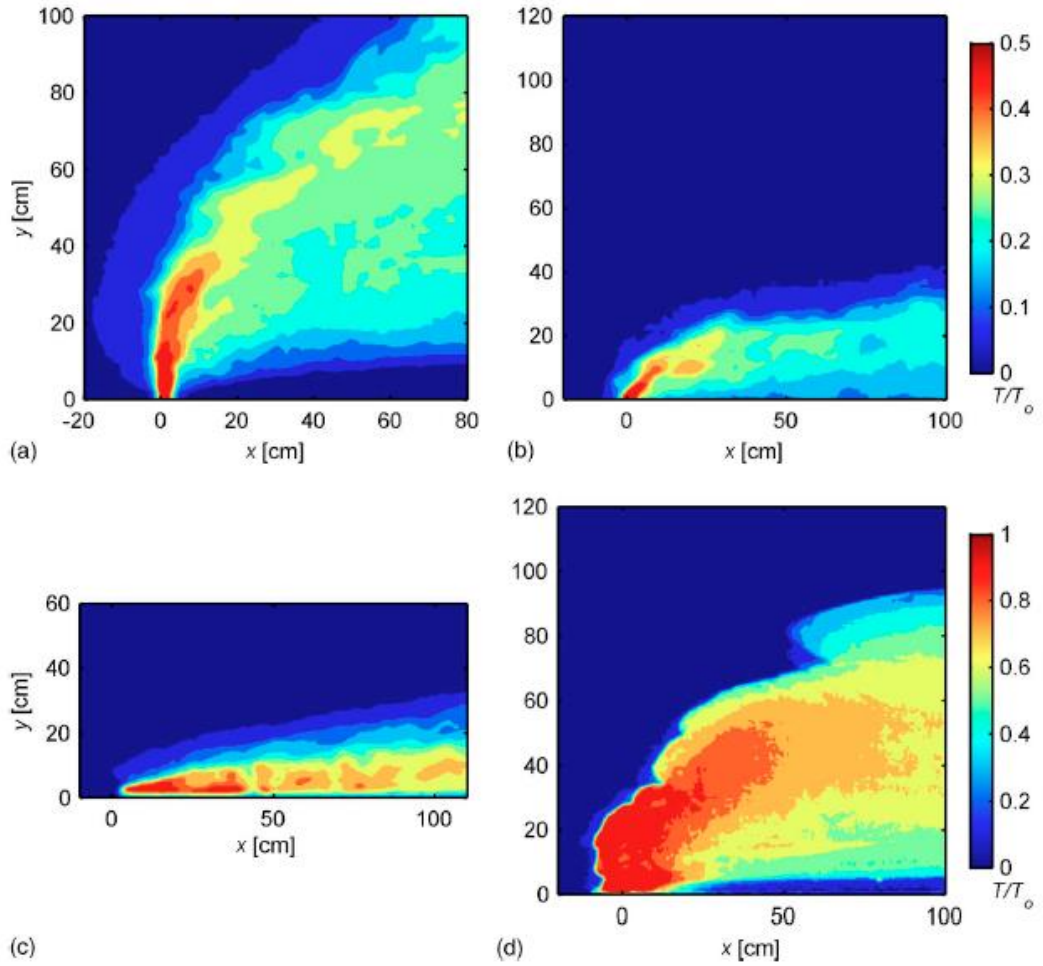

Figure 1.2: Modelled plumes, images obtained from laser-induced fluorescence (LIF), measured in large modelling basins. Dimensions are all in cm. The four major flow categories of buoyant surface discharges are, (a) Buoyancy dominated free jet into deep ambient waters (L_Q=2.5 cm, L_m=30 cm, L_b=170 cm, L_M =14 cm, H=10 cm); (b) Shoreline attached jet into deep ambient waters (L_Q=2.5 cm, L_m=9.2 cm, L_b=1.4 cm, L_M=23 cm, H =10 cm); (c) Wall jet into shallow ambient waters (L_Q=2.5 cm, L_m=11 cm, L_b=3.5 cm, L_M=20 cm, H=4 cm); and (d) Upstream intruding plume into deep ambient waters: (L_Q=2.5 cm, L_m=5.7 cm, L_b=64 cm, L_M=1.7 cm, H=10 cm). Adapted from Nash and Jirka (1995), taken from Jones *et al.* (2007).

1.3.1 Origins

Freshwater plumes in coastal environments usually originate from rivers, sewer out falls and stormwater run-off. Stormwater run-off has become a major source for water pollution (Lee *et al.*, 2007). The increase in impervious surfaces (e.g. roads, buildings) due to increases in infrastructure means the problem is growing

(Lee *et al.*, 2007). Many local authorities now require stormwater monitoring in order to obtain consent.

The problem has grown such that it has become necessary to implement stormwater-monitoring programs. According to Lee *et al.* (2007) regions with a distinct dry season show a phenomenon called 'first flush' at the beginning of the wet season, typically occurs after large rainwater events.

1.4 Tannins and resin acids

Tannins and resin acids are molecules that can be found in plants, especially in the bark of trees. These molecules can be washed out and then end up in the storm water. Tannins, when in large enough concentration, discolour the water. This staining usually takes the form of a brownish 'tan'. This 'tan' presents the port of Tauranga with a considerable aesthetic problem. Tian *et al.* (1994) found that the 'yellow substance' concentrations in the stormwater runoff from the port are high. This 'yellow substance' is partly responsible for the water discolouration.

Resin acids are environmentally persistent and accumulate in the sediments of receiving waters (Tian *et al.*, 1998). According to Tian (1993) the storm water runoff from the log handling area at the Port of Tauranga has a similar chemical composition to the effluents of pulp and paper mills in terms of containing the same fatty and resin acids.

1.5 Study aim and objective

For my thesis, I will use field observations to characterize the storm water runoff plume in Tauranga Harbour under present log handling and harbour conditions, with particular emphasis on investigation of dispersion and dilution processes. The data will allow determination of mixing length scales and the maximum plume extension. A related project (conducted by fellow MSc student David Culliford) will undertake a toxicity assessment of the storm runoff using caged arrays of filter-feeding bivalves, as currently the effects of resin acids and leachates on mussels are unknown.

Finally, the overarching aim is to explore linkages between the responses of the biota and the physical forcing conditions of the plume. In particular we will

examine the dependence of accumulation rate of toxins on distance from source and depth within the water column. This analysis should also indicate any potential hot spots of pollutants and possible effects of future storm events. The combination of both projects will not be included in this thesis owing to differential start dates so here we focus purely on the plume dynamics.

1.6 Thesis outline

In order to achieve the study aims and objectives this thesis is organised in the following way.

- Chapter One

  Chapter One gives a brief description and background information on what the thesis is about.
- Chapter Two

  A description and history of the study site.
- Chapter Three

  A literature review on work done previously in Tauranga Harbour.
- Chapter Four

  Description of field deployment and field work set-up.
- Chapter Five

  Results presentation, data analysis, and plume parameter calculations.
- Chapter Six

  Discussion of findings and encountered problems as well as indication of future work

1.7 Summary

- Pollution can be defined as a deviation from the natural state by anthropogenic means.
- Plumes are buoyancy driven currents that occur in the estuarine environment. The buoyancy difference can be driven by several factors.
- The origins of plumes are usually freshwater input into the marine or estuarine environment.

- Tannins and resin acids are leftover products in waste from timber operations such as timber handling for export or paper mills.

Chapter Two

Study Site

2.1 Tauranga Harbour

2.1.1 Geology

Tauranga Harbour is a barrier enclosed estuary on the north-eastern coast on the North Island of New Zealand (Figure 2.1, left panel). The barrier comprises two tombolos and a 24 km long sand barrier as seen in the right panel of Figure 2.1. Both tombolos are of volcanic origin and the sand barrier consists of Holocene beach ridges (Davies-Colley & Healy, 1978a; Davis & Healy, 1993; de Lange, 1988). The bathymetry within the harbour is such that the northern and southern part of the lagoon can be viewed and treated as two separate basins as there is little to no water exchanged between them (Spiers *et al.*, 2009; Tay *et al.*, 2013). The large tidal flat areas (41 km^2) in the harbour are exposed during low tide. The harbour has a spring tidal range of 2m (Heath, 1976). The main freshwater input for the harbour is the Wairoa river which has a mean flow of 17.6 m^3/s (Tay *et al.*, 2013). The harbour entrance is interrupted by an ebb tidal delta (Price, 1968) with a deep dredge channel to facilitate shipping. The main flood-tidal delta in the inlet is known as the Centre Bank. The main tidal flow goes through the western channel and the Maunganui channel. Centre Bank was dredged to create an artificial channel (Cutter Channel) to facilitate better shipping to and from the Port (Davies-Colley & Healy, 1978a). The harbour sediments contain mainly sandy mud and shell (Inglis *et al.*, 2008).

2.1.2 Hydrodynamics

The hydrodynamics in the harbour area are predominantly forced by tidal currents and wind waves (Davies-Colley & Healy, 1978a) with smaller influences from tidal wave surge, baroclinic circulation and seiching. According to (Phleger *et al.*, 1969) a tidal wave surge is when a part of the oceanic tidal wave transmissions into a lagoon. In the case of Tauranga Harbour it causes a delay of high water and

peak current times. Baroclinic circulation is observed after heavy rain events. At these times the normally low freshwater content is increased and weak salinity-density currents appear (Davies-Colley & Healy, 1978a).

2.1.3 Tide

According to Tay *et al.* (2013) the tide constituent that dominates the tide in Tauranga harbour is the M2 with a height of 0.66m. Constituents S2, N2, and K1 together contribute about 0.07 m of tidal amplitude and the O2 constituent O2 contributes a further 0.015m. Due to the entrance constriction the M2 amplitude attenuates by 4% over the 500m of the entrance. At Omokoroa Point a strong ebb-dominance can be observed while flood-dominance prevails in the Lower Western Channel and Entrance. Behind Mount Maunganui and west of the flood tide delta there are back-eddies. The harbour near mouth and western channel is relatively well flushed with an average residence time of 2 to 4 days. Although storms can reduce this residence time considerably by 24-39% depending on season (Tay *et al.*, 2013).

2.1.4 Stormwater runoff plume

The log handling area produces about 7500 $m^3ha^{-1}a^{-1}$ of runoff water (Tian, 1997) which discharges into the main tidal channel of the estuary via ~20 storm water runoff pipes (Figure 2.2). The log handling produces significant amounts of bark leachates and resin acids, which get discharged during and after rain events. This leachate mixture consists mainly of suspended solids, floating solids, and fatty and resin acids. The leachate is responsible for a serious discolouration of the water (Tian, 1997). The plume can be easily identified in the field by the water colour and floating particles (Figure 2.4).

According to (Tian, 1993) the runoff is similar to pulp and paper mill effluent but the chlorinated compounds are absent. Conventional treatments would be able to remove resin acids effectively. The impact of the resin acids is limited to about 100 m from discharge point (Tian, 1997).

The freshwater plume from the log handling areas of the Port of Tauranga enters the harbour at Stella Passage (Figure 2.3). The hydrodynamics of the area generally force shoreline attached plumes. Furthermore, depending on the timing

of the discharge in relation to the tidal cycle, the plume may undergo flow reversal, which can complicate the flow dynamics and impact on where the runoff water ends up (Jones *et al.*, 2007; Nash & Jirka, 1996). The natural salinity stratification in Stella Passage depends on the weather. Wind drag and pressure gradient have the greatest influence on the plume during flood tide. The plume typically remains within the top 2 to 3 meters of the water column. (Tian, 1997). Of social concern is the possibility that the plume may advect to the Whareroa Marae (Figure 2.3), however, Tian (1997) concluded that this advection was an unlikely scenario because the plume dispersion and mixing is efficient enough for the plume to be dispersed before it would ever reach the Marae.

2.1.5 Sediments

The sediment sources for Tauranga Harbour are the freshwater streams and the inner shelf. The sediments from the freshwater streams are fine grained sediments (muds) from the catchments (Boulay, 2012). The sediment from the inner shelf is typically delivered by littoral drift and tidal currents. These marine sediments consist mainly of sands (Davis & Healy, 1993). The average shell content in the harbour sediment is 30%, however can reach up to 90% in the channel. Mud content throughout the harbour is relatively low at 1 % (Kwoll, 2010).

2.1.6 Wind and waves

The prevailing wind direction in the Bay of Plenty is from the west through to south-west. The harbour is sheltered from these winds by the Kaimai-Mamaku Range (Kwoll, 2010). Therefore the maximum wind speeds are low (de Lange, 1988). In summer cyclones occur occasionally. As these cyclones undergo formation over the warm waters in the tropics (north) they can bring fast winds, large amounts of rain, and storm surges to the Bay of Plenty (de Lange, 1988).

The Bay of Plenty wave climate is a low energy wave climate compared to the rest of New Zealand. Wave periods (T_z) typically are between 7 – 9 s, with significant wave heights (H_s) ranging from 0.7 m to 1.5m (de Lange, 1988). According to Kwoll (2010) the dominant wave directions are from north to north-east. The offshore mean Hs is 0.5m (de Lange & Healy, 1990).

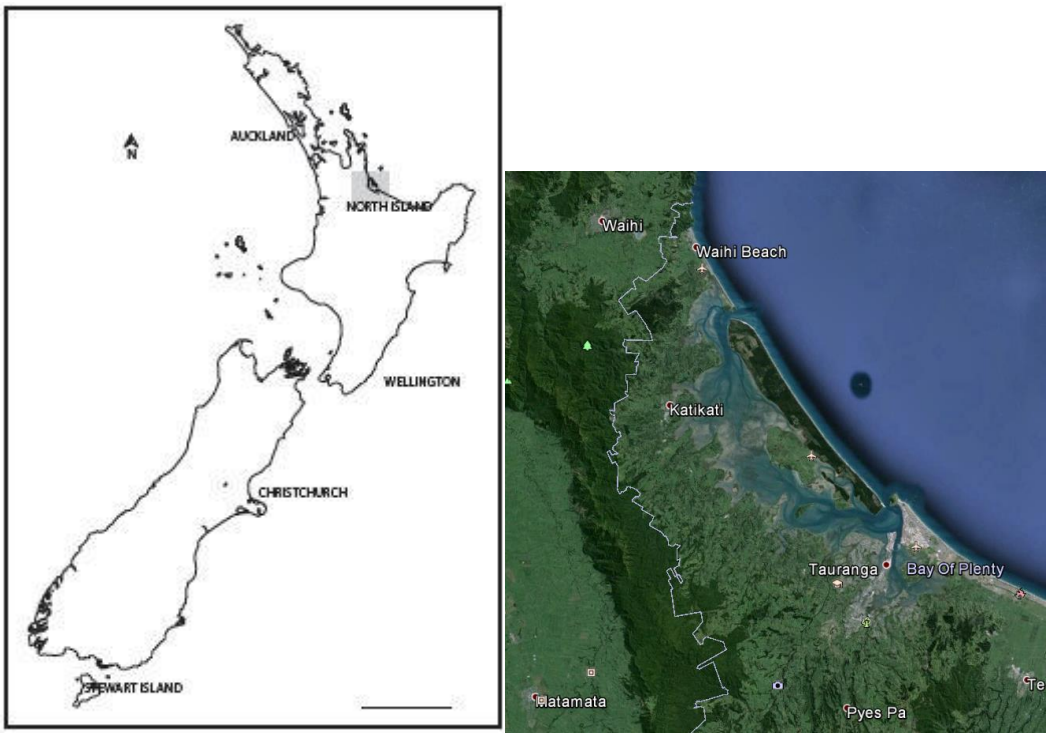

Figure 2.1: Left panel shows New Zealand and the approximate study site location in grey. Right panel shows Tauranga Harbour with Matakana Island (image credit: Google Earth).

2.2 Field Site

The field site for my thesis research is located in the southern basin of Tauranga Harbour, adjacent to the Port of Tauranga wharf in Mount Maunganui on Stella Passage (Figure 2.3).

2.2.1 Port of Tauranga

The Port of Tauranga is the largest import/export port in New Zealand and was officially established in 1973 (Inglis *et al.*, 2008). The expansion of the Port required dredging of the entrance channel and Cutter Channel to accommodate the larger ships (Michels & Healy, 1999). The first timber export occurred in 1957 to Japan (Inglis *et al.*, 2008). Presently, the main timber export is *Pinus radiata.* The Port started exporting timber around 1960 and the export volume has increased over the years. Log handling inevitably produces bark chunks (Healy *et al.*, 1997). Some of the logs are treated on site which can leave residues of the treatment used on the impervious ground.

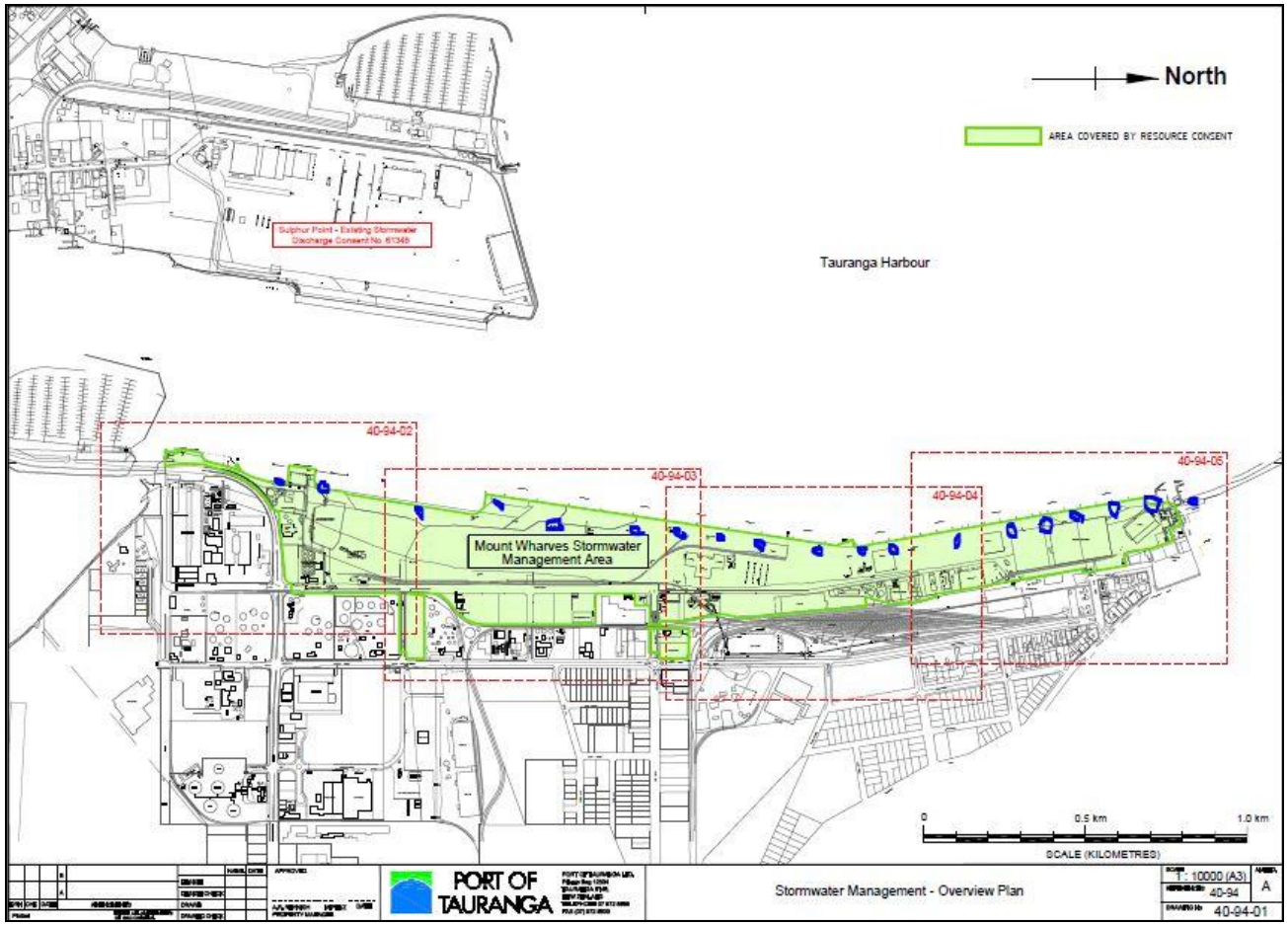

Figure 2.2: Port of Tauranga discharge overview plans. Blue rings/dots indicate approximate locations of stormwater outfall pipes (image credit: Port of Tauranga).

Figure 2.3: Overview of the geographical features within Tauranga Harbour (image credit: Google Earth). Timber export area (green) drawn on Goggle Earth Pro after information from Port of Tauranga.

Figure 2.4: Photo of stormwater runoff plume (dark/brown water at bottom of photo) edge to harbour water (greenish/blue) in upper part of photo (photo credit: Nadine Brunschwiler).

2.3 Biology

2.3.1 Flora and fauna

Cole et al. (2000) studied the bivalve distribution in Tauranga Harbour and found that across 27 sites 314 different bivalve taxa can be found. Centre Bank houses substantial populations of bivalves. Sea grass covers over 22.5% of the harbour area (Inglis et al., 2008).

2.3.2 Environment Bay of Plenty 1994

Park and Donald (1994) carried out an extensive survey of the species found in Tauranga Harbour. The following sections list some of the key species. The complete list can be found in Park and Donald (1994).

2.3.3 Macroalgae

Sea grass (*Zostera sp*) was the most common species of macroalgae found in the harbour during the Harbour ecology study by Park and Donald (1994). Sea grass showed an average cover of over 22%. The algae were represented by sea lettuce (*Ulva sp*) with 3.78%, *Hormisira banksii* (2.38%), *Gracilaria secundata* (0.38%), *Corallina officinalis* (0.64%), *Gelidium caulacantheum* (0.16%), and *Ceramium sp* (0.03%).

2.3.4 Macrofauna

Among the benthic macrofauna the most abundant bivalves include cockle (*Austovenus stutchburyi*), pipi (*Paphies australis*), wedge shell (*Tellina itilana*), nut shell (*Nucula hartvigiana*), green-lipped mussel (*Perna canaliculus*), and others. The gastropods are represented by snails, chitons, and limpets. The common octopus (*Octopus macrum*) is the only member of the Cephalopods found in the harbour. The most abundant opisthobranch in the harbour is the black sea hare (*Apiysia Juliana*). The crustaceans are represented by crabs, crayfish, shrimp, amphipods, isopods, malacostraca, ostracods, and barnacles. There are anemones and holothurians (sea cucumbers). Starfish and urchins are common in the harbour. There are a large number of polychaetea species. There are sea squirts, worms and sponges. The fish in the area are sharks, stingrays, eels, and finfish like mullets, flounders, moki, kahawai, kingfish, snapper, sea horse, stargazer, and others as well as amphioxus, a chordate.

2.3.5 Resin acid

As of yet the effects of the tannins and resin acid on the mussels is unknown. A related toxicity assessment to determine the potential effects on the marine life from the stormwater runoff is being conducted by David Culliford. Therefore the study will explore if linkages between the plume waters and any biota can be detected.

Resin acids are lipophilic compounds. As such they can bio-accumulate in liver, bile, and plasma of aquatic organisms (Fåhræus-Van Ree & Payne, 1999). Gravato et al. (2005) found that resin acid causes liver bio-transformation and possibly genotoxicity in fish. Resin acids in the water usually coincide with

particulate matter in the water, from log handling for example. The Tauranga port stormwater runoff discoloration is mostly due to particulate matter. Particulate matter is known to be able to negatively affect feeding behaviour in filter-feeding organisms (Fåhræus-Van Ree & Payne, 1999).

Rosin is a major by-product from pine resin and consist mostly of abietic and primaric acids (Fåhræus-Van Ree & Payne, 1999). During chemical treatment of water containing these acids the acids can change their composition and/or their chemical structure, affecting their behaviour/reactivity with aquatic organisms. Water treatment can possibly lower the resin acid level in the water. If the resin acid is change chemically and this new chemical stays in the effluent water, the toxicity of the water might not have decreased even though the resin acid was removed/lowered as the new compound might be more toxic to aquatic organisms. Several other studies examined resin acids and their behaviour in water (Borga *et al.*, 1996a; Borga *et al.*, 1996b; Kanber *et al.*, 2006, 2008).

2.4 Summary

The study site is located in Tauranga Harbour on the North Island of New Zealand. Even though the estuary has two inlets, there are two distinct basins that can be treated as separate entities in regard to hydrodynamics.

- The study site is located in the southern basin just off of Mount Maunganui.
- The dominant hydrodynamic forces are tidal currents and wind waves.
- The hydrodynamics at the study site generally force shoreline attached plumes from the wharf runoff.
- The sediments in the area are predominantly fine grained; muds from the catchments and sand/shells from the shelf.
- The dominant wind direction is from the west.
- Tauranga Harbour has a diverse flora and fauna.

Chapter Three

Literature Review

3.1 Previous research undertaken focusing on Tauranga Harbour

Many previous scientific studies have been conducted in Tauranga harbour. The social and economic drivers such as Port expansion and dredging of the entrance channel have ensured that these studies predominantly focused on the southern basin in proximity to the Port, Stella Passage, and the ebb tidal delta. In particular there is a wide range of studies focusing on the hydrodynamics of the entrance channel, and the effects of dredging (de Lange & Gibb, 2000; Michels & Healy, 1999; Spiers & Healy, 2009; Spiers *et al.*, 2009; Tay *et al.*, 2013). I review some of the key results here.

3.1.1 Hydrodynamics

Tay *et al.* (2013) investigated the hydrodynamics of the southern basin of Tauranga Harbour Figure 3.1. They used the ELCOM model with data from a 1999 field study for calibration. The paper discusses the main circulation patterns and the effects of temperature and salinity. Different wind conditions and their influence on the circulation were characterised. Figure 3.2 shows the residual currents for the southern basin. The salinity stratification within the estuary is weak and influenced by the tide. The flood tide brings marine water to the intertidal flats eventually, and the ebb tide drains this water first. During the later stages of the outgoing tide and the early stages of the incoming tide the water is confined to the tidal channels which results in higher salinity in those when averaged over all tidal stages. The salinity, temperature, and retention time were modelled and Figure 3.3 shows the model results, demonstrating that wind seems to largely influence water temperature and retention time however, has a lesser effect on salinity. Temperature varies mostly diurnally and wind driven circulation can cool the water over the tidal flat areas by 2-4°C (Figure 3.3, B).

Large freshwater inputs intensify the stratification. These large freshwater inputs are mostly influenced by discharges from the Wairoa River. The southern basin is ebb-dominant at Omokoroa Point and ebb-dominant at Motuhoa and in the channels. There is a back eddy behind Mount Maunganui and on west of the flood tide delta.

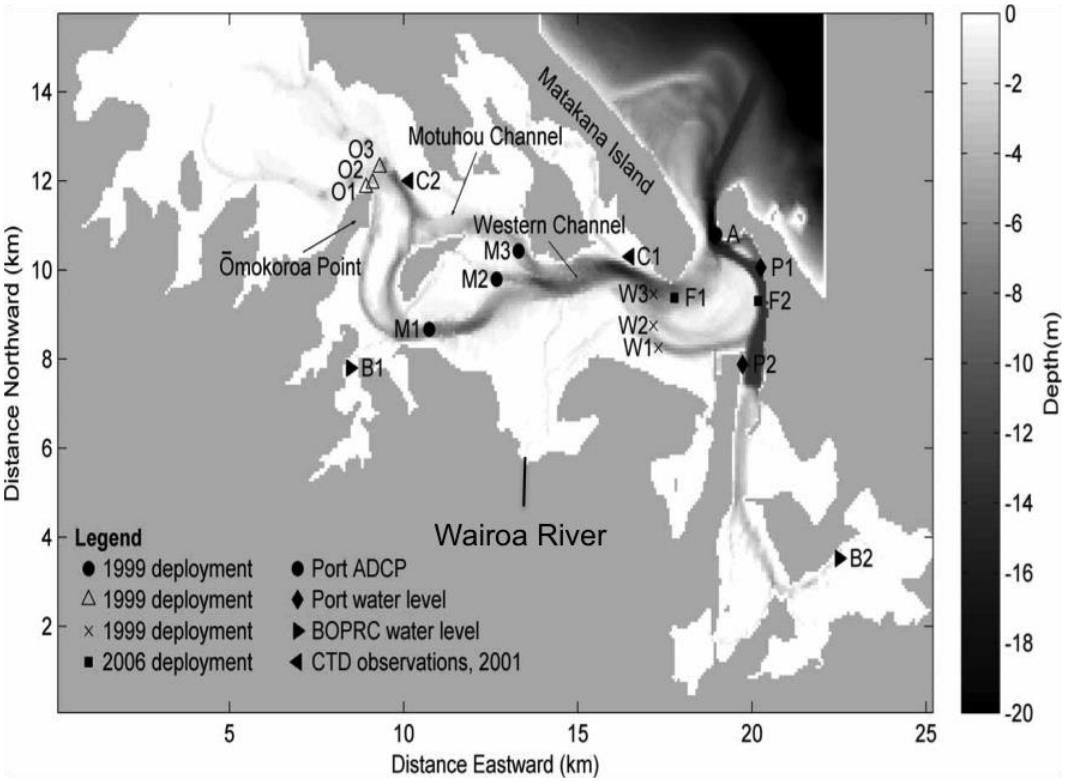

Figure 3.1: Site map of the deployment locations. Omokoroa point (O1, O2, O3), Motuhou (M1, M2, M3), Western Channel (W1, W2, W3), all used for model calibration. FSI current meter deployment (F1, F2), Port of Tauranga (P1, P2), and Bay of Plenty Regional Council water level recorders (B1, B2). The bathymetry grid in the background is from the ELCOM model. Source: (Tay *et al.*, 2013).

The harbour is relatively well flushed with residence times near the harbour mouth of 2 to 4 days. Storm winds seem to reduce residence time considerably by 39% for winter winds, and 24% for summer storms. The direction of these winds influences the residual currents. Easterly winds cause the Wairoa River water to flush faster towards the estuary mouth and thus decrease the residence time.

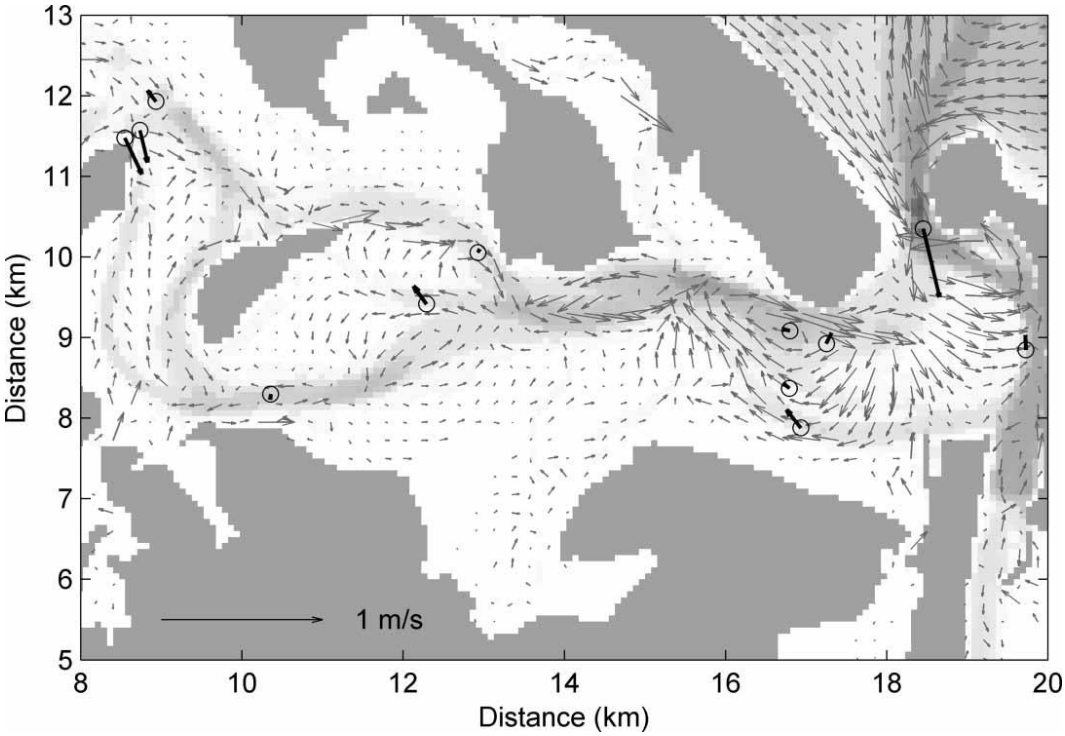

Figure 3.2: Residual currents in Tauranga Harbour. The solid grey indicates land mass, and the grey scale is water depth. Arrows indicate residual currents. Grey arrows: modelled residual current speed and direction, black arrows with circles: observed residual currents. Source: (Tay *et al.*, 2013).

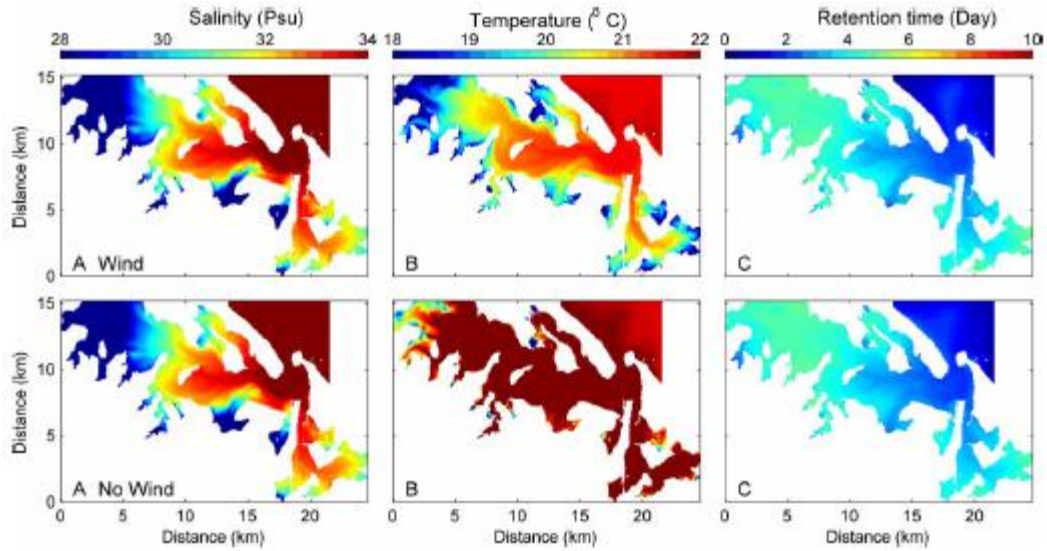

Figure 3.3: Modelled, depth-averaged salinity (A), temperature (B), and residence time (C) of the harbour. The top panels show dominant wind condition scenarios, bottom panels show no wind condition scenarios for summer. A spring to neap tide cycle (14 days) was averaged for the results. Source: (Tay *et al.*, 2013).

3.1.2 Sediment dynamics

Davies-Colley (1976) examined the sediment dynamics in Tauranga Harbour, focusing on the flood and ebb-tidal deltas. Their conceptual model describes the sediment transport pathways. These pathways are defined by tidal currents, bed forms (size and alignment), sediment discharge, and sediment transport rates. According to their findings sediment enters into the harbour via flood currents and then spreads across Centre Bank. The sediment leaves the harbour with the ebb currents. They also identified two major eddies; one eddy is south of Matakana Island, the other eddy is in Pilot Bay. Sediment can get trapped and eventually settle out. Davies-Colley (1976) also found that the tidal asymmetry varies with the magnitude and direction of the peak ebb and flood tide current velocity measurements. This variation was especially noticeable in the eddies. The longer durations of ebb flow current velocities within Pilot Bay result in dominant ebb residual currents (de Lange, 1988).

The impact of wind waves on sediment transport in the harbour is limited to the shallow regimes of beaches and tidal flats as that is the area where the wave orbitals reach the bottom and can have high enough velocities to entrain the sediment into the water column (Davies-Colley & Healy, 1978b). Figure 3.4 shows the proposed sediment transport patterns around the Tauranga Harbour Entrance. These directions of the sediment transport are determined by the residual tidal currents (Davies-Colley & Healy, 1978a).

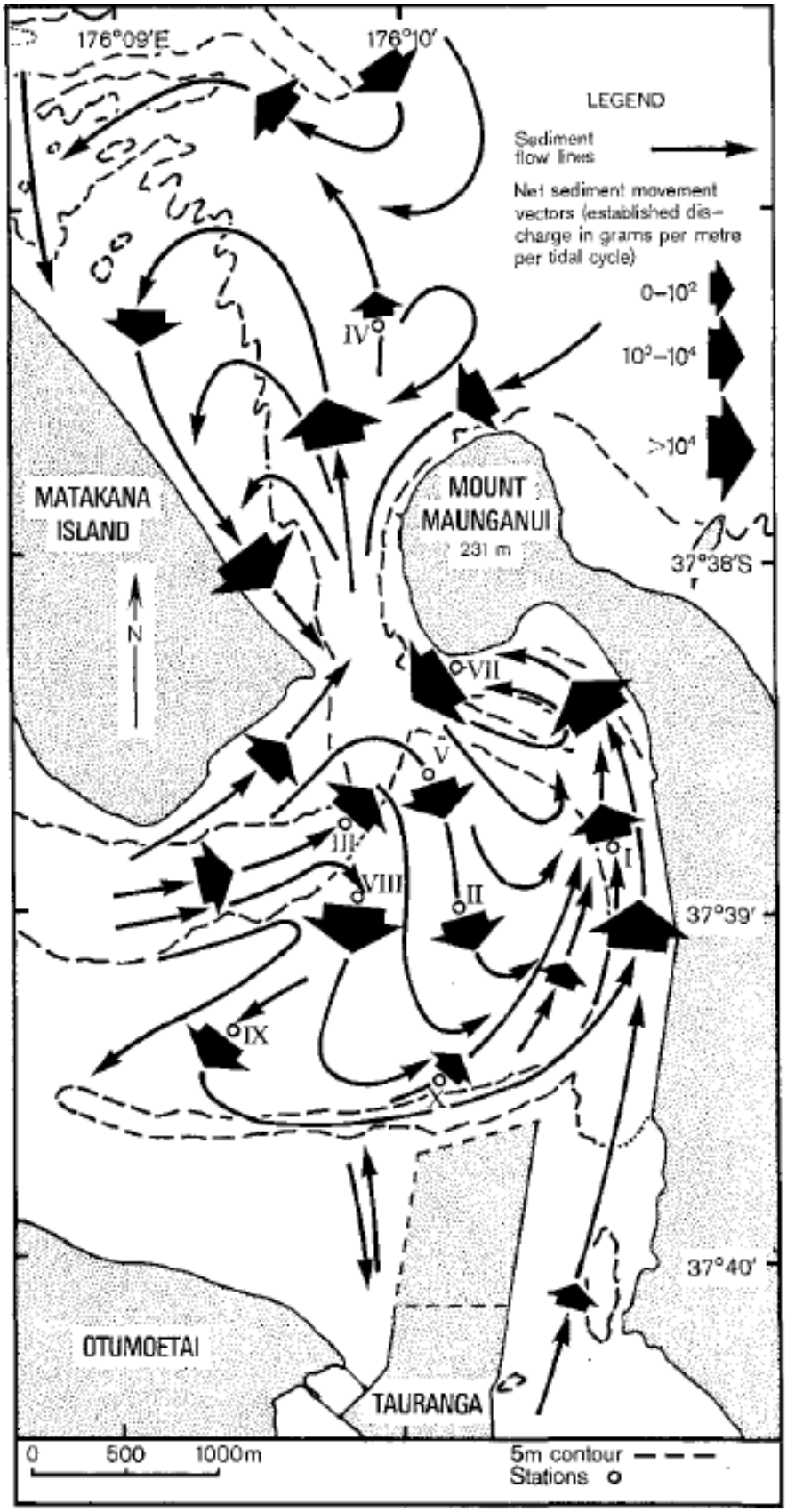

Figure 3.4: Sediment transport pattern model for the Tauranga Entrance. Source: (Davies-Colley & Healy, 1978b).

de Lange (1988) studied the wave climate and sediment transport in Tauranga Harbour. He found in his residual current analysis that Pilot Bay has ebb dominant flows. In the harbour the short period waves are mainly wind generated and the long period waves are generally seiches. The wave action is responsible for sediment transport on the shallow tidal flats as the short period wave orbital velocities are capable of entraining sediments to a depth of 2m below still water. His measurements indicate that there is an eddy in Pilot Bay. He detected flood dominance in Cutter Channel and ebb dominance in Pilot Bay channel which causes long period ebb currents (8-11 hours) in Pilot Bay.

3.1.3 Dredging

Mathew (1997) studied morphologic changes on the tidal deltas due to dredging and dumping. He found that dredging increased the current velocity in the lower West Channel and also increased flood velocity in Cutter Channel. He also found that the peak velocities decreased in the north of Cutter Channel, in Tauranga Entrance, and at Sulphur Point Wharf. Consistent with these results, Brannigan (2009) in his study of changes in geomorphology and hydrodynamics of the Tauranga Harbour found that the flow pattern in Stella Passage showed no changes before 1954 (no dredging). However, after the capital dredging which increased the water depth the current velocity decreased. Figure 3.5 shows the changes in the ebb tide velocities for the Tauranga Entrance and Figure 3.6 shows the changes in the flood tide velocities. On a comparing of both Figures, a clear difference between ebb tide and flood tide path in the Entrance is recorded, especially for post dredging (Cutter Channel).

Boulay (2012) in his MSc thesis mapped the sediments of Tauranga Harbour. He used acoustic mapping techniques; multibeam echosounder and side scan sonar. The data was mapped and then ground truthed using underwater camera and seabed sampling. He then compared the new maps to previous studies, identifying changes. He found that sand dunes that were identified by Davies-Colley (1976) were no longer there, and attributed this change to the on-going maintenance dredging in the area. The dredging also reduced the current velocities in Stella Passage. In the area of relevance to the work presented here, around Stella Passage, we see that the sediment is mainly fine sand, according to Figure 3.7. In

the area of Town Reach and Bridge Marina the morphological changes between 1985 and 2011 were found to be minor.

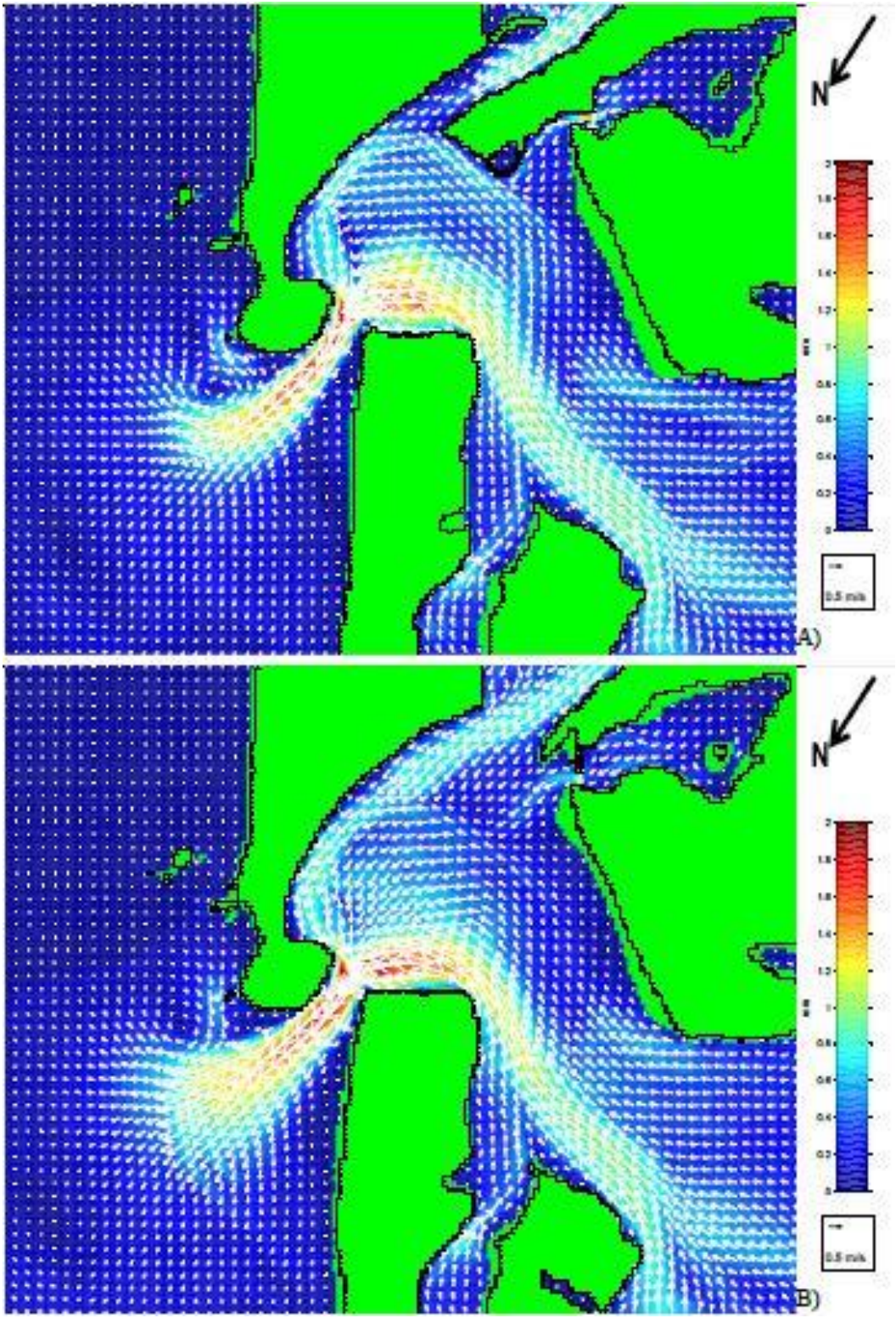

Figure 3.5: Vector plot of mean spring tide peak ebb velocity 2006 after dredging (A), and 1954 (B), showing every third vector, scale maximum set at 2m/s. Source:(Brannigan, 2009).

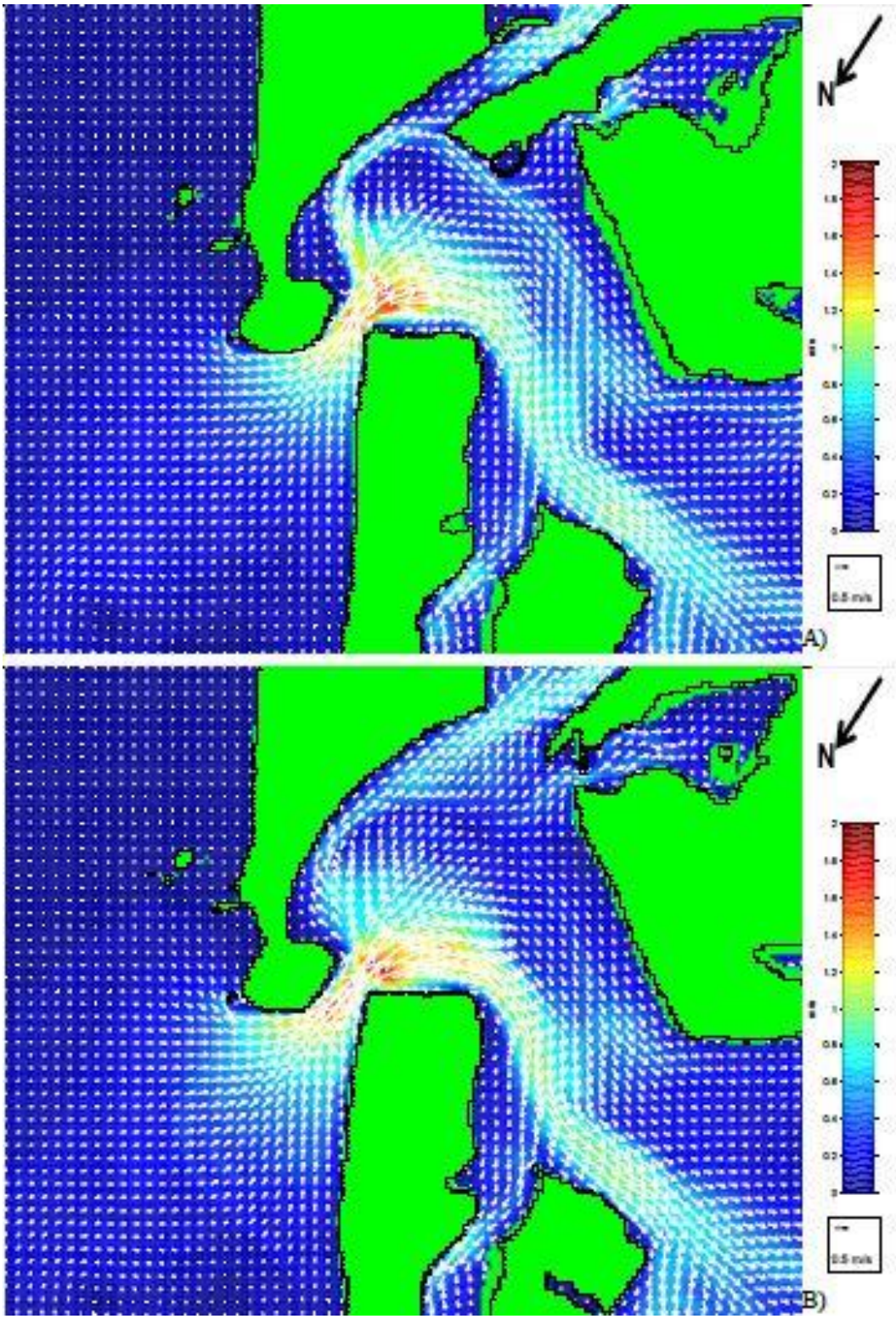

Figure 3.6: Vector plot of mean spring tide peak flood velocity 2006 (A), and 1954 (B), showing every third vector, scale maximum set at 2m/s. Source: (Brannigan, 2009).

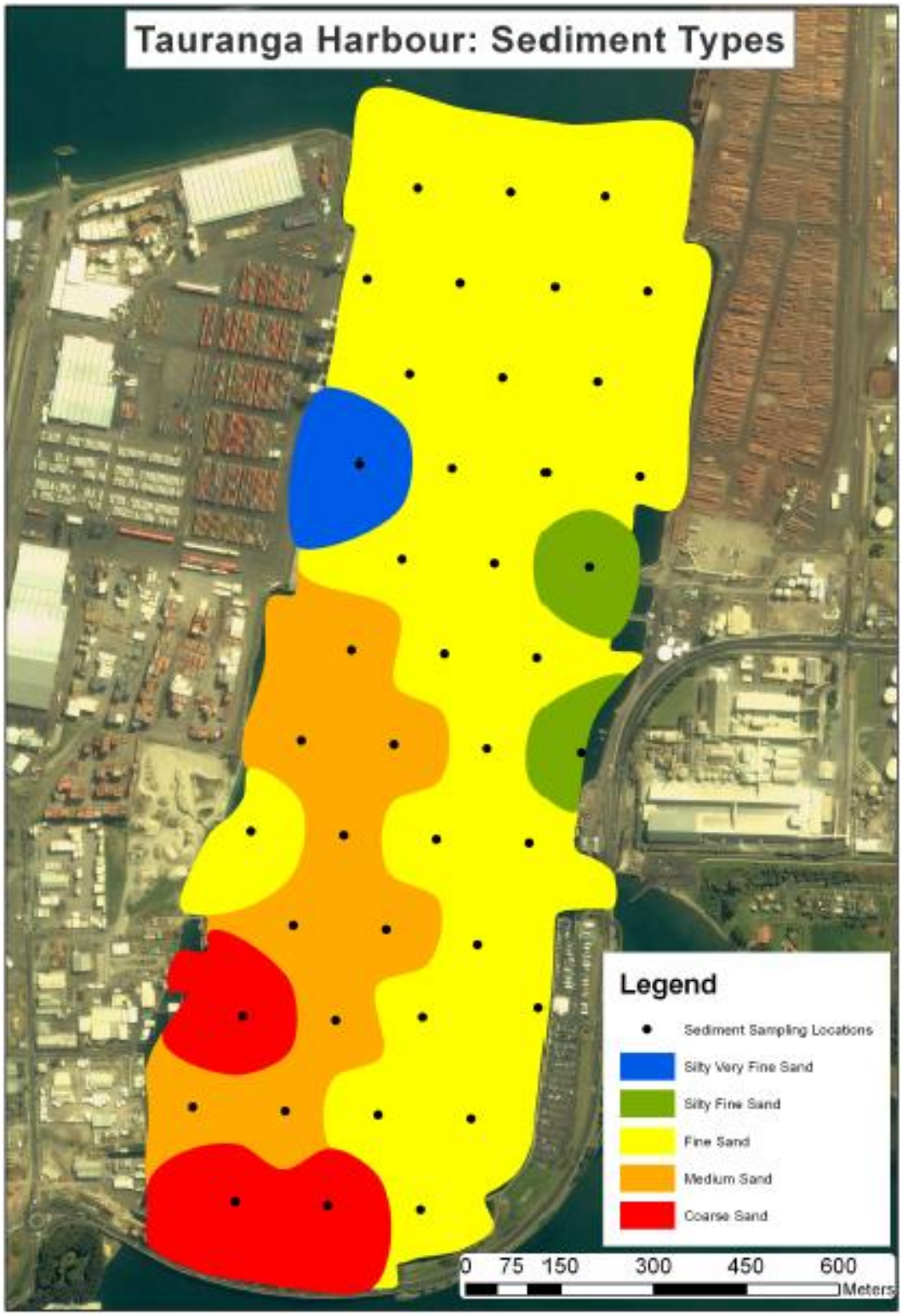

Figure 3.7: Map of surface sediment of Stella Passage, Town Reach, and Bridge Marina in Tauranga Harbour. The colour-coding groups similar sampling sites. Map does not represent actual sediment class boundaries of the area. Source: (Boulay, 2012).

3.1.4 Runoff

Tian conducted several studies around the port of Tauranga (Tian, 1993, 1997; Tian *et al.*, 1994; Tian *et al.*, 1998). According to Tian (1997) about half of the annual precipitation at the port becomes surface runoff. This runoff has a strong effect on the optical water quality which is about 1% of the receiving waters. In his study he treated each daily rainfall as a discrete event. He found that when the cumulative rainfall was low, no runoff was produced. With a high cumulative rainfall there is no difference in runoff volume if the rain is from one or several events once the ground is wet. The duration of the rain event does not play a role in runoff production.

3.1.5 Rainfall and runoff calculations

The following formula was used by Tian (1997) to calculate the runoff.

$$v_r = K(s - C) \qquad \text{Equation 3.1}$$

where v_r is runoff volume in m^3, s is accumulated rain in m, C is depression storage in m, and K is the runoff coefficient. According to Auckland regional Council C for impervious surfaces like the sealed log storage area have a C of 0.002m. The runoff coefficient K for the sealed area is 0.9 as the bark and logs take time to wet.

$$v_{rs} = 0.9 * A(s - 0.002) \qquad \text{Equation 3.2}$$

where v_{rs} is the runoff volume and A is the area that produces runoff in m^2.

I calculated the area for this study in Google Earth Pro using the Polygon measuring tool. The polygon in Figure 3.8 was produced by taking the area schematic provided by the Port (Figure 2.2). The calculated area is 735756 m^2. This number is very close to the number that was provided to me by the Port (total catchment area is 745000 m^2).

The rainfall data was calculated from the environmental data provided by the Port using MATLAB. Table 3.1 gives the data for the two storms that were surveyed. Using equation 3.2 to calculate the runoff volume (v_{rs}) and assuming a constant discharge rate, this then in time could be used to calculate u0, the discharge flow rate.

Table 3.1: Cumulative rain, storm duration, calculated runoff volume vrs, and flow rate u0 for the storm events on April 17th 2014 and July 12th 2014.

	17-Apr	12-Jul
rain (mm)	124.8	67.6
duration (sec)	51840	25860
vrs (m3)	826388	446310
u0 (m/s)	15.915	17.2587

To calculate flow rates

$$v_{fr} = v_{rs}(A_{dis}) \qquad \text{Equation 3.3}$$

where v_{fr} is flow rate velocity in m/s, v_{rs} is runoff volume in m^3, and A_{dis} is area of pipe holding water during discharge. Figure 3.9 gives the pipe area as 1.2 meters, which equates to a radius r of 0.6 m. To calculate A_{dis}

$$A_{dis} = x * \pi r^2 \qquad \text{Equation 3.4}$$

where x is the fraction of the pipe that is under water, π is π (3.1415), and r is pipe radius 0.6 m. As x is unknown, flow rates can only be approximated.

Tian (1997) calculated a flow rate of 0.32 m/s for a runoff of 0.72 m^3/s. For this he assumed that the discharge pipes were half full during the flooding event. Thus he calculated A_{dis} as 2.26 m^2.

Figure 3.8: Port area, to calculate runoff producing area with Google Earth Pro polygons. Area approximated from Figure 2.2.

The depression storage C in Equation 3.1 refers to the fact that rain on dry ground will not immediately produce runoff. The first rain is to wet the ground, fill up the depression storage; after C is full, any additional rain is converted into runoff.

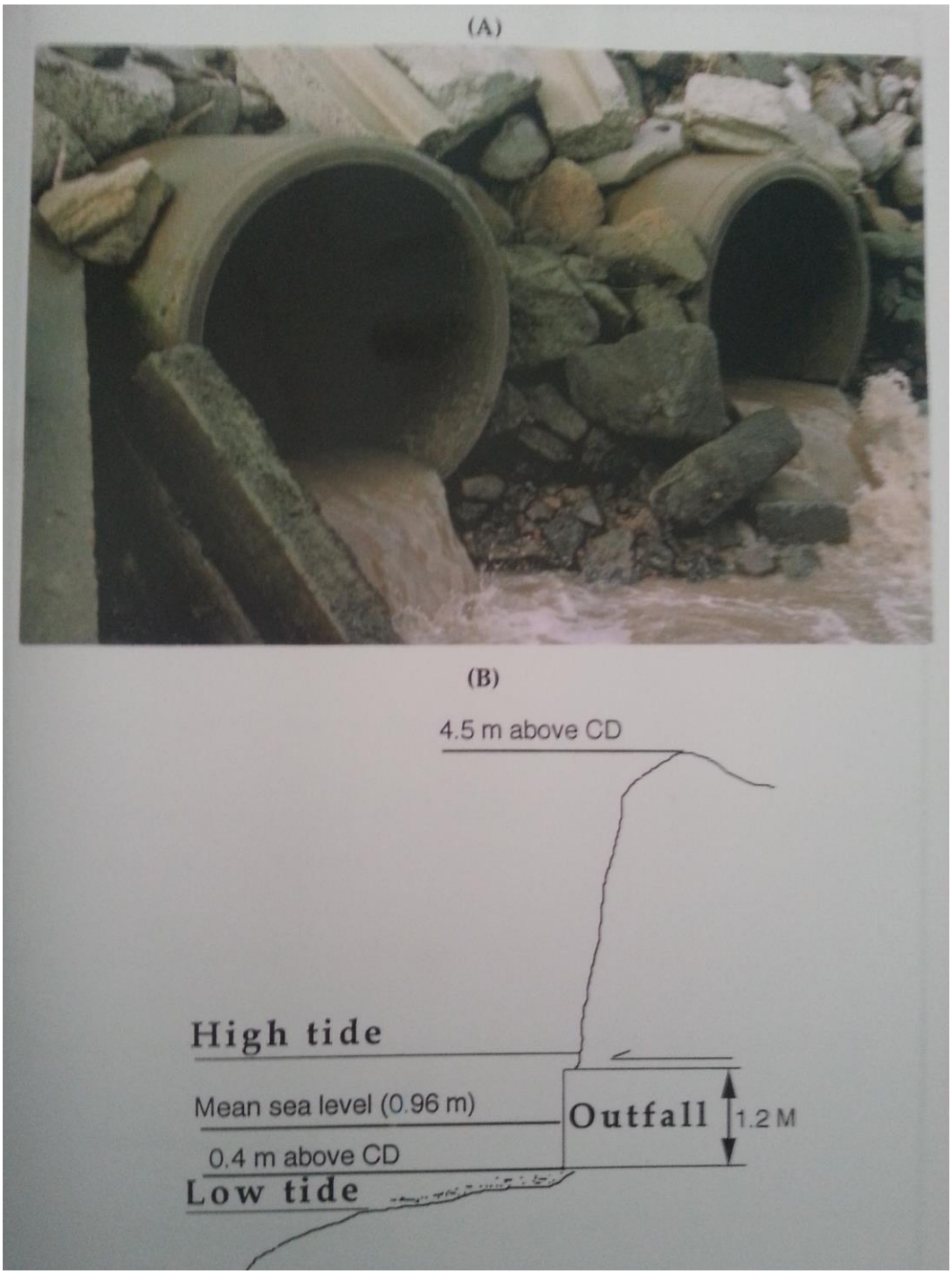

Figure 3.9: (A) Photo of southern outlet pipes. (B) Dimensions and elevations of outlet pipes relative to mean sea level. CD: Port datum. Source: (Tian, 1997).

3.1.6 Log handling and treatment

The timber export in Tauranga harbour requires the stripping off the bark from the logs. Some of the logs are treated against fouling. Both these treatment types produce different compounds. Stripping the logs from their bark leaves a

considerable amount of bark particles. These particles are swept up and removed but this removal is not completely effective and a considerable amount of bark pieces are left behind, especially pieces smaller than 2mm (Tian, 1993). These residues contribute to suspend and floating solids as well as fatty and resin acids in the stormwater runoff. The stormwater contains bark, soil particles, and nutrients. The large bark pieces are removed mechanically by sweeping the area after the logs are removed. This sweeping is relatively efficient for pieces larger than 4 mm. Small pieces stay on the impervious surface and usually are washed away during rainfall. The runoff passes through retention cages which can remove pieces down to sizes of 0.2 mm. These suspended solids are mainly responsible for the discolouration of the water (Tian, 1993).

Conventional water treatment techniques are effective in removing resin acids and suspended solids from the runoff. The impact of those resin acids is limited to about 100 meters from the discharge points. The acids tend to accumulate in the surface sediments of Stella Passage at a rate of 300-370 ppb per year. In Stella Passage the natural salinity stratification is dependent on weather conditions. Freshwater plumes in that area are affected by wind drag and pressure gradients, especially during the flood tide. At all times the plume seems to stay within the top 2-3 meters of the water column. Tian (1997) found in his field campaign that the salinity differences during the rain event was 5.2 psu over the first 4.5 meter while it was only around 0.2 psu over the same distance during dry days. The model predictions show a plume depth of around 2 meters (Tian, 1997).

Amounts of resin acids accumulated in the sediments have been found to be between 820 and 3900 ppb. These concentrations were measured after the main expansion dredging in 1990 and 1992. Before 1992 background concentrations were around 31-84 ppm. Considering the new concentration, the accumulation-rates were estimated as 300 and 370 ppb/year for the southern and northern (370 ppb/year) outfall pipes, respectively. Resin acid concentration was found to attenuate with increasing distance from source (Tian *et al.*, 1998).

The sampling regime used by Tian (1997) was limited which resulted in a coarse spatial and temporal resolution. Also, the instruments have improved since his study was undertaken.

3.1.7 Modelling

Tian (1997) used the fully coupled 3-d circulation and transport hydrodynamic numerical model 3DD. He used the eulerian scheme hydrodynamics coupled with eulerian and lagrangian advection and diffusion scheme as this would allow for better results of plume mixing with wind and tidal current forcing that the study site requires. The 3DD model is based on discretisation and numerical solution of the momentum and mass conservation equations. A 300 meter grid was used to establish boundary conditions for the 75 meter grid used for the plume modelling. To model the vertical plume 11 vertical layers were established in the 75 meter grid. Several scenarios were model to account for different wind speeds and direction as well as different timing in relation to tidal stage. With all model results he was able to show that the plume never reached depths deeper than 3 meters. He was also able to show that under certain wind and tidal conditions the plume can reach all the way across Stella Passage. The plume is usually advected south on an incoming flood tide and north on the outgoing ebb tide with the wind direction either increasing the advection effect or decreasing it if wind direction is against the tidal current.

Model results for scenario one with 30 knots north-easterly winds show that the plume reaches across Stella passage Figure 3.10. In Figure 3.11 we can see that the plume is very thin, only in the top two layers. Looking at Figure 3.12 and Figure 3.13 we see that the plume does not go below 2 meters water depth but does reach across the channel (Figure 3.13).

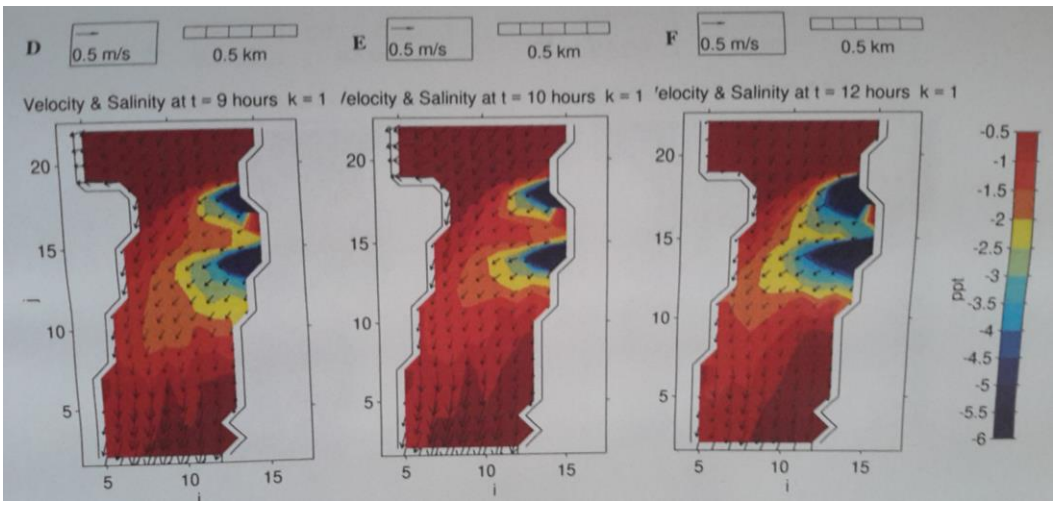

Figure 3.10: 30 knot north-easterly wind, time at 9 (D), 10 (E), and 12 (F) hours, layer 1. Source: (Tian, 1997)

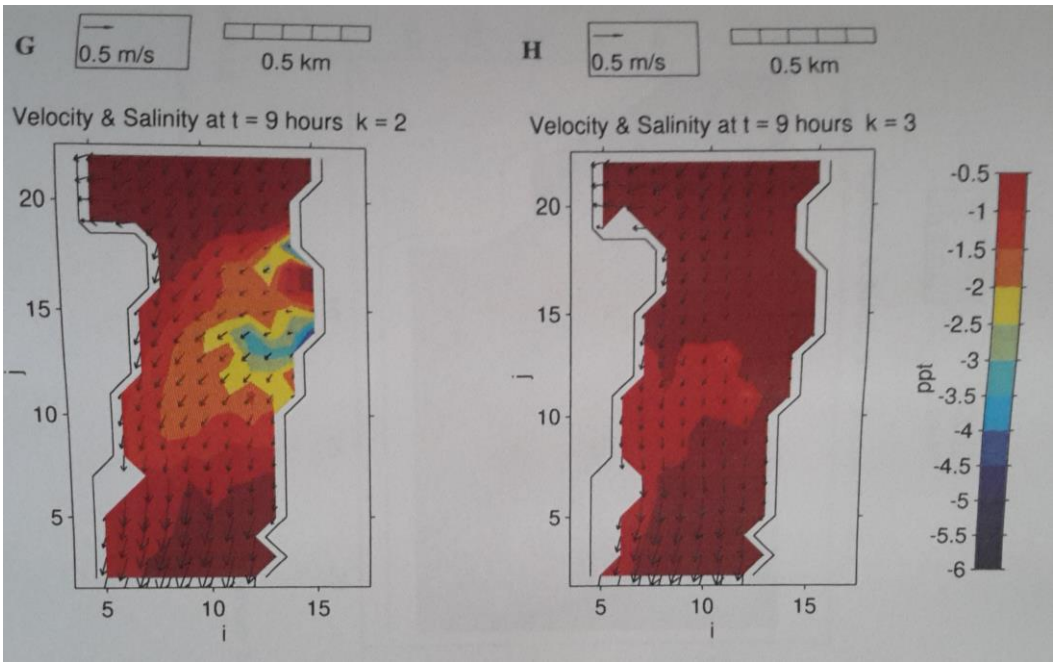

Figure 3.11: 30 knot north-easterly wind, time at 9 hours, depth layer 2 (G) and 3 (H). Source: (Tian, 1997)

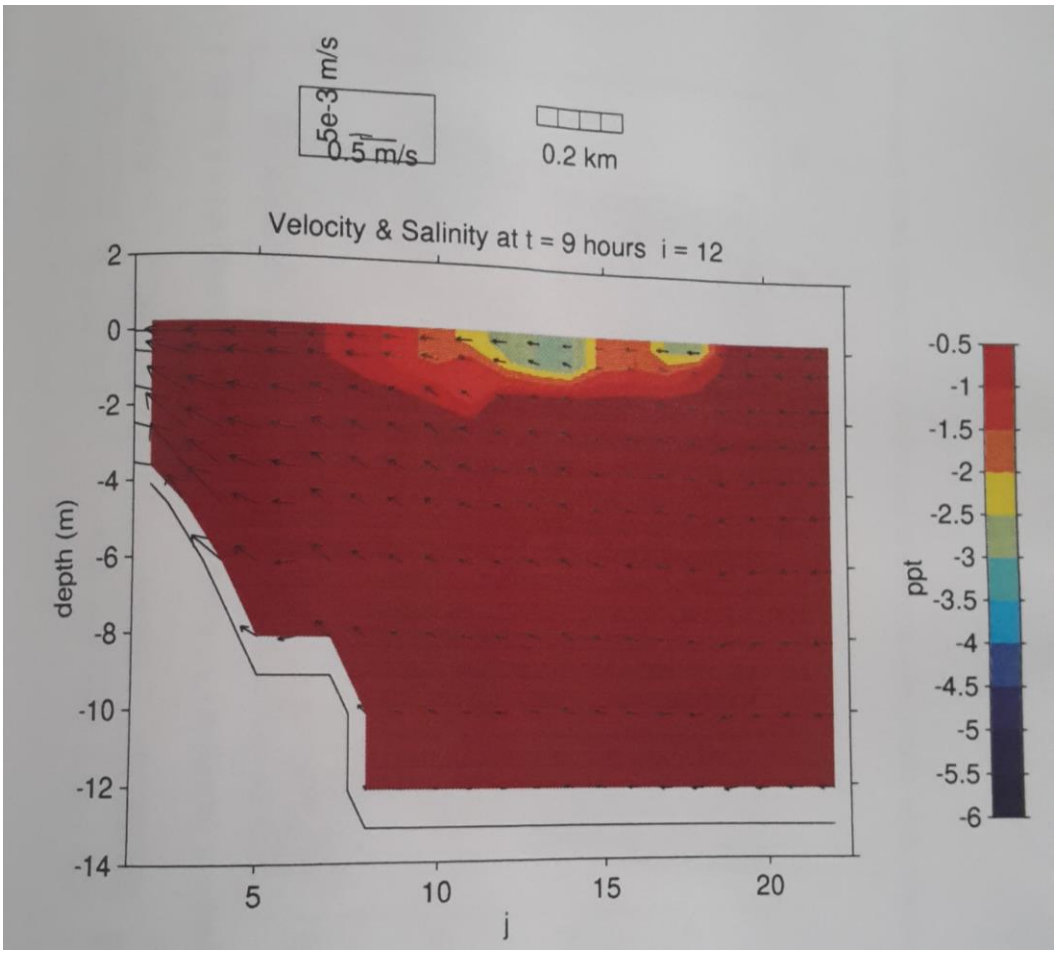

Figure 3.12: 30 knot north-easterly wind, time at 9 hours, and depth profile section along Stella Passage. Source: (Tian, 1997)

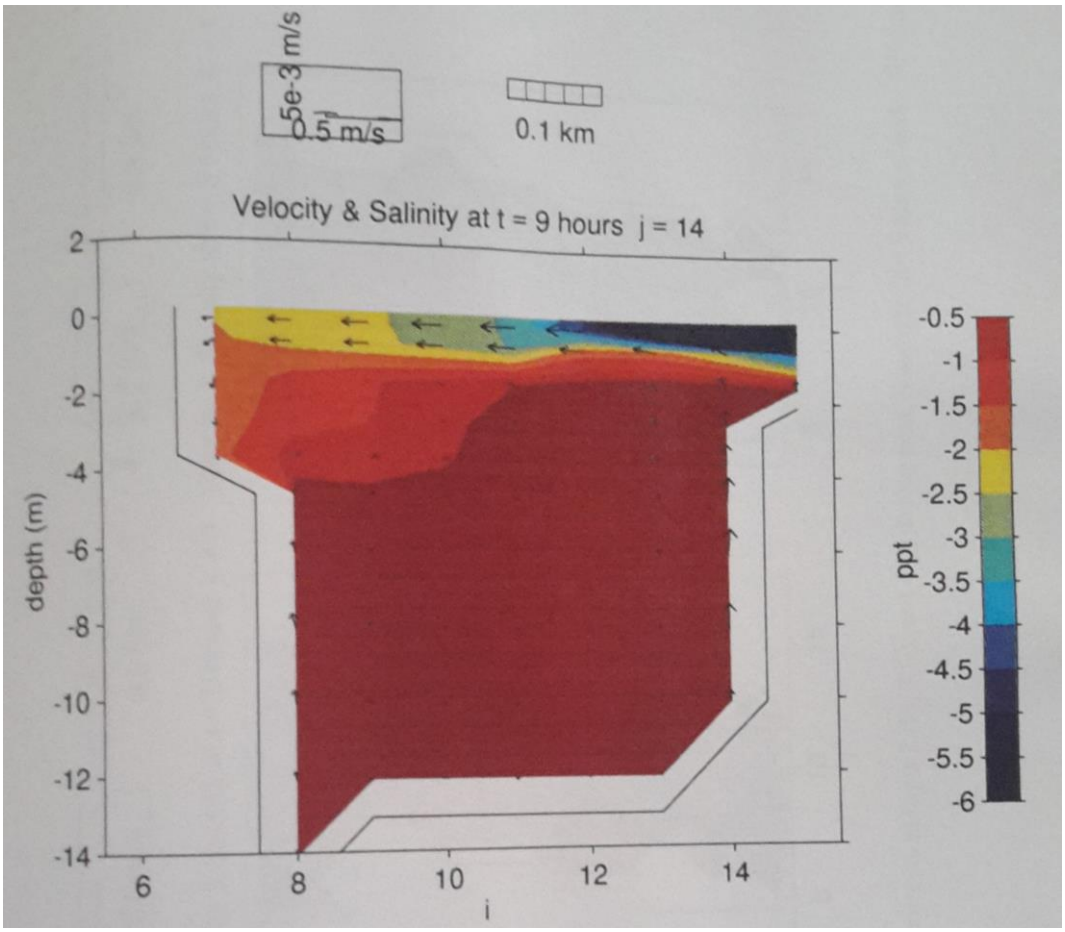

Figure 3.13: 30 knot north-easterly wind, time at 9 hours, depth profile, and section across Stella Passage. Source: (Tian, 1997)

One of the modelled scenarios, started right after high tide with 30 knots southerly winds. The outgoing tide strongly advects the plume to the north (Figure 3.14). Figure 3.15 shows that the plume is very shallow, less than 2 meters deep.

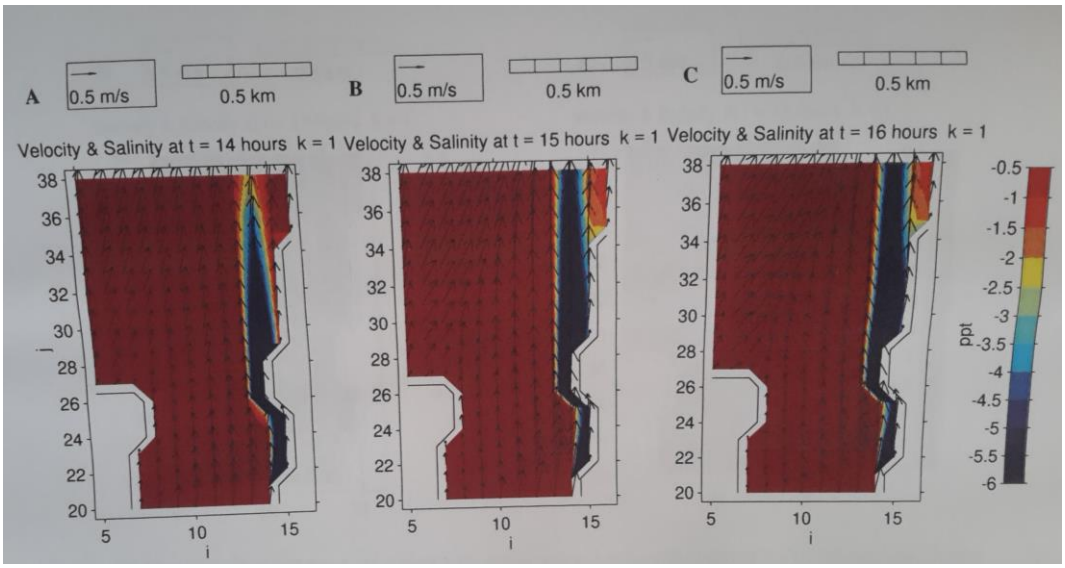

Figure 3.14: 30 knot southerly wind, 2 hours (A), 3 hours (B) and 4 hours (C) after high tide, surface layer. Source: (Tian, 1997)

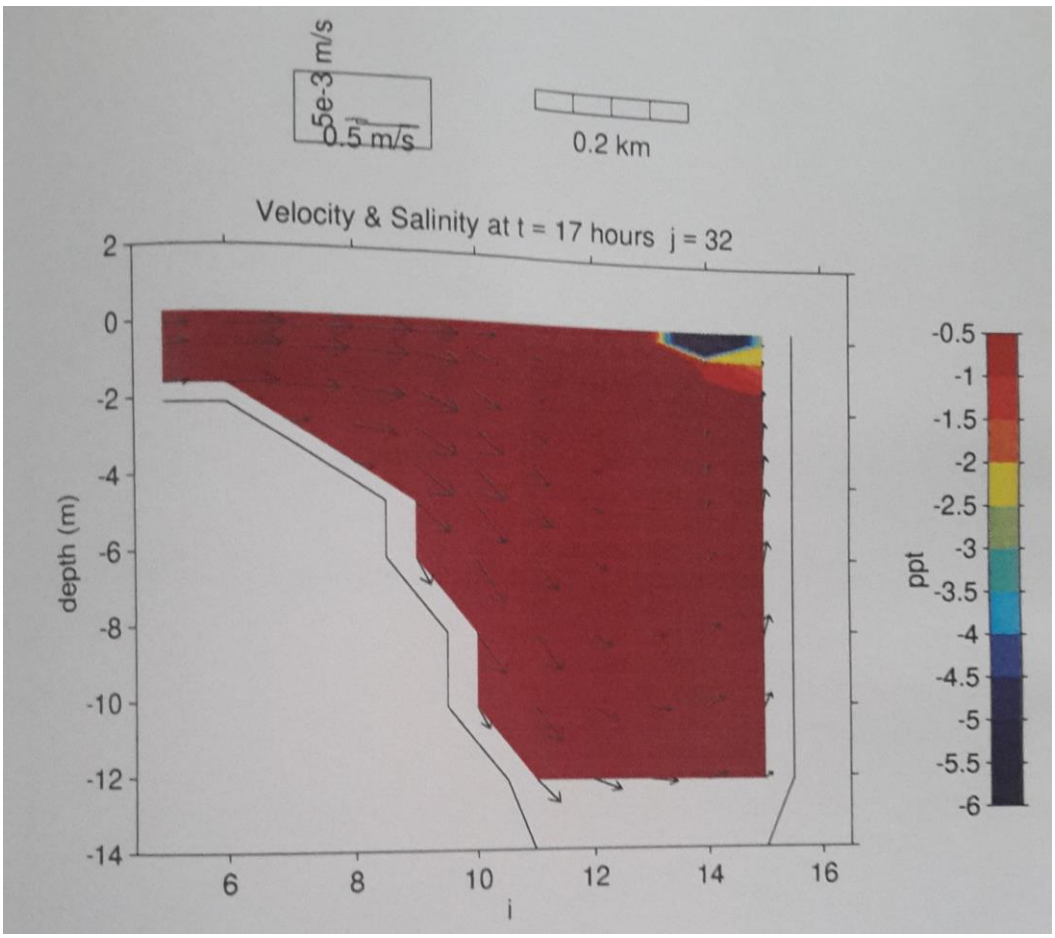

Figure 3.15: 30 knot southerly wind, 5 hours after high tide, depth profile across Stella Passage. Source: (Tian, 1997)**.**

Using the Delft3D modelling suit coupled with a SWAN wave model, Kwoll (2010) predicted erosion to occur primarily in the major sediment transport pathways. The smaller the grain sizes the larger the predicted erosion. Sediment transport on the intertidal flats was predicted to be minimal and the deposition was generally limited to smaller grain sizes (<350μm) due to limited entrainment potential of the weak current velocities. In the inner harbour the larger grain sizes (>350μm) were dominant.

3.1.8 Calculated Plume numbers from Tian (1997)

Horizontal eddy diffusion was calculated using

$$F = -N_h \frac{dC}{dx} \qquad \text{Equation 3.5}$$

where N_h is eddy diffusity in direction x and C is particle concentration. The vertical mixing was calculated using

$$E_v = \kappa D u * \frac{z}{D}\left[1 - \frac{z}{D}\right] \qquad \text{Equation 3.6}$$

where E_v is the vertical eddy viscosity, u* the shear velocity, D the water depth, κ the von Karman constant (0.4). The Richardson number for stratified water columns was calculated using

$$R_i = -g\left(\frac{\partial \rho}{\partial z}\right) / \rho\left(\frac{\partial u}{\partial z}\right)^2 \qquad \text{Equation 3.7}$$

where g is gravitational acceleration (9.81m/s^2) and ρ is water density.
The mixing length was given as

$$l_m = \kappa z\left(1 - \frac{z}{h}\right) \qquad \text{Equation 3.8}$$

$$N_z = l_m{}^2\left[\left(\frac{\partial u}{\partial z}\right)^2 + \left(\frac{\partial v}{\partial z}\right)^2\right]^{\frac{1}{2}} \qquad \text{Equation 3.9}$$

where κ = 0.4, z is the distance for sea bed, h is water depth, u and v are orthogonal velocities.

3.1.9 Biology

Cole *et al.* (2000) studied the bivalve distribution in Tauranga Harbour and found that across 27 sites 314 different bivalve taxa can be found. Centre Bank houses substantial populations of bivalves. Sea grass covers over 22.5% of the harbour area (Inglis *et al.*, 2008).

Chapter 2 gives a good description of flora and fauna found in Tauranga Harbour. For the detailed list consult Park and Donald (1994).

According to Boulay (2012) the area around the Tauranga bridge is an important source of seafood and juvenile shellfish for the shellfish beds on Centre Bank.

3.2 Previous freshwater plume studies

Several freshwater plume studies have been conducted. The studies I examined were mostly focusing on southern Californian waters (Lahet & Stramski, 2010; Lee *et al.*, 2011; O'Donnell, 1997; Reifel *et al.*, 2009; Svejkovsky *et al.*, 2010; Washburn *et al.*, 2003; Wu *et al.*, 1994)

Wu *et al.* (1994) used field observations to examine plume structure and dynamics. They employed high resolution towed survey of physical and bio-optical variables with current measurements to determine the plume structure and dynamics. They found the plume mixing to be strongly dependent on background current velocities.

O'Donnell (1997) employed ship mounted instrument arrays to measure near-surface currents and density distribution in plumes and frontal systems. The array provided current velocities at four levels and temperature and conductivity at five levels in the upper 3 meters of the water column, thus providing a high depth resolution. At a ship speed of 1 to 2 m/s the horizontal resolution is 5 meters. He found salinity differences of 20 psu in less than 10 meters going into the plume.

Lahet and Stramski (2010) studied runoff plumes using MODIS imagery to determine horizontal plume extent.

3.3 Summary

Previous research in the study area shows that:

- Salinity is influenced mainly by freshwater input and weather conditions.

- The harbour is weakly stratified.
- Sediment transport relies mostly on residual currents and wave action on shallow tidal flats.
- Dredging had a major influence on the hydrodynamics of the harbour, changing the residual tidal current patterns and sediment transport pathways.
- Runoff can have an influence on the sediments for up to around 100 meter downstream of the outlet pipe.
- The resin acid concentrations in the sediment attenuate with increasing distance from the source.
- The runoff plume always stays in the upper 3 meters of the water column.
- The plume spreading depends on tidal stage when released and wind direction during the spreading.
- There is abundant flora and fauna in the Harbour that could potentially be affected by the runoff.
- Other plume studies used similar approaches like temperature and conductivity arrays as well as current velocities.
- Optical measurements were also used to determine plume horizontal extent, spreading, and dispersion rates.

Chapter Four

Field Deployment

4.1 Introduction

Field measurements were undertaken focusing on the area adjacent to the stormwater run-off pipes. Longer-term time series were obtained to provide information about baseline hydrodynamic conditions (velocities and densities). A series of surveys of velocities, salinities, temperatures were also conducted over shorter time scales to provide measurements with no outflow from the pipes (control transects), and during large rain events to map the extent and dissipation of the freshwater plume from the stormwater outflow pipes.

Figure 4.1 shows the locations where the different instruments were deployed. Table 4.1 gives the corresponding instrument type and serial number, sampling type and deployment depth.

Figure 4.1: Deployed instrument locations in Stella Passage and Cutter Channel (image credit: Google Earth)**.**

4.1.1 Longer term time series (current measurement)

A series of instruments were deployed from 10 April 2014 to 17 May 2014. The array consisted of the following instruments:

- Current profiling instruments to provide 3 components of velocity at fixed depths in the water column (Sontek Argonaut ADP (Figure 4.2), 2MHz Nortek Aquadopp (Figure 4.3)).
- Fixed point; current meters to give 3 components of velocity at a single depth point close to the bed (Sontek triton Acoustic Doppler velocimeters (ADVs, Figure 4.4) and Interocean S4 electromagnetic current meters (Figure 4.5).

The summary of locations, sampling rates (all instruments burst sampled), and deployment depths are provided in Table 4.2.

Figure 4.2: Sontek ADP (photo credit: Nadine Brunschwiler).

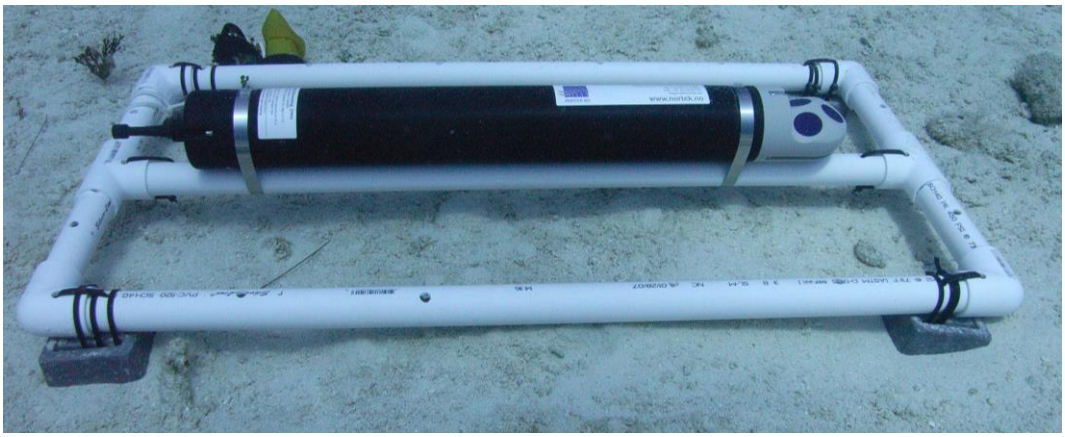

Figure 4.3: Aquadopp (photo credit: http://people.uncw.edu/finellic/images/adp2.jpg).

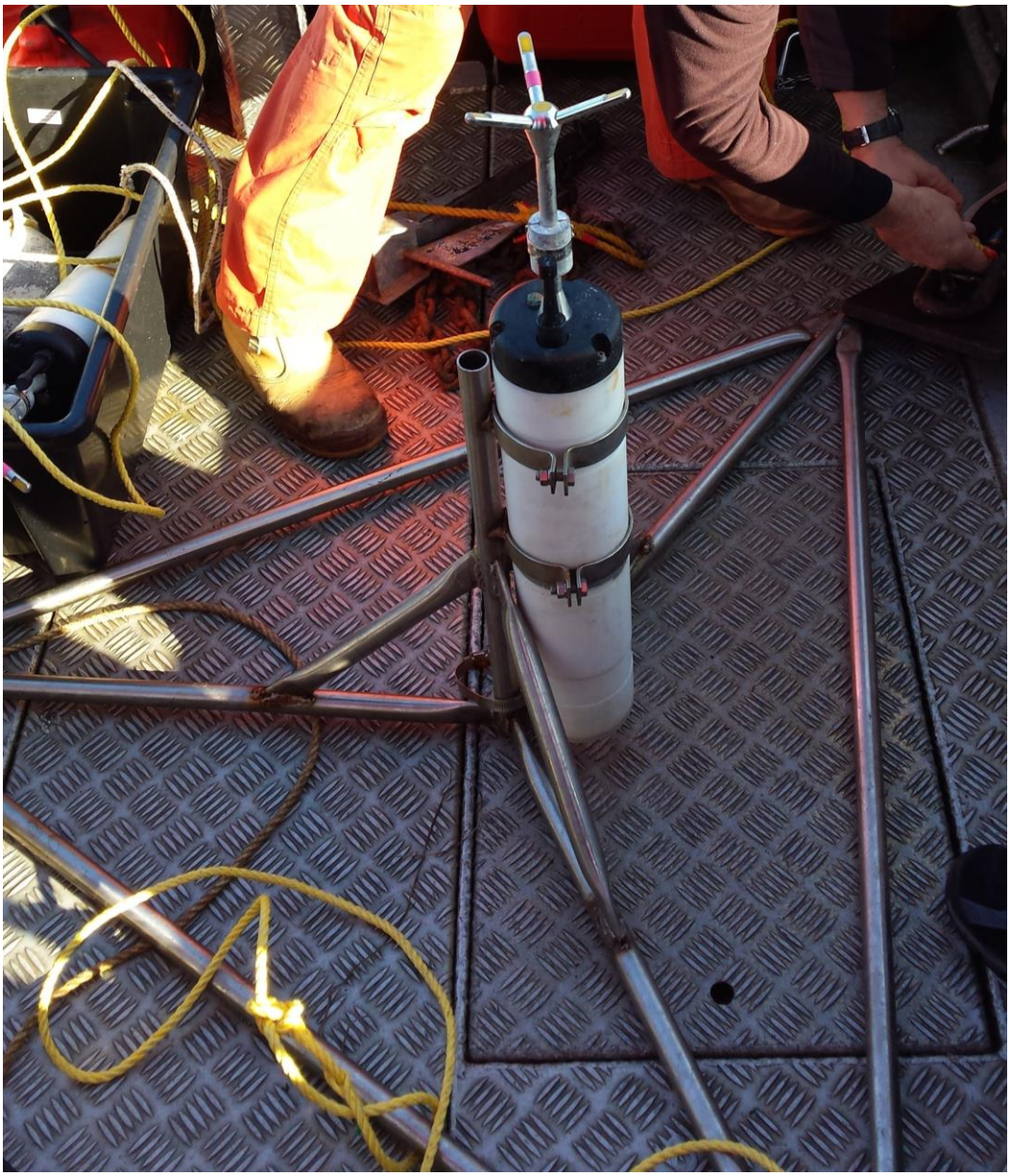

Figure 4.4: Sontek ADV (photo credit: Nadine Brunschwiler).

Figure 4.5: Interocean S4 (photo credit: Nadine Brunschwiler).

The S4 program did not provide a date vector, only a time vector therefore a date vector for each file was created in MATLAB.

Table 4.1: Fixed instrument locations (number and Latitude and Longitude), serial numbers, sampling type (p: profile sampling, f: fixed sampling depth), and deployment depth. The location numbers correspond to numbers in Figure 4.1.

Locations	Instrument	Latitude (S)	Longitude (E)	sampling	depth (m)
1	ADP	37.6492	176.1793	p	10.5
2	S4 07581610	37.6661	176.1765	f	7
3	S4 05452199	37.6411	176.1722	f	8.6
4	S4 08767065	37.6406	176.1779	f	9
5	ADV R259	37.6378	176.1698	f	8.9
6	ADV R252	37.6426	176.1755	f	9.6
7	ADV R228	37.6752	176.1750	f	6.6
8	Aquadopp 6858	37.6568	176.1763	p	11.9

Table 4.2: Summary table of fixed deployed instruments. Location, instrument, measurements, make, model, serial number, averaging interval, sampling interval, cell size, and sensor height above sea bed.

Location	Instrument	Measurements	Make	Model	serial number	averaging interval (s)	sampling interval (s)	cell size (m)	sensor height above bed (m)
1	ADP	P, T, u, v, w	Sontek	Argonaut XR	E2506	120	300	0.6	0.2
2	S4 3	u, v, w	Interocean	Argonaut XR	07581610	300	900	N/A	1.1
3	S4 2	u, v, w	Interocean	Argonaut XR	05451299	300	900	N/A	1.1
4	S4 1	u, v, w	Interocean	Argonaut XR	05782065	300	900	N/A	1.1
5	ADV 1	P, T, u, v, w	Sontek Triton	10000Hz	R259	120	600	N/A	1
6	ADV 2	P, T, u, v, w	Sontek Triton	10000Hz	R252	120	600	N/A	1
7	ADV 3	P, T, u, v, w	Sontek Triton	10000Hz	R228	120	600	N/A	1
8	Aquadopp	P, T, u, v, w	Nortek	2MHz	AQD6858	120	300	25	0.3

4.1.2 Longer time series (Conductivity-Temperature (CT) measurements and mussel deployment)

In addition to current measurements, Odyssey CT sensors (Figure 4.6) were deployed around the harbour, focusing on the wharf (Figure 4.7). Conductivity can be calibrated to give salinity. Although not of high accuracy these sensors were used to provide an indication of plume extent. All instruments were set to sample every 5 minutes. In some cases CT sensors were also co-located with a cage containing mussels which would be used for the toxicology assessment (conducted by David Culliford and Nick Ling). CT locations are listed in Table 4.3 and shown in Figure 4.7.

Table 4.3: CT sensor locations (Latitude, Longitude), association with mussel cage (yes/no). Locations are shown in Figure 4.7.

Place	Instrument	Latitude (S)	Longitude (E)	mussel cage
1	CT 2830	37.6378	176.169722	n
2	CT 4053	37.6378	176.169722	n
3	CT 4054	37.6375	176.166667	n
4	CT 4053	37.6658	176.176389	y
5	CT 2828	37.6597	176.181111	y
6	CT 2827	37.6597	176.181111	y
7	CT 2829	37.6592	176.181389	y
8	CT 4055	37.6592	176.181389	n
9	CT 2826	37.6489	176.179167	y
10	CT 2831	37.6378	176.169722	y

There were 3 main deployment periods with the CT sensors (Table 4.4) trying to catch major rain events and overlapping with survey data.

We note that unfortunately sensor 4056 was stolen and CT sensor 2827 malfunctioned owing to a corroded battery link.

Figure 4.6: Odyssey CT sensor (photo credit: Nadine Brunschwiler).

Figure 4.7: CT sensor locations in Stella Passage and at Mount Maunganui (control) (image credit: Google Earth).

Table 4.4: CT sensor deployment periods, giving sensor serial number and deployment start and stop dates.

Sensor	start1	stop1	start2	stop2	start3	stop3
CT 4056			17-Jul-14	12-Sep-14		
CT 4054			17-Jul-14	12-Sep-14		
CT 2882	4-Jun-14	15-Jul-14			19-Dec-14	18-Mar-15
CT 2830			17-Jul-14	12-Sep-14	19-Dec-14	18-Mar-15
CT 2828	4-Jun-14	15-Jul-14				
CT 2827	4-Jun-14	15-Jul-14				
CT 2829	4-Jun-14	15-Jul-14				
CT 4055	4-Jun-14	15-Jul-14				
CT 2826	4-Jun-14	15-Jul-14				
CT 2831	4-Jun-14	15-Jul-14			19-Dec-14	18-Mar-15
CT 4053			17-Jul-14	12-Sep-14		

4.2 Calibration

The CT sensors were calibrated against solutions of known densities in the laboratory using the following procedure:

Two buckets containing (2 and 0.4 litres respectively) of tap water were kept at 20 degrees Celsius. The large bucket was used for calibration measurements and the smaller bucket was used to store the additional loggers between measurements in order to keep them at the same temperature and salinity. During the calibration process the logger was suspended in the solution from a stand to about 4 cm under the rim along with the YSI sensor. The sensor measurements are given in voltages and were recorded in an excel spread sheet. Salt was incrementally added to make solutions of increasing salinities and measurements from an Anton Paar DMA35 density meter and an YSI were used to calibrate against. Measurements were taken at six calculated salinities (0, 10, 15, 25, 30, and 35 PSU). The Odyssey software provides a 'Probe Trace Mode' interface which provides raw data value readings for temperature and conductivity. At each level a single reading for temperature was taken for each measurement and for the conductivity measurements an average of the first seven readings was calculated. The process was then repeated with solutions held at 15 degrees Celsius. For these calibration iodised cooking salt (CEREBOS) was used. To increase the salinity of the solutions by 5 PSU 10 gram salt were added to the two litre bucket and 2 gram to the 0.4 litre bucket.

The odyssey software includes a calibration interface in which data sets have to be produced for each logger, one for temperature and one for conductivity. Temperature calibration requires two readings with an approximate temperature difference of 5 degrees and simply assumes a linear response between reading and temperature. The conductivity calibration fits a polynomial set which requires six data points. While entering the recorded data, the units can be selected.

4.2.1 Example Calibration

The first CT sensors (4053, 4054, 4055, and 4056) were calibrated September 20 2013 and recalibrated November 30 2013. The calibration and recalibration

figures for both density (Figure 4.8) and salinity (Figure 4.9) are shown. To calibrate the sensors for salinity and density the average raw sensor reading for a specific salinity/density was taken from the Anton Paar DMA35 density meter (density) and the YSI (salinity). With these numbers density and salinity were calculated in MATLAB using a linear regression. The calibration was carried out at a water temperature of 20°C. Figure 4.9 shows that at the high end of the salinity spectrum that the sensors were calibrated for they show a bit of divergence after the recalibration. This phenomenon is not observed in the density calibration (Figure 4.8).

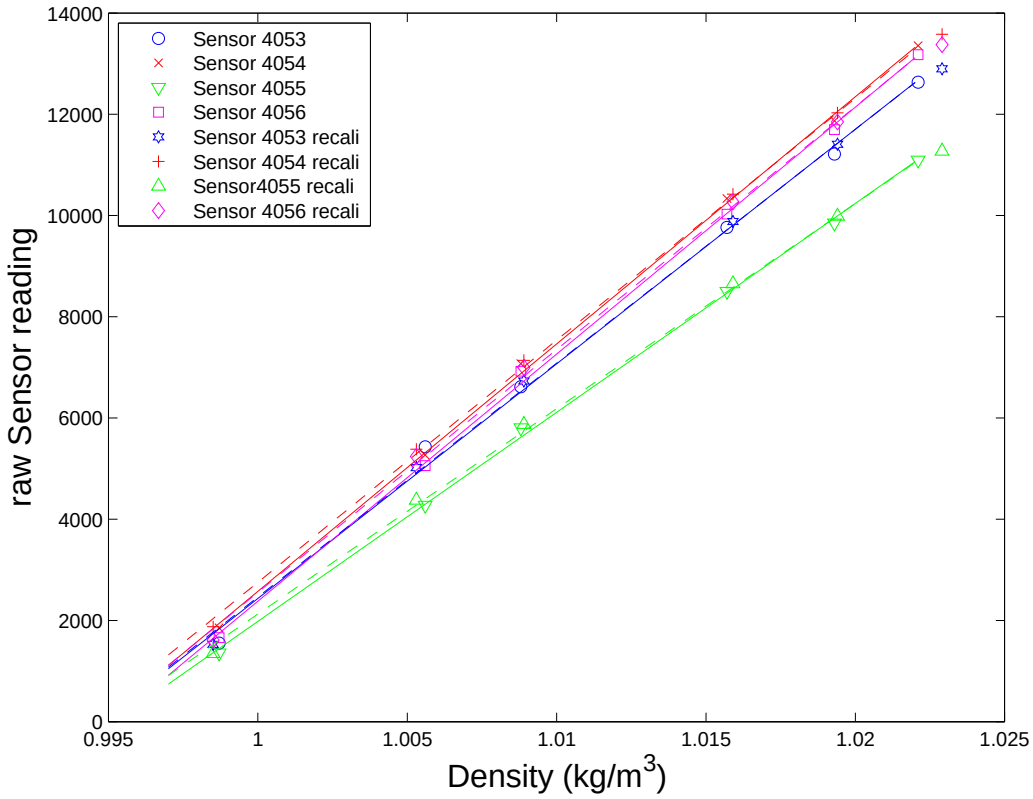

Figure 4.8: Example results of a calibration (solid lines) and recalibration (dashed lines) for density. Sensor 4053; blue lines, circle for calibration measurement, star for recalibration measurement. Sensor 4054; red lines, x for calibration measurement, + for recalibration measurement. Sensor 4055; green lines, v for calibration measurement, ^ for recalibration measurement. Sensor 4056; pink lines, square for calibration measurement, diamond for recalibration measurement.

The temperature was calibrated similarly, although only two points were measured. Figure 4.10 shows an example the temperature calibration. The

recalibrations gave rise to the same values and hence are not plotted. The calibration therefore provided some confidence that the temperature sensors do not drift significantly over the periods of interest.

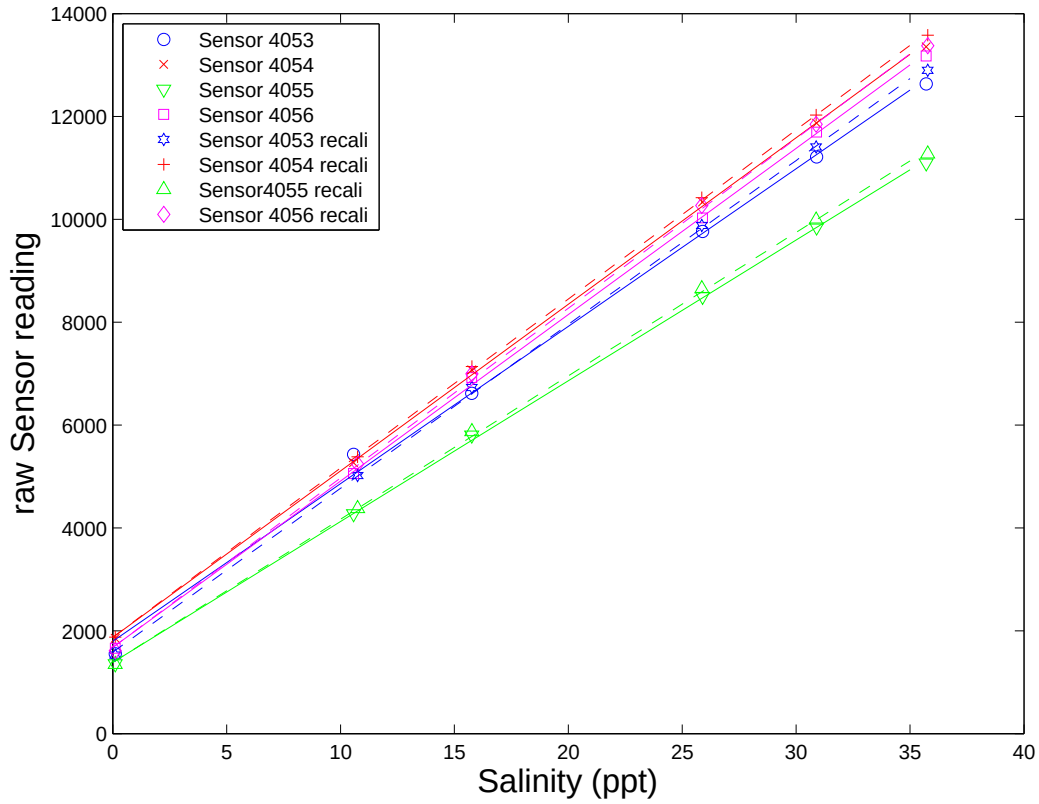

Figure 4.9: Example results of a calibration (solid lines) and recalibration (dashed lines) for salinity. Sensor 4053; blue lines, circle for calibration measurement, star for recalibration measurement. Sensor 4054; red lines, x for calibration measurement, + for recalibration measurement. Sensor 4055; green lines, v for calibration measurement, ^ for recalibration measurement. Sensor 4056; pink lines, square for calibration measurement, diamond for recalibration measurement.

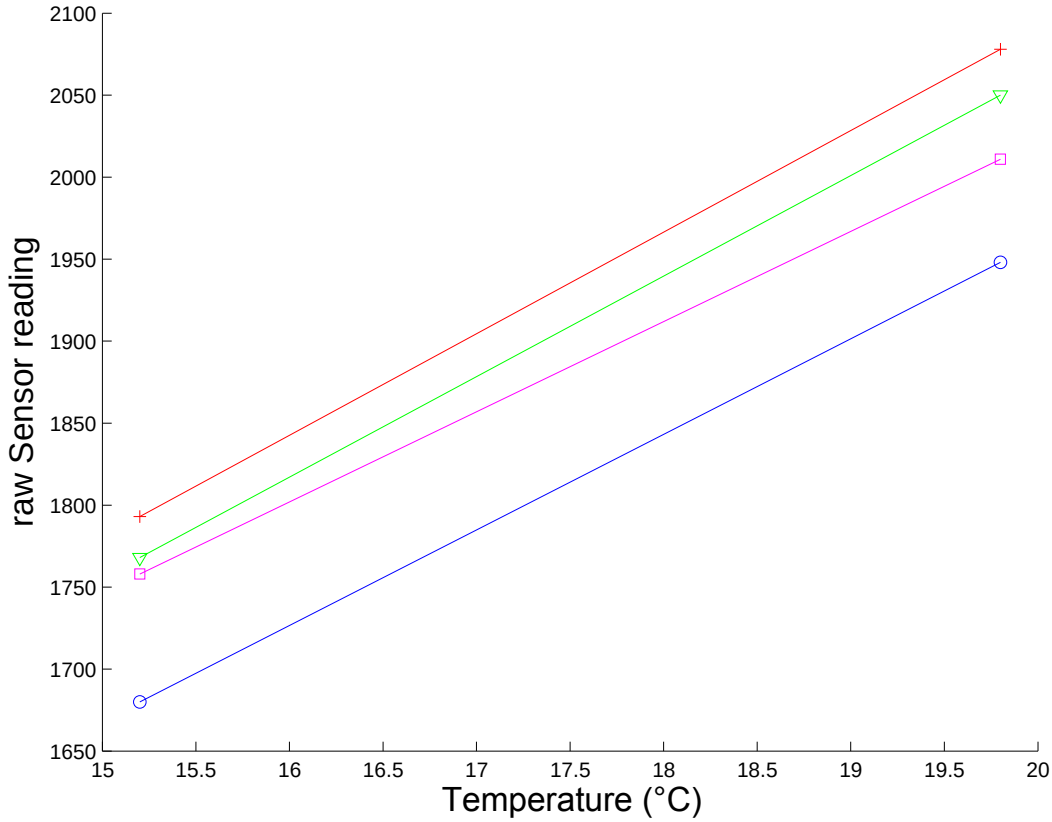

Figure 4.10: Example results of a calibration (solid lines) for temperature. Sensor 4053; blue line, circle for calibration measurement. Sensor 4054; red line, + for calibration measurement. Sensor 4055; green line, v for calibration measurement. Sensor 4056; pink line, square for calibration measurement.

4.3 Transect/Survey

Repeated boat surveys were also undertaken. These surveys involved repeated surveys of the area around the wharf with a boat mounted ADCP (RDI 1200kHz workhorse, sampling at 1200kHz, with depth bins of 0.25m, from 0.6 meters below surface to bottom, Figure 4.11) to capture 3 components of velocity. Boat motion was measured by GPS and removed from measurements within the RDI processing software. Water column stratifications were also observed using a seabird 19plus V 2.1 Conductivity-Temperature-Depth (CTD, Figure 4.12) profiler (serial number 6165). Salinity can then be calculated from conductivity using an algorithm pre-programmed into the Seabird software.

Figure 4.11: Julia Mullarney is disassembling the RDI ADCP workhorse after a day in the field (photo credit: Nadine Brunschwiler).

Typically a circuit system was followed consisting of both across and along channel transects (Figure 4.13). Each across channel (EW) transect was conducted twice; once with just ADCP sampling and the across channel section was repeated with stops for CTD casts. Three CTD casts were carried out per transect, east, middle, and west. The transects were named A, B, C, and D, the western most being A. Following this labelling structure the CTD drop locations were called A1, A2, A3, etc, see Figure 4.14.

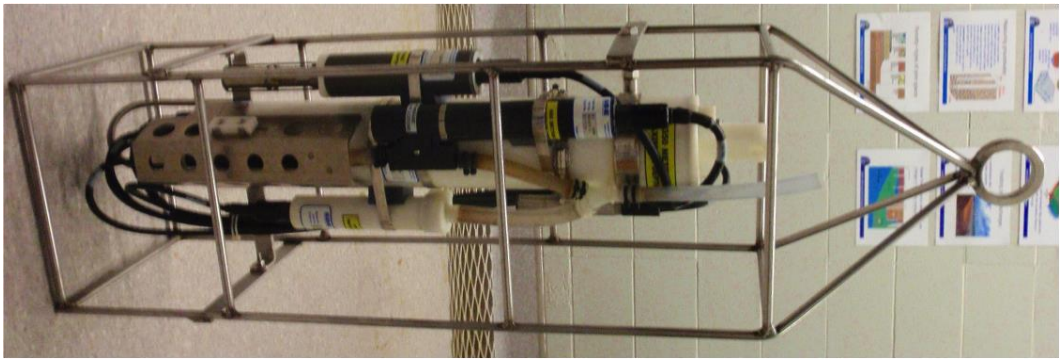

Figure 4.12: Seabird Electronics CTD (photo credit: Nadine Brunschwiler).

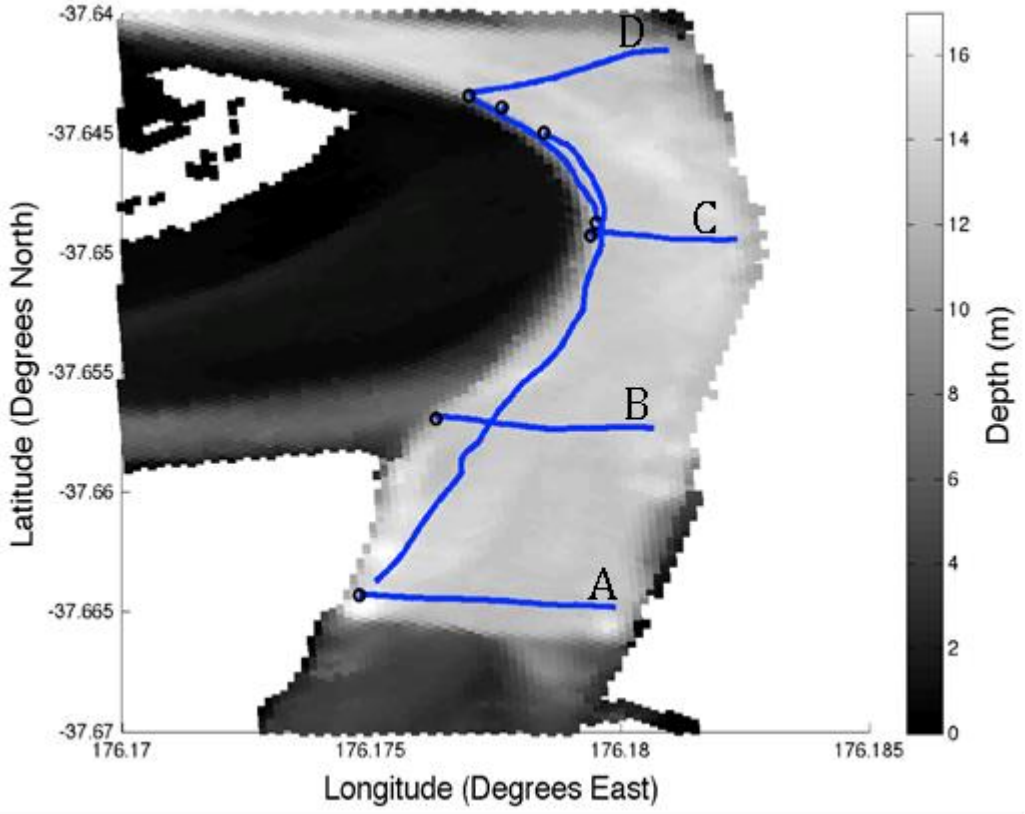

Figure 4.13: Example map of ADCP transects from 19 November 2013, letters A to D represent transect labelling used throughout the Thesis.

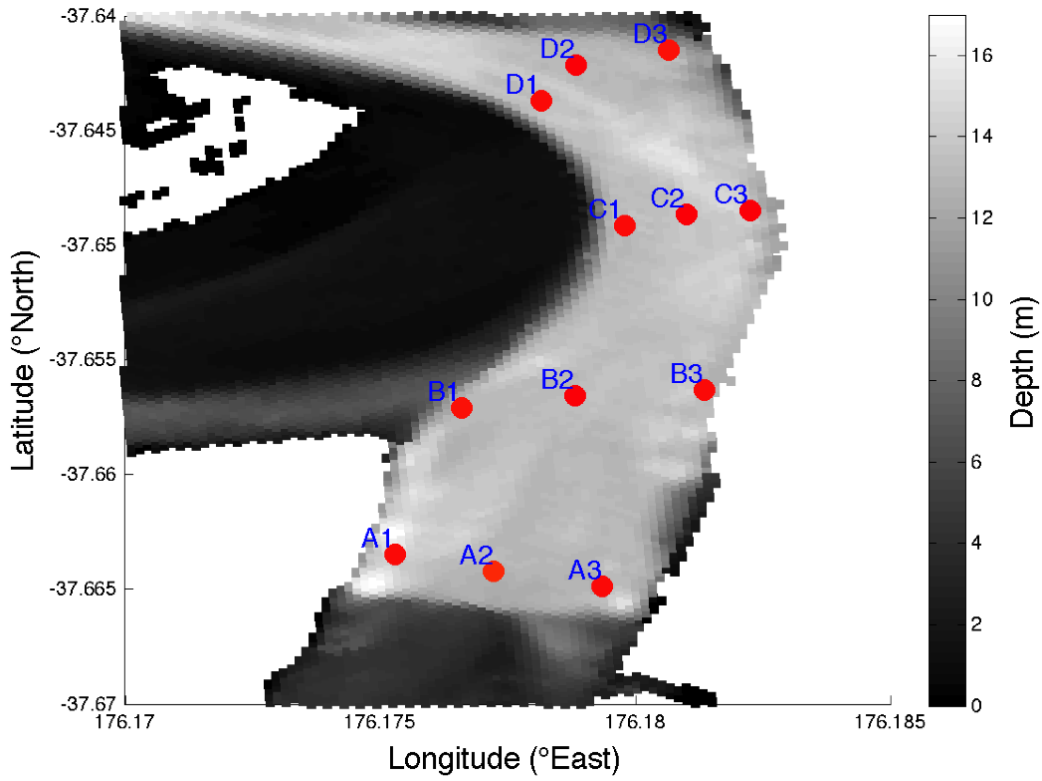

Figure 4.14: CTD drop locations and labels for the cross channel transects.

Multiple surveys were undertaken as defined below.

4.3.1 Preliminary survey (24th September 2013)

A preliminary survey was carried out on the 24th September 2013 to familiarize with field procedures and gain an idea of how well the stormwater runoff plume can be detected with the proposed instrumentation of CTD and ADCP.
On this preliminary test the transect rotation had not been set and the boat was driven around/through different sections of the plume.

4.3.2 Dry survey (19th November 2013)

A dry survey of the field site was carried out on the 19th November 2013. This survey was necessary to gain some insight into currents under 'non-discharge' conditions which allows for comparison of the stratification of the water column between these background and rainy conditions. Circuits were carried out over a full tidal cycle.
Figure 4.13 shows the four transects across the channel that were used at the field site during the dry survey. On the most estuarine/western transect (A) four CTD casts were taken on each round and on the other three transects three casts were taken. With the time it took to do this we were able to compile seven circuits of the field site within one tidal cycle.
The procedure was as followed:

- Across channel ADCP transect, repeat of across channel transect while 3 or 4 CTD casts were taken at specific locations
- Take along channel ADCP transect measurements between across channel transects
- Take along channel ADCP transect measurement on the far side on the way down to transect A

4.3.3 Wet survey 1 (17th April 2014)

The transects established for the dry survey were followed closely with the key difference that the link along-channel ADCP transects were taken on the wharf

side of the channel. This change was implemented in order to catch the plume output from the pipes along the wharf. A second change was going from 4 CTD casts on transect A (dry survey) to only three on all across channel transects.
Time and man power allowed for six circuits on that day. As the weather cleared up later in the afternoon we managed to get measurements of how fast the plume disperses once rain and discharges reduced significantly.

4.3.4 Wet survey 2 (12th July 2014)

On the second day for wet survey we replicated the procedure form the first wet survey exactly.
Due to lack of man power and difficult weather conditions we only managed to measure four circuits. Visual observations indicated that the first two circuits were conducted before the discharge created a significant plume output through the pipes from the port.

4.4 Summary

- The field site is located in Tauranga Harbour in the Cutter Channel and Stella Passage.
- A long time series deployment was undertaken for background current velocities and backscatter.
- Long CT time series were taken to cover a wide range of weather conditions.
- Two wet surveys provide the main plume data collected for analysis.

Chapter Five

Results

5.1 Environment

The environmental data was collected and provided by the Port of Tauranga and is shown in Figure 5.1. The environmental data consisted of metrological data (rainfall in mm, wind speed in km/hr and wind direction) from a weather station located at the port, and water temperature in °C (Figure 5.1) from ADCP set up in Entrance channel. Wind speed and direction are an average of 12 values every minute. Rainfall records are cumulative rainfall every minute.

The main wind direction is west-southwest and typical wind speeds are between 5 and 15 km/h. For the water temperature in Figure 5.1 values where T equalled 0 °C were removed.

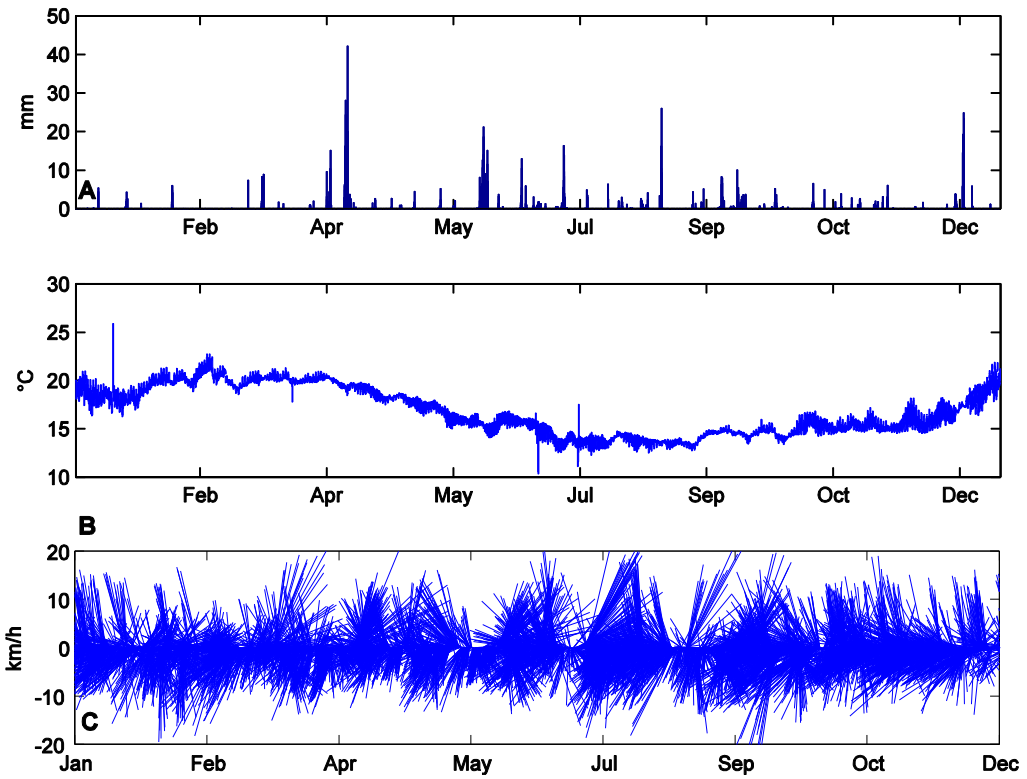

Figure 5.1: Weather data for 2014. A: hourly rainfall in mm, B: water temperature in °Celsius, C: wind speed in km/h.

5.2 Fixed Deployment

The fixed instruments were deployed from 10th April 2014 (yearday 101) to 8th May 2014 (yearday 123). Chapter 4 provides details of the deployments including sampling regimes and data processing.

5.2.1 ADP

The ADP was deployed in the Channel, Figure 4.1, which shows deployment locations). The tidal amplitude for this location is about 1 meter from the amplitude of the main tidal constituents, Table 5.1. Figure 5.2A shows a clear tidal signal in the pressure measurements. There is also a semi-diurnal signal in the temperature superimposed onto a steady decrease (Figure 1.2B). Figure 5.3 shows the heading pitch and roll, which indicates some small movements (tilting of a few degrees) during the first half of the deployment period until around yearday 111, after which the instrument appears to have stabilized. However, the instrument software applies a correction for these tilts when applying the internal rotation to transform from measurements in beam coordinates to Earth coordinates so the effect of these changes have been compensated for. Applying t_tide (Pawlowicz *et al.*, 2002) in MATLAB to the data after removing the noisy data at the beginning reveals that the main tidal constituents are M2, N2, S2, O2, K2, MKS2, LDA, and L2. The dominant directions are east-west, maximal velocities are 6.38 m/s and the velocity magnitudes are relatively depth-uniform (Figure 5.5 D). Table 5.1 lists the constituents with their frequency and amplitude. The main tidal constituents (M2, N2, and S2) combined amplitude amounts to about 1 meter.

Table 5.1: Significant tidal constituents (Tide) and their frequency and amplitude for ADP record. Extra columns show amplitude error, phase, phase error, and signal to noise ratio.

Tide	frequency	amplitude	amp_err	pha	pha_err	snr
*2Q1	0.0357064	0.1761	0.117	156.66	40.25	2.3
*N2	0.0789992	0.2087	0.092	126.4	27.36	5.1
*M2	0.0805114	0.6213	0.093	91.34	8.84	45
*S2	0.0833333	0.2149	0.092	307.04	25.32	5.5
*MO3	0.1192421	0.1073	0.057	173.4	34.41	3.5
*M3	0.1207671	0.1018	0.071	348.82	37.89	2
*MK3	0.1222921	0.102	0.065	171.87	38.91	2.5
*SK3	0.1251141	0.1302	0.066	161.54	27.99	3.9
*2MK5	0.2028035	0.0537	0.023	222.34	26.88	5.6
*2SK5	0.2084474	0.0593	0.027	218.7	29.38	4.8
*3MK7	0.2833149	0.0459	0.014	352.96	14.37	11
*M8	0.3220456	0.0532	0.006	203.47	6.3	84

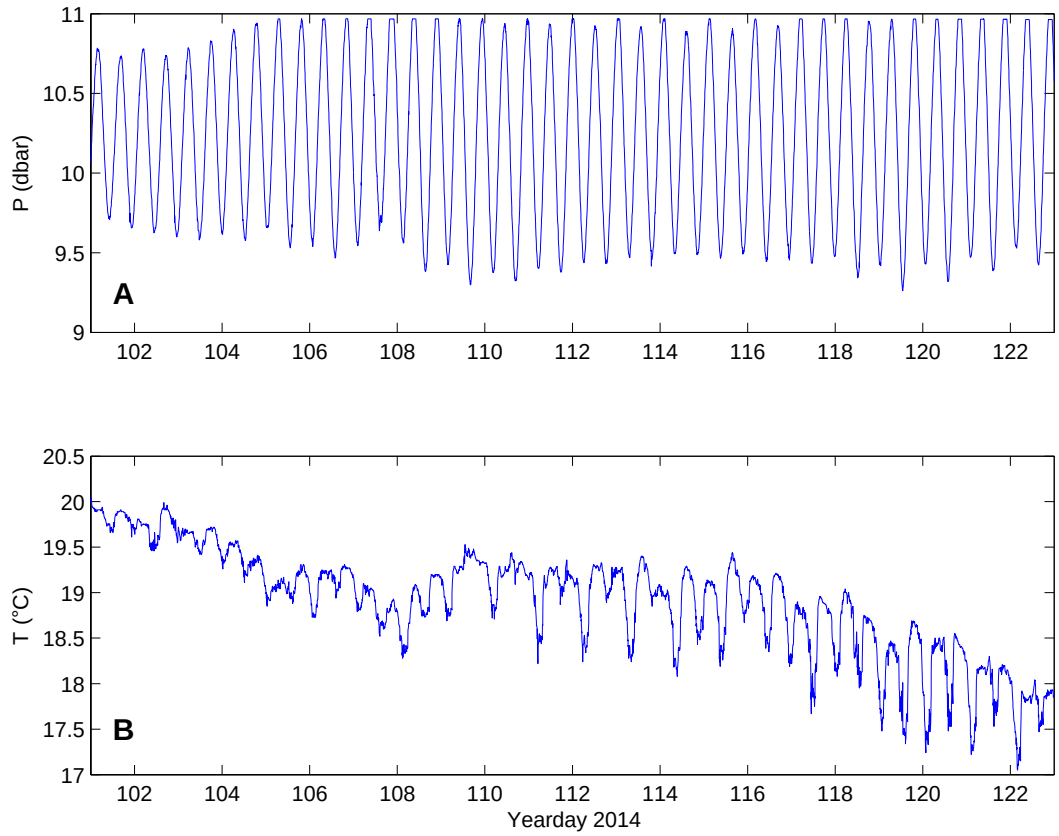

Figure 5.2: ADP pressure (A) and Temperature (B) measurements.

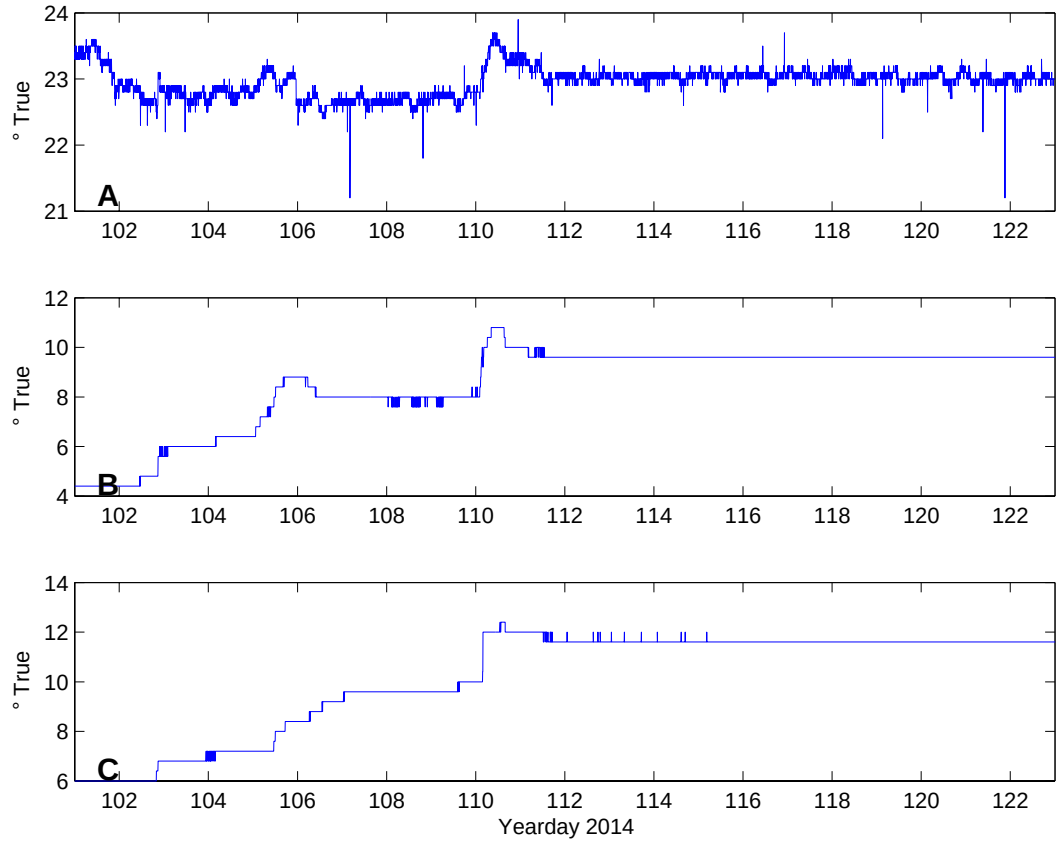

Figure 5.3: ADP instrument information, including heading (A), pitch (B), and roll (C).

Figure 5.4 depicts the backscatter for the three beams of the ADP. There are some periods of very low backscatter (close to zero counts around yearday 110, yearday 113, yearday 116, and yearday 120). These periods are likely owing to the sensors being covered with seaweed or algae and these times have subsequently been removed from the velocity data. Figure 5.5 shows the velocities from the ADP. Although the profile does not cover the full water column, the velocities are close to depth-uniform throughout the profile length (as to be expected in such an energetic region) and dominated by tide.

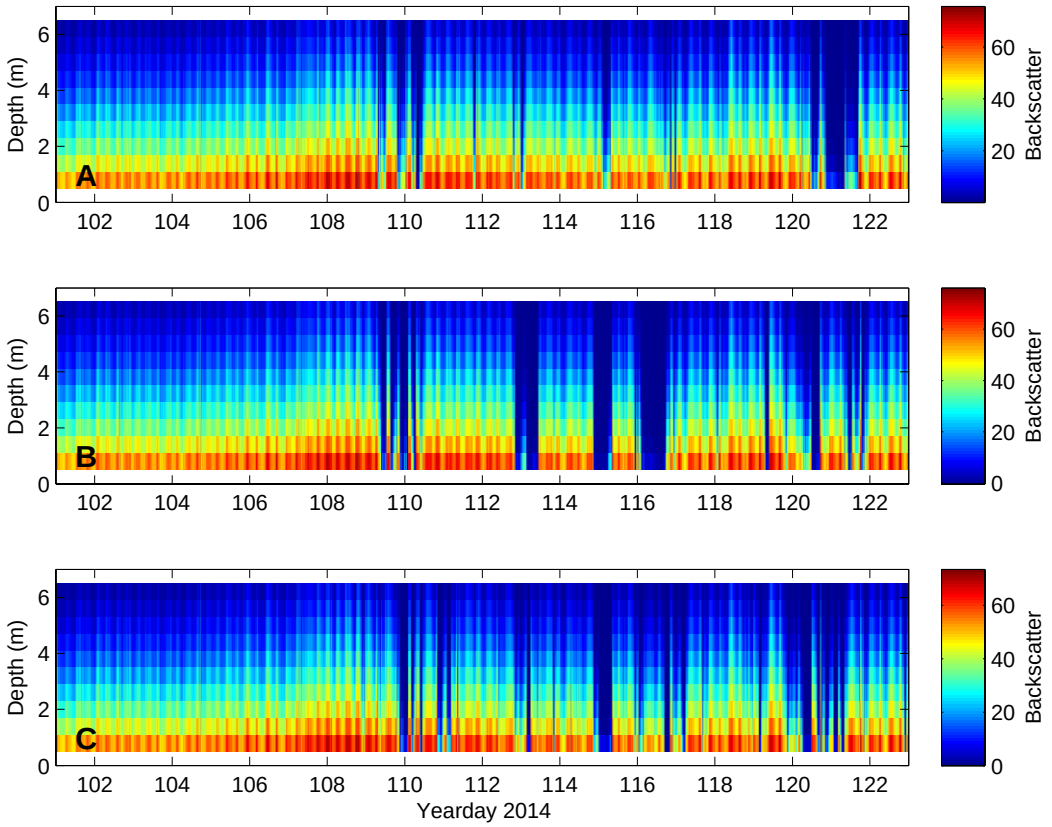

Figure 5.4: Backscatter data for the three beams of the ADP; A: beam one, B: beam two, C: beam three. Where the backscatter was low all the way through the profile the respective beams were most likely covered by something. The white strip at the bottom of the column is due to blanking distance, instrument cannot measure right from instrument surface. The top white strip is due to instrument being deployed in water depth deeper than the maximum instrument profile length.

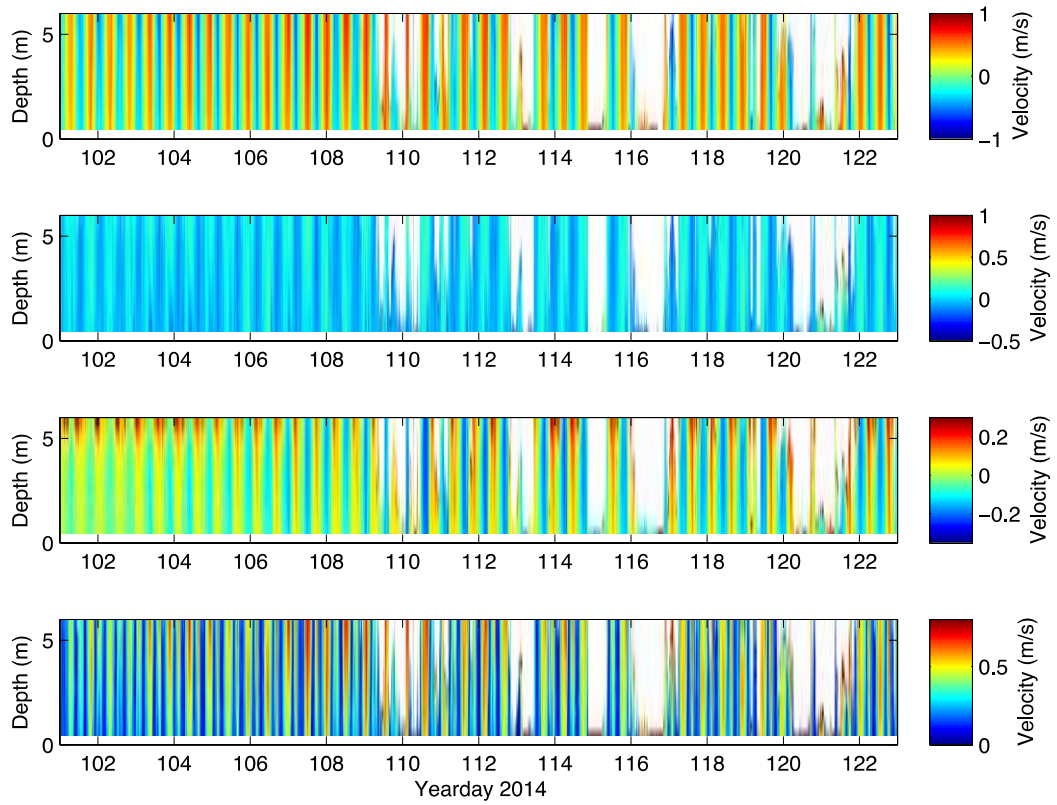

Figure 5.5: Velocity data for the three beams of the ADP; A: north-south, B: east-west, C: vertical, D: horizontal velocity magnitudes. White spaces over the column correspond to removed data due to fouling. The white strip at the bottom of the column is due to blanking distance, instrument cannot measure right from instrument surface.

5.2.2 ADV

Three ADVs were deployed in the main channel (Figure 4.1). From here on out the instruments will be referred to as ADV1 (R259), ADV2 (R252), and ADV3 (R228) with the numbers increasing from North (ADV1) to South (ADV3). The colour coding in the following ADV figures is as follows: ADV1 is the solid red line, ADV2 is the dotted blue line, and ADV3 is the dash-dot green line. Refer to Table 4.2 for deployment locations and depths.

Figure 5.6 shows the temperature and pressure measurements from the ADVs. The temperature sensor for ADV3 malfunctioned. The pressure sensors in all three ADVs recorded the tidal signal in respect to their deployment water depth. The temperature varies with the tide. The temperature is high during ebb tide and low during flood tide. The temperature seems to be similar at both locations. Only the high temperatures measured by ADV2 are a bit higher which could be

attributed to it being further up the estuary. Heading, pitch, and roll for the three ADVs (not shown) indicate the instruments remained close to stationary throughout the deployment (with the exception of small movements ~2 degrees) on ADV3 between year day 106 and 112 coordinates. According to the measured velocities in Figure 5.7 the north-ward component is strongest in location 6 (up to 1.07 m/s). As this is located in the Cutter Channel it can be expected as the Cutter Channel points east-west. The east-ward component is smaller in location 7 (about 0.86 m/s) and it is dominantly west velocities in location 5 (0.453 m/s). Panel C in Figure 5.7 shows the up/down velocities and it seems there is down-welling in location 5. As location 7 (ADV3) is far up in Stella Passage the dominant direction is expected to be north-south.

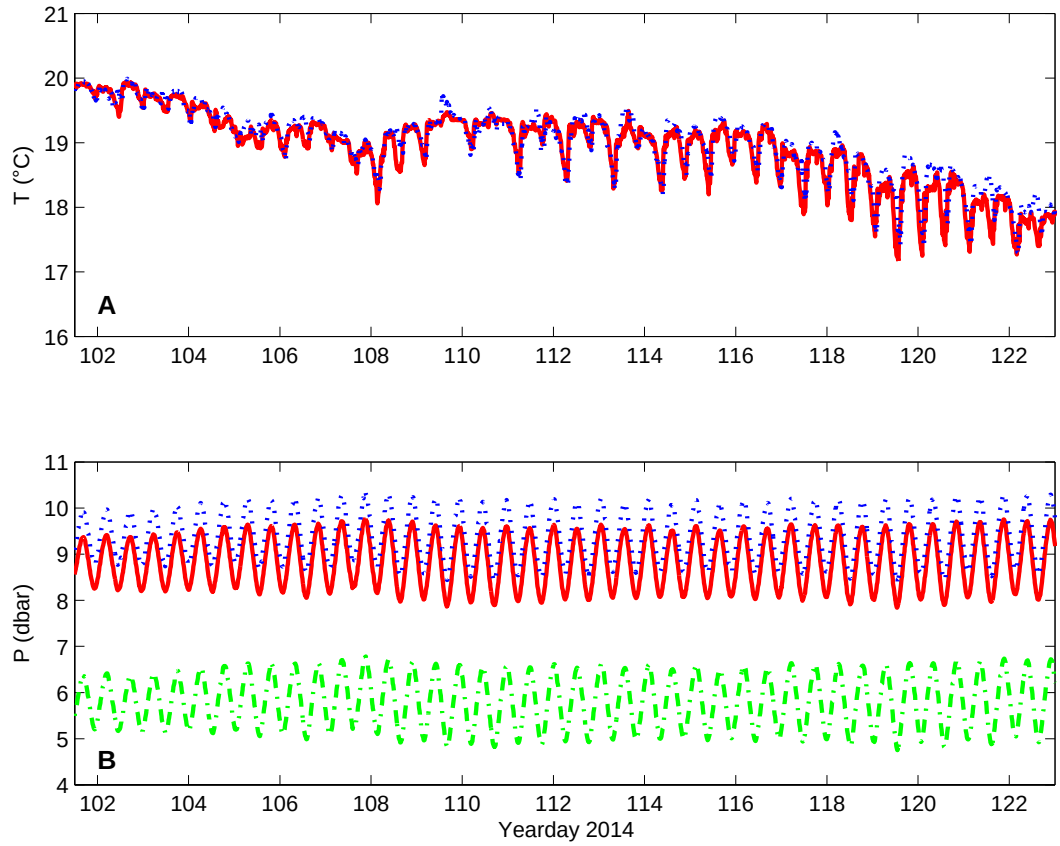

Figure 5.6: Temperature (A) and pressure (B) measurements of the three ADVs. Red (---) for ADV1, blue (....) for ADV2, green (-.-.-.) for ADV3. Note there is no ADV3 temperature measurement as the sensor malfunctioned.

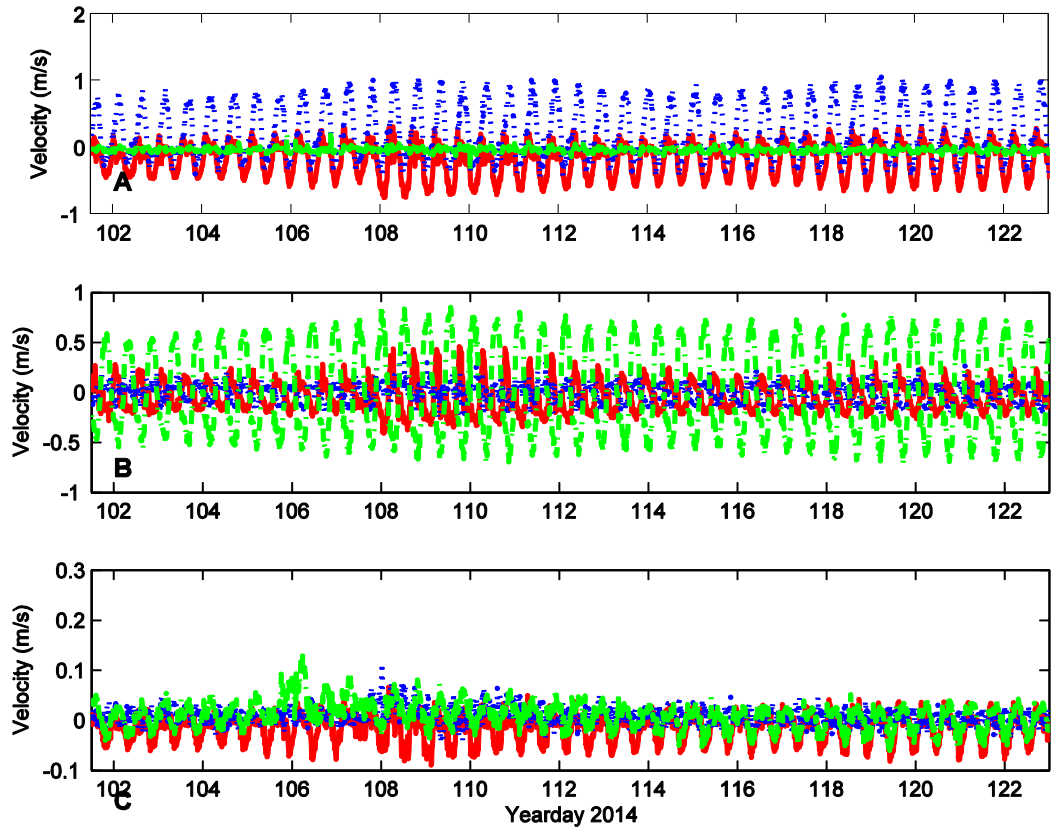

Figure 5.7: Velocities in m/s for the three ADVS. A: north-south velocities, B: east-west velocities, C: up-down velocities. Red (---) for ADV1, blue (....) for ADV2, green (-.-.-.) for ADV3.

5.2.3 Nortek Aquadopp

The aquadopp is located in Stella Passage (Figure 4.1). In Figure 5.8 a clear tidal signal can be seen both in the pressure data and the temperature data. The temperature shows the same steady decrease as the temperature measured by the ADP (Figure 5.2). It also shows the same temperature tidal stage relationship; high temperatures during low tide, and low temperatures during high tides.

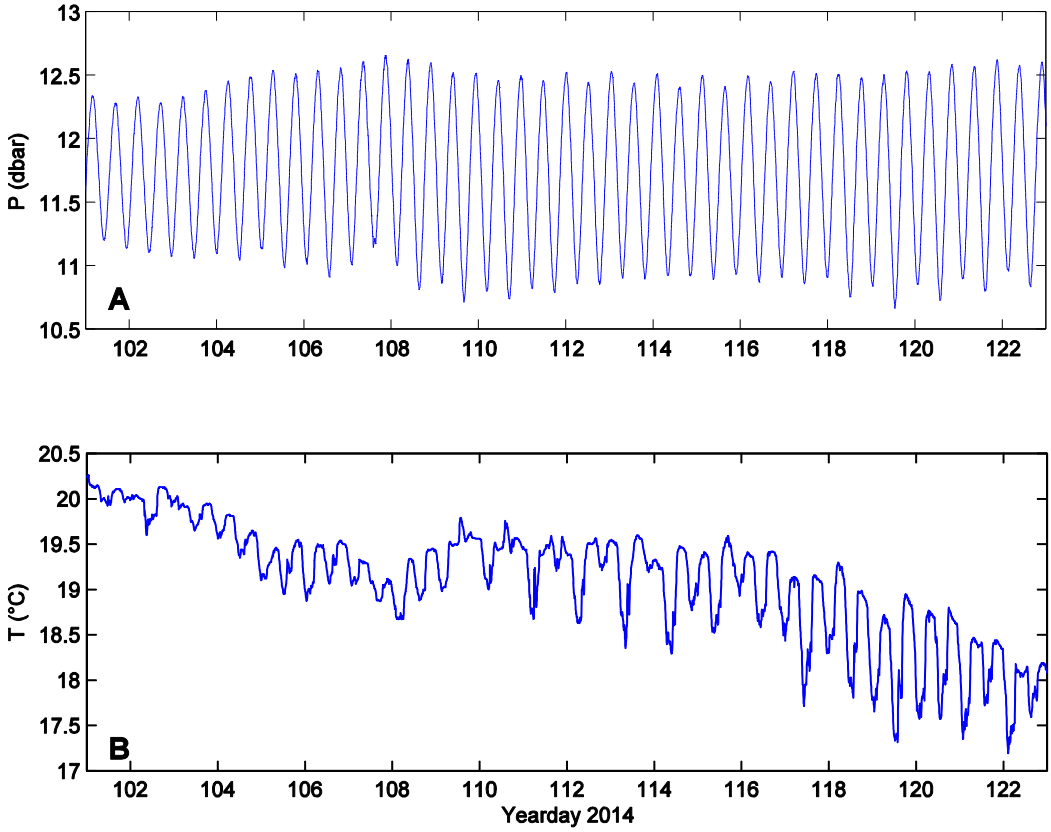

Figure 5.8: Aquadopp pressure (A) and temperature (B), from the Centre Bank side of Stella Passage, opposite the Mount Maunganui wharf.

The heading, pitch, and roll data, not shown, indicate that the instrument was steady for most of the deployment period. The heading changed slightly on the last three days of the deployment.

The backscatter data shows an increased backscatter signal around yearday 107 (Figure 5.9). Yearday 107 corresponds to 17th April 2014, our first wet survey days and thus a rain event. Figure 1.1 also shows this constituted the first large rain event of the year, possibly washing significant particulate matter into the harbour. Around this time we see a noticeable increase in backscatter throughout the water column.

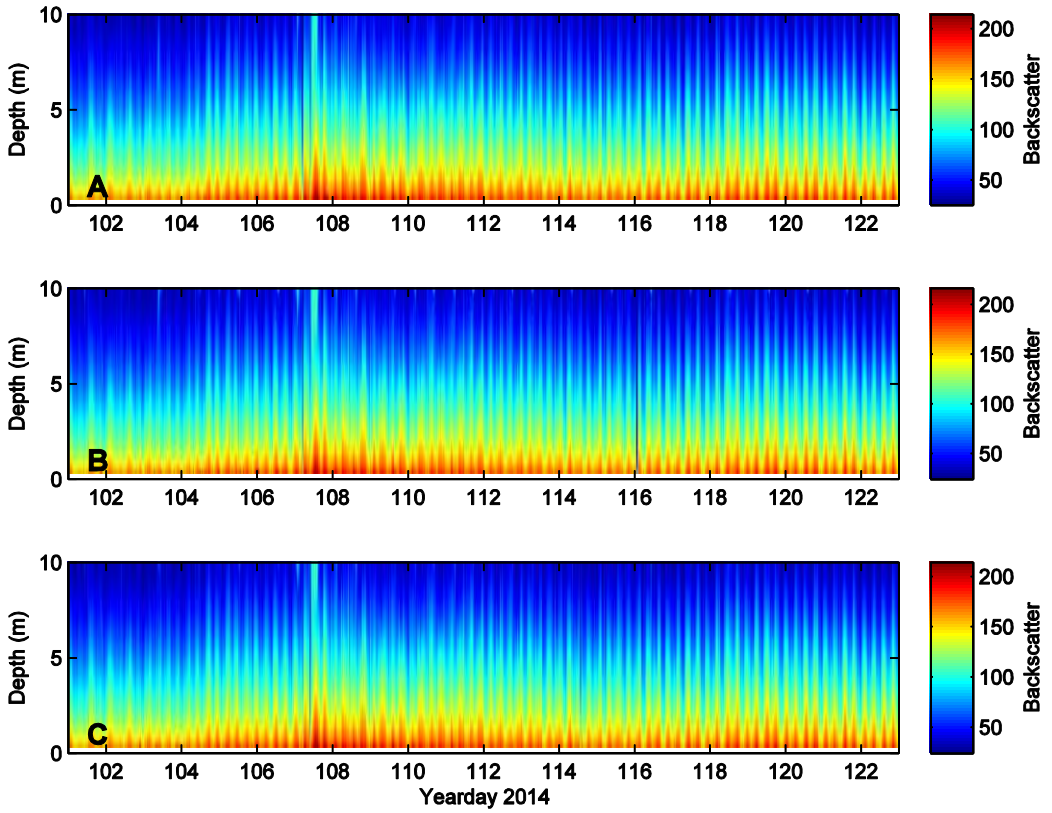

Figure 5.9: Backscatter from the three different beams of the Aquadopp. A: beam one, B: beam two, C: beam three.

The velocity plot in Figure 5.10 shows clearly that the Aquadopp measured the tidal velocities. There vertical velocities are predominantly downwards, indicating a down slope component to the flow, which is consistent with the instrument positioning at this location. The instrument was deployed too deep and was not able to capture surface velocities and backscatter in the top 1-2 m of the water column. In Figure 5.10D we can observe a slight shear in horizontal velocities during the high tide. Even though the plume was observed to occasionally reach this location (discolouration of the surface water here was visible during the boat surveys), there is no sign of changes in backscatter and velocities during the rain events, thus indicating that any effects of the plume on circulation within the harbour were at the very least confined to the top of the water column at this distance from the source. There is almost no vertical structure as backscatter signal would get lower with increasing distance from the instrument. Even though the backscatter shows a change during the April rain event, the velocities do not show any different behaviour during this time.

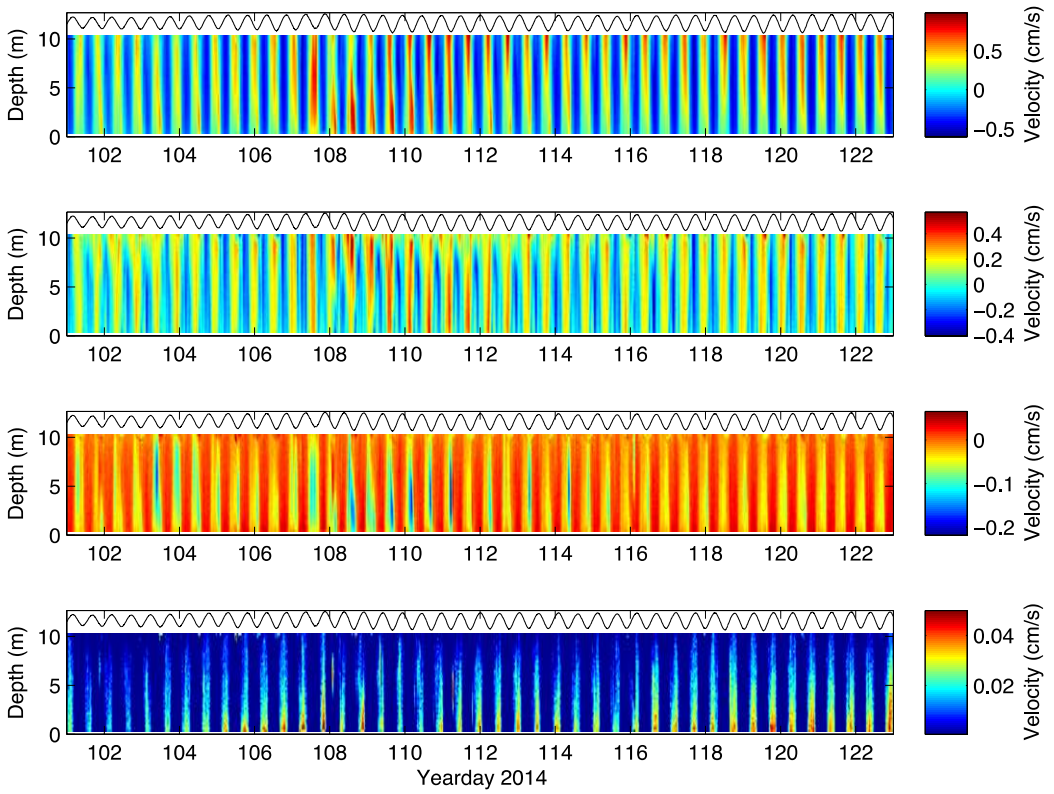

Figure 5.10: Aquadopp measured velocities with pressure measurements on top to compare to tidal stage. A: north-south velocities, B: east-west velocities, C: vertical velocities, D: horizontal velocity magnitudes.

5.2.4 S4

The S4 data output from the software provided 10 measurement points every 10 minutes. It was not possible to obtain higher resolution data owing to computer memory constraints. The program did not provide a date vector, only a time vector therefore a date vector for each file was created in excel.

Figure 5.11 shows the current directions and speed for the three S4s on 17th April 2014 (a wet survey day) and on 27th April 2014 as a non-rain control day. Comparing the dominant wind direction during the 17th April storm and the normal condition winds (Figure 5.11 G and H) shows that during the storm the wind direction changed completely from dominantly east-west during calm to exclusively north-east. Also the wind speeds during calm days are up to 15 km/h and during the April 17th storm wind speeds reached up to 50 km/h.

The S4_1 in location 4 (Figure 5.11 C and D) shows that the currents during calm conditions (C) are predominantly north-west in accordance with channel direction,

the maximum current speed is about 0.70 m/s. During the storm (D) the currents are slightly stronger, up to 0.74 m/s and differ a lot in direction. The strong north-east current could possibly be attributed to wind waves as the fetch for this location is considerable.

S4_2 in location 3 (Figure 5.11 A and B) show similar patterns. During the calm conditions (B) the currents are small (up to 1m/s) and only along channel direction. During the storm (A) the currents are stronger (up to 6m/s) and go north-east and north-west. The north-east component could be explained by the dominant strong wind during the time and the considerable fetch.

S4_3 in location 2 (Figure 5.11 E and F) supports the previous findings. During the calm day (F) the currents are just in line with the channel in Stella Passage and of strength of about 0.8m/s. During the storm (E) the currents are still in line with the channel but they increase significantly in strength (up to 6m/s). The current direction does not change because at this location there is no fetch.

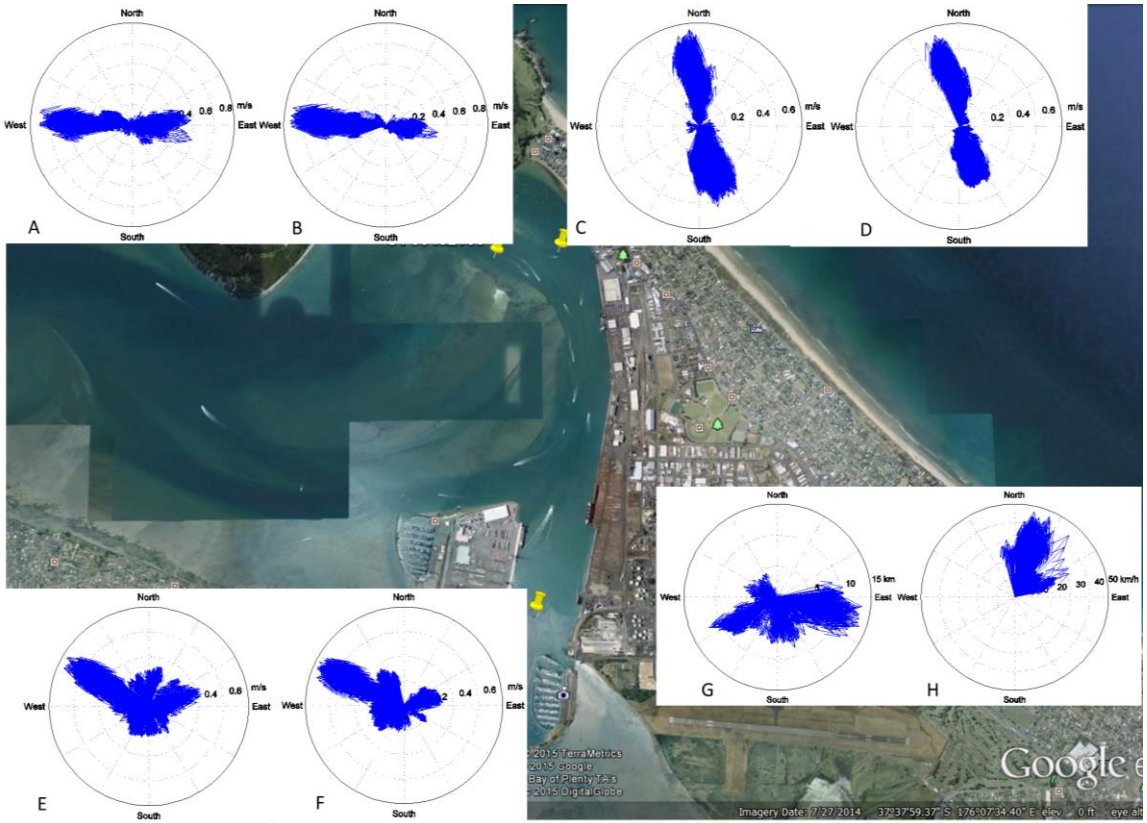

Figure 5.11: Current and wind directions and speed for the three S4s. A: S4_2 currents during storm conditions on 17th April 2014, B: S4_2 currents during calm conditions on 27th April. C: S4_1 currents during calm conditions on 27th April 2014, D: S4_1 currents during storm conditions on 17th April. E: S4_3 currents during storm conditions on 17th April 2014, F: S4_3 currents during calm conditions on 27th April. G: wind currents during calm conditions on 27th April 2014, H: wind currents during storm conditions on 17th April. Yellow pins on map show S4 locations. Underlying map (image credit: Google Earth).

5.3 CT sensors

The conductivity/temperature sensors were deployed over three separate deployments. I will discuss the results from each deployment period. The corresponding weather data (rain and wind) are plotted for each deployment period for ease of comparison and interpretation. All measurements have been converted from conductivity into salinity before plotting. Due to an issue with the calibration file inside the software provided by Odyssey, this conversion was carried out in MATLAB (instead of the download software). The deployment locations can be checked in Chapter 4 Table 4.3.

The salinity and temperature resolution of these CT sensors is not very good (Odyssey), however the sensors should give sufficient information to provide an overview of how the salinity changes under large rain events at varying locations.

For the deployment the sensors were deployed at one of two depths. The surface deployment was 20 cm under the water surface on floating buoys to keep the distance to the surface constant at all times. The deep deployment was at 2m. Occasionally, there was a problem with the surface deployment, in which the rope and buoy set up around the pylon did not slide up and down correctly and some of the sensors got stuck on the pylon out of the water. The data from these times manifests as unrealistic low values or short spikes, dropping to close to zero salinities.

5.3.1 Deployment 1 (4 June to 15 July 2014)

In Figure 5.12 we show the first set of salinity data from deployment 1. The salinity shows a semi-diurnal variation with the tidal signal. Immediately after deployment, there was a large rain event (8 to 15th June). As expected for a surface deployment, a subsequent drop in salinity is seen and this lower salinity persists for around 7 days (even accounting for variation with tides). Figure 5.13 shows a close up of that first rain event. Zooming in on the second rain event (Figure 5.14) again shows the surface rain signal. As this event was smaller (less rain) and the sensors came out a day later there is no information about the persistence of the signal.

(CT sensor 2827 was also deployed during this period but due to a corroded battery link no data was recorded.)

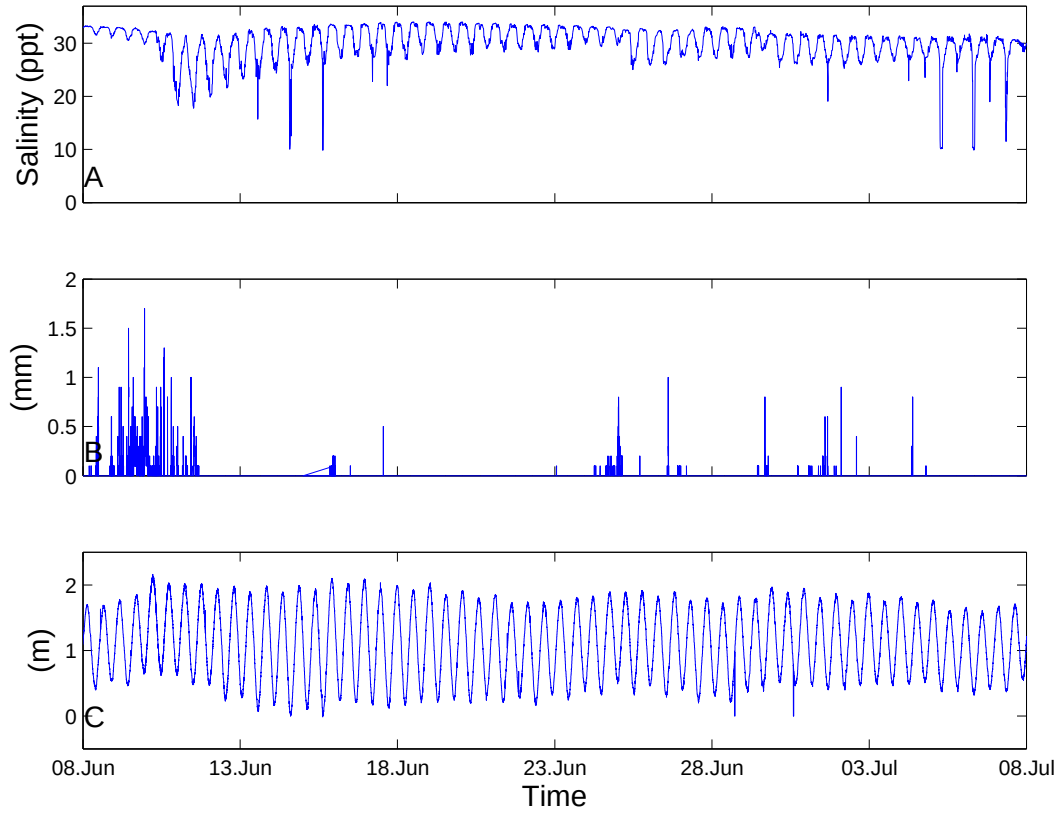

Figure 5.12: CT sensor 2882, July deployment at marker 13 near surface. A: salinity, B: hourly rain (mm), C: tide (m).

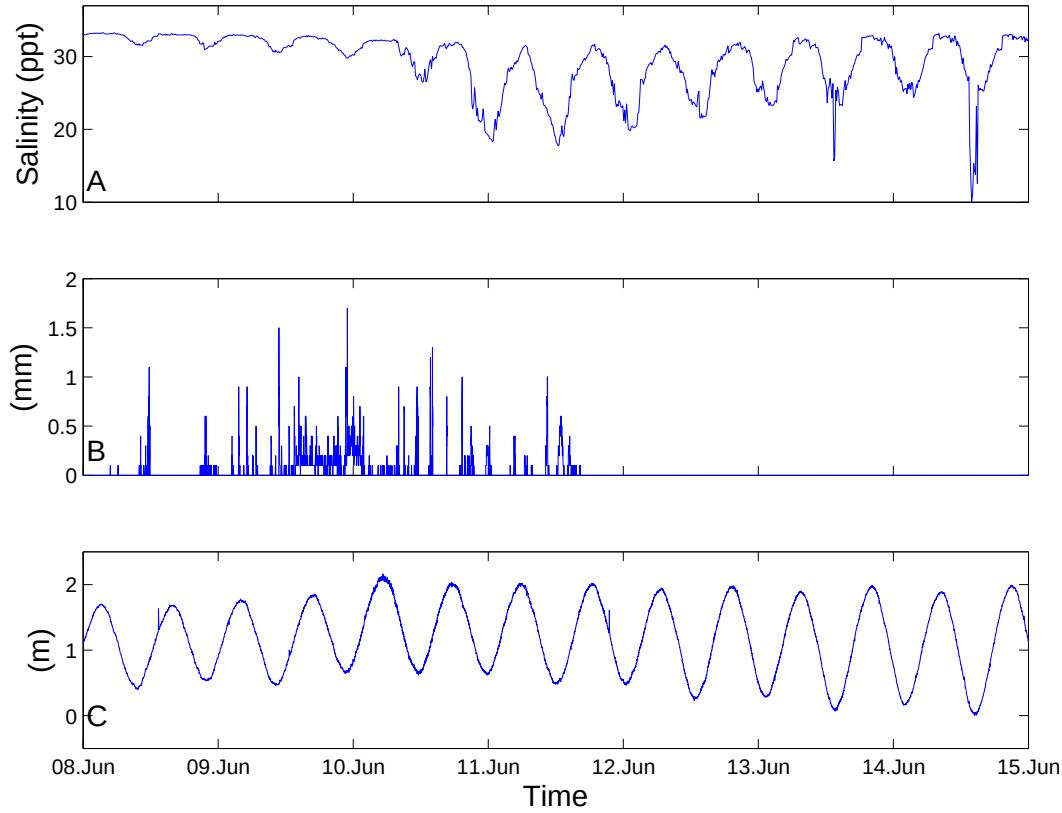

Figure 5.13: Zoom in on Figure 5.12 on the first rain event before June 13th. A: salinity, B: hourly rain (mm), C: tide (m).

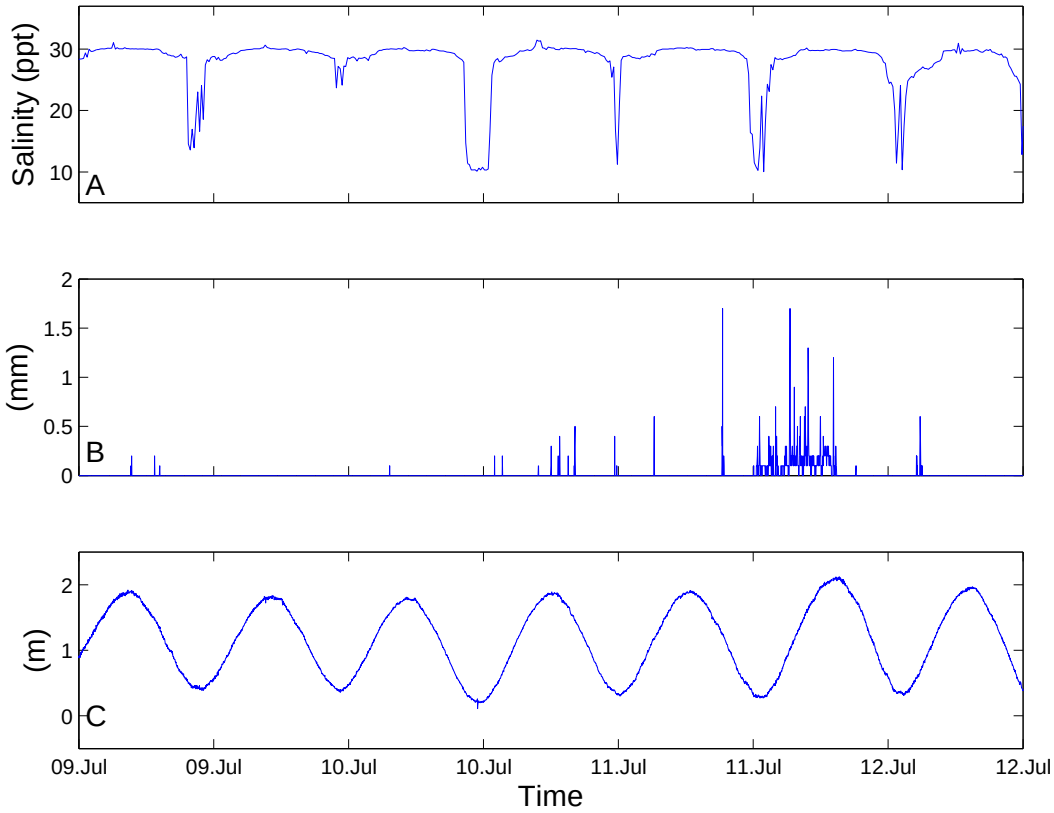

Figure 5.14: Zoom in on **Figure 5.12** on the second rain even on July 11th/12th which coincided with a wet survey. A: salinity, B: hourly rain (mm), C: tide (m).

Looking at the sensors in Figure 5.15 we see the freshening of the surface waters on all three sensors from the middle of the rain event onwards. The salinity slowly readjusts to before rain levels over the next four days. The signal has a delay time of about one day before it is picked up by the CT sensors. The recovery period seems to be a few days, the same as with CT2882 (Figure 5.13). The two times the salinity in Figure 5.15 B drops to below 10 is when the respective sensor was reported to be out of the water during low tide.

Figure 5.16 shows the second rain event of the deployment period and a similar response at the sensors is observed. However, there also exist two sharp changes in salinity in the sensor at 2 m depth under the wharf shortly after the start of each rain event (Figure 1.16B 10th June, around noon and Figure 1.17B 11th June around 3 am). These are likely associated with the freshwater output from the pipes directly discharging past the sensor and are consistent with the short lived nature of these spikes.

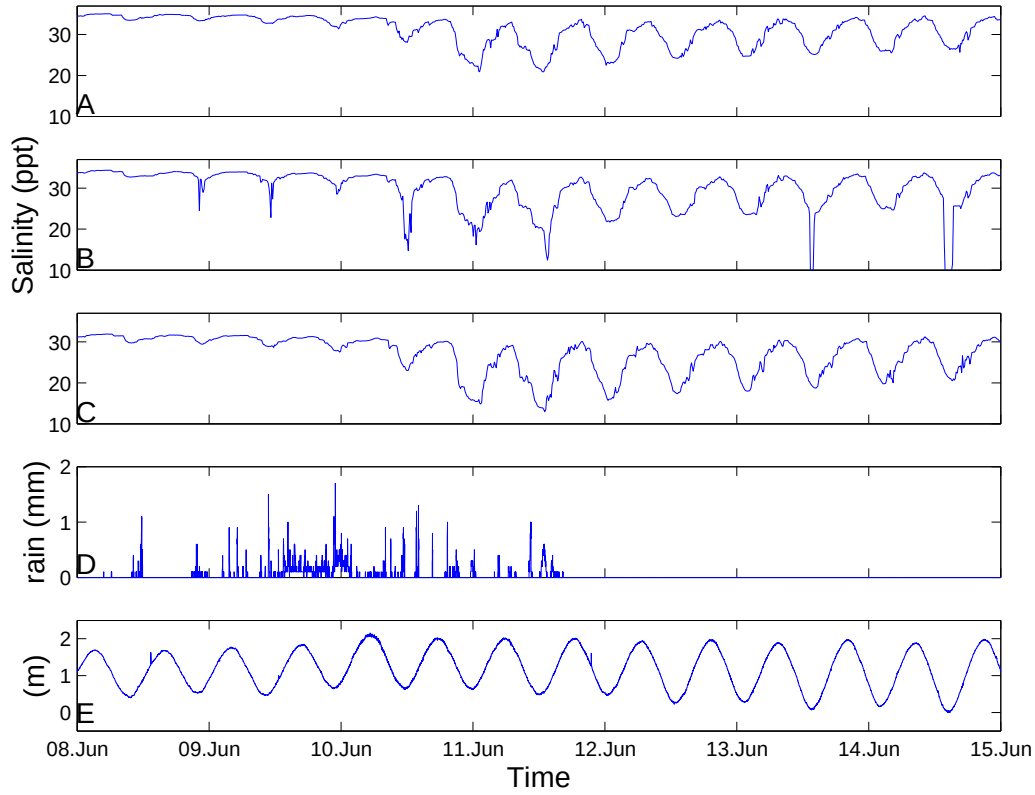

Figure 5.15: A: salinity for CT sensor 2828, outside wharf at surface, B: salinity for CT sensor 2829, under wharf at surface, C: salinity for CT sensor 4055, under wharf deep, D: hourly rain (mm), E: tide (m) during first rain event of deployment around June 10th 2014.

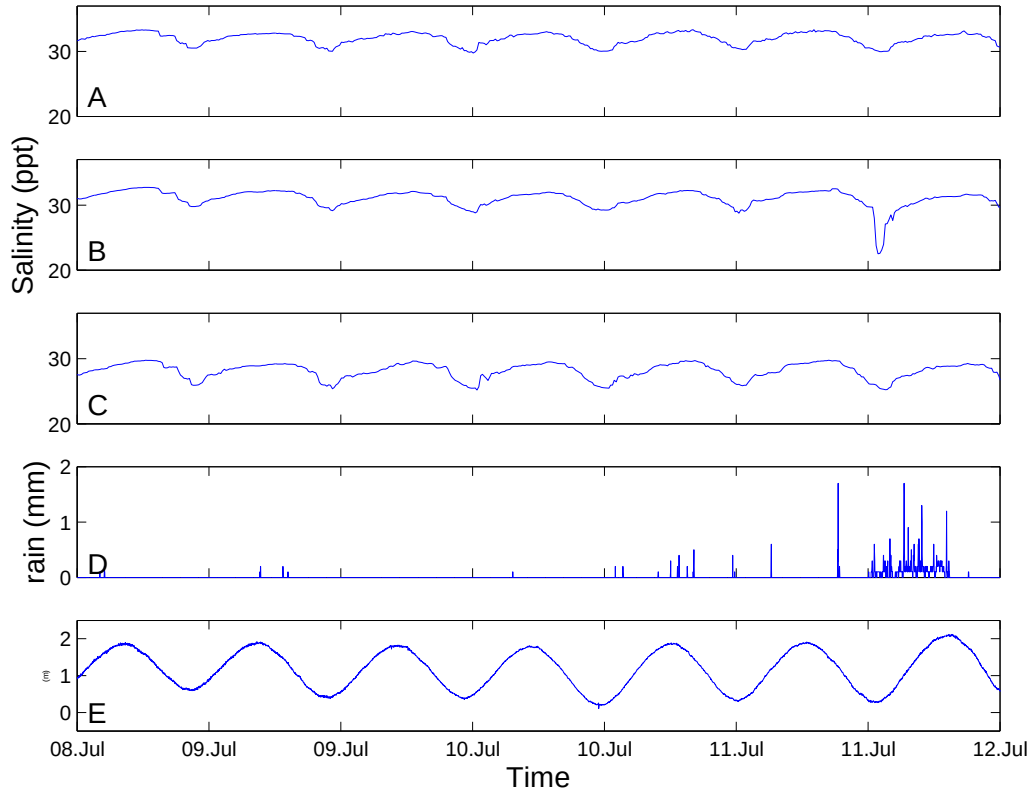

Figure 5.16: A: salinity for CT sensor 2828, outside wharf at surface, B: salinity for CT sensor 2829, under wharf at surface, C: salinity for CT sensor 4055, under wharf deep, D: hourly rain (mm), E: tide (m) during second rain event of deployment around July 11th 2014.

5.3.2 Deployment 2 (17 July to 12 September 2014)

During this deployment period seven sensors were put out but here we only show the data of four of them as the other sensors do not show any clear response to the rain signals. Figure 5.17 shows the salinity measured by the sensors that actually picked up on some of the rain events during the deployment period. There was a rain even before August 12 but none of the sensors show any change in salinity. For the rain event on August 17 all four sensors measured a small decrease in salinity. The signal is small but the delay time was shorter than a day (short in comparison to delays measured during deployment 2). The recovery period is about five to six days in all four sensors. A zoom in on the rain event (Figure 5.18) shows that all four sensors picked up on the surface rain.

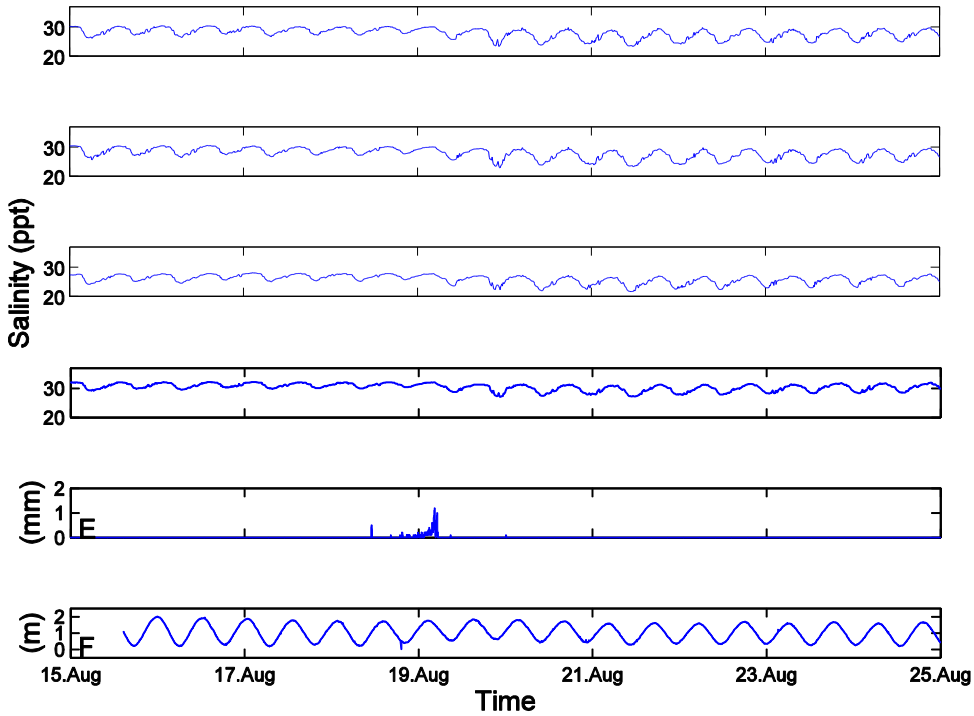

Figure 5.17: A: salinity for CT sensor 4056, Marker21 at surface, B: salinity for CT sensor 4054, Butters wharf at surface, C: salinity for CT sensor 4053, 'the Leaner' at surface, D: salinity for CT sensor 2830, Marker1 at surface, E: hourly rain (mm), F: tide (m), September 2014 deployment.

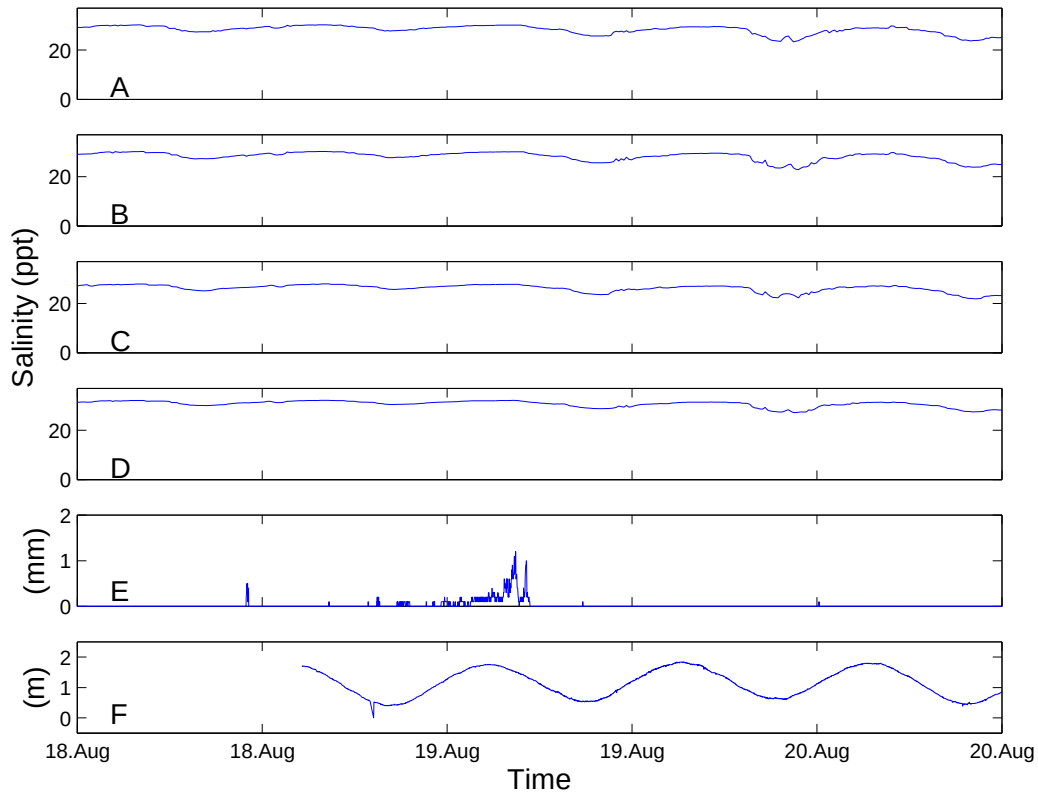

Figure 5.18: A zoom in on the rain event of August 19th 2014. A: salinity for CT sensor 4056, Marker21 at surface, B: salinity for CT sensor 4054, Butters wharf at surface, C: salinity for CT sensor 4053, 'the Leaner' at surface, D: salinity for CT sensor 2830, Marker1 at surface, E: hourly rain (mm), F: tide (m) September 2014 deployment.

5.3.3 Deployment 3 (27 December 2014 to 17 March 2015)

Figure 5.19 covers the last CT sensor deployment period over the summer 2014/15. Figure 5.19 D reveals that there was no rain event large enough to register on the sensors regardless of their position. In Figure 5.19 A the salinity data for sensor 2882, which was located outside the wharf at 20 cm depth, can be seen. All three sensors exhibit a tidal signal. The other variations that can be examined do not seem to correlate to the weather at all. The spikes in Figure 5.19 C are inexplicable as this sensor was deployed at a water depth of 2 meters and was thus well out of the danger of being stuck out of the water at low tide.

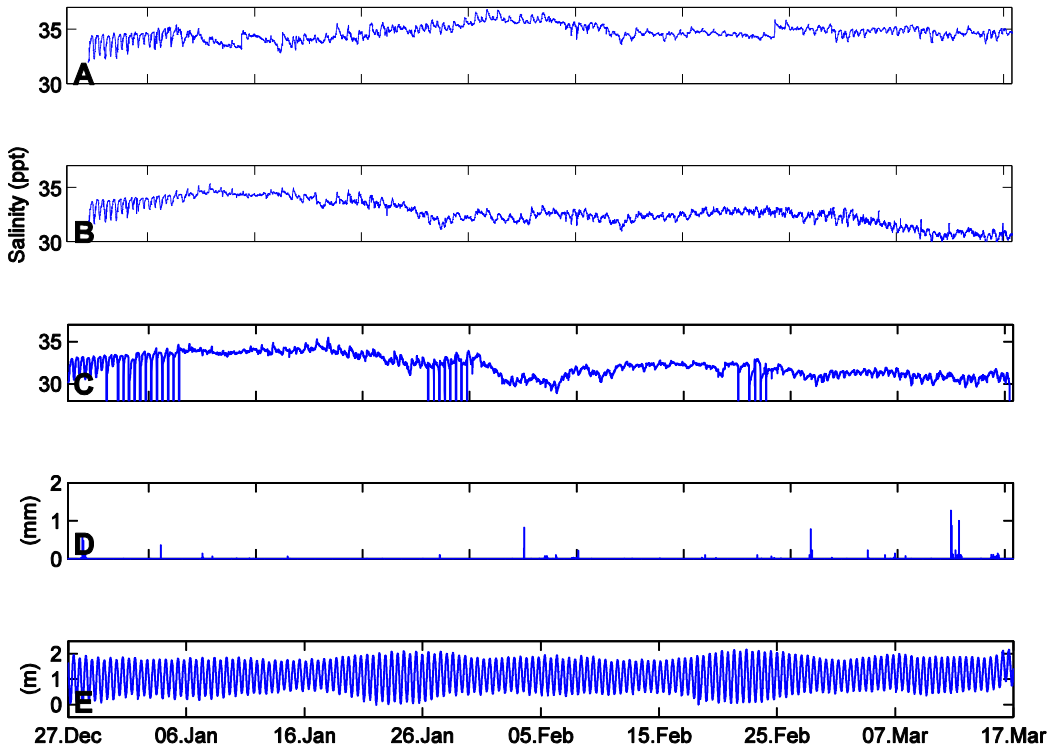

Figure 5.19: December 2014 to March 2015 deployment. A: salinity for CT sensor 2882 outside wharf at surface, B: salinity for CT sensor 2831 under wharf at surface, C: salinity for CT sensor 2830 outside wharf deep, D: hourly rain (mm), E: tide (m).

5.3.4 CT sensor summary

Given the similar response across all sensors, from the sensor under the wharf that was observed to be inside the plume (as seen by the discoloration of the water) and those that were not (the sensors located on the far side of Stella Passage), we can conclude that the plume did not have a strong salinity signal above that associated with rain input over most of the harbour (despite being initially freshwater) indicating that mixing occurred quickly. For the times when the sensors under the wharf appeared to discern the plume, the response was short-lived and the spike in lower salinity water disappeared within a tidal cycle.

5.4 Surveys

Figure 5.20 shows a schematic of the locations within the harbour at which the CTD casts were made. The letters A to D correspond to the ADCP transects established earlier. The numbers 1 to 3 refer to the three different drop locations

on each transect, with 1 corresponding to the west side of Stella Passage, 2 is in the centre and 3 is the cast on the eastern side of the passage. Later on I will discuss surface salinities at these locations.

Each circuit took about 90 to 100 minutes to complete including the two way ADCP and CTD transects in the across channel direction and some time to return directly to the starting point (i.e. from D3 to A1).

Figure 5.21 and Figure 5.22 show some example CTD casts from the survey on July 12th, which demonstrate that the variations in density are strongly controlled by variations in salinity and not temperature. Indeed, the temperature variations throughout the profiles are generally small (<0.5°Celsius over 15m water depth). Hence, for the remainder of this section I focus on the salinity measurements as these are the dynamically important variations.

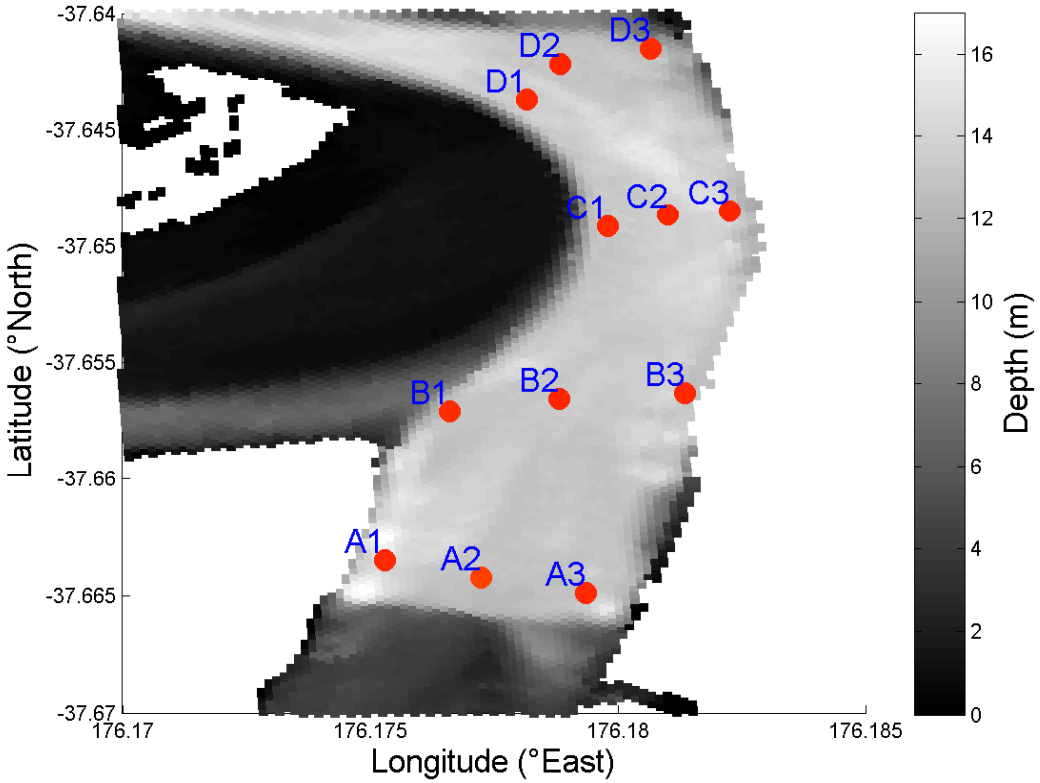

Figure 5.20: CTD cast location references. The grey scale depicts the bathymetry, solid white is land.

5.4.1 Calculations for ADCP and CTD

In order to create the surface data and the profile figures the raw data was processed as described below.

The ADCP backscatter for surface was averaged over top two meters of water depth (noting that due to transducer depth and positioning the top 0.6 meters were not measured at all). Then the first 6 bins were averaged to provide a measurement for the top 2 meters.

In the case of the CTD salinity surface plots also the top two meters were averaged. The operating procedure of the CTD requires that it is kept at the surface for one minute and so there are a lot of shallow measurements. A part of these measurements were removed prior to averaging in order to reduce bias. Only the points over which depth increased steadily were used for the surface average. For the salinity profiles the first few measurements were removed (same issue here with bias towards the top). Then the measurements were averaged over 20 cm depth bins as above.

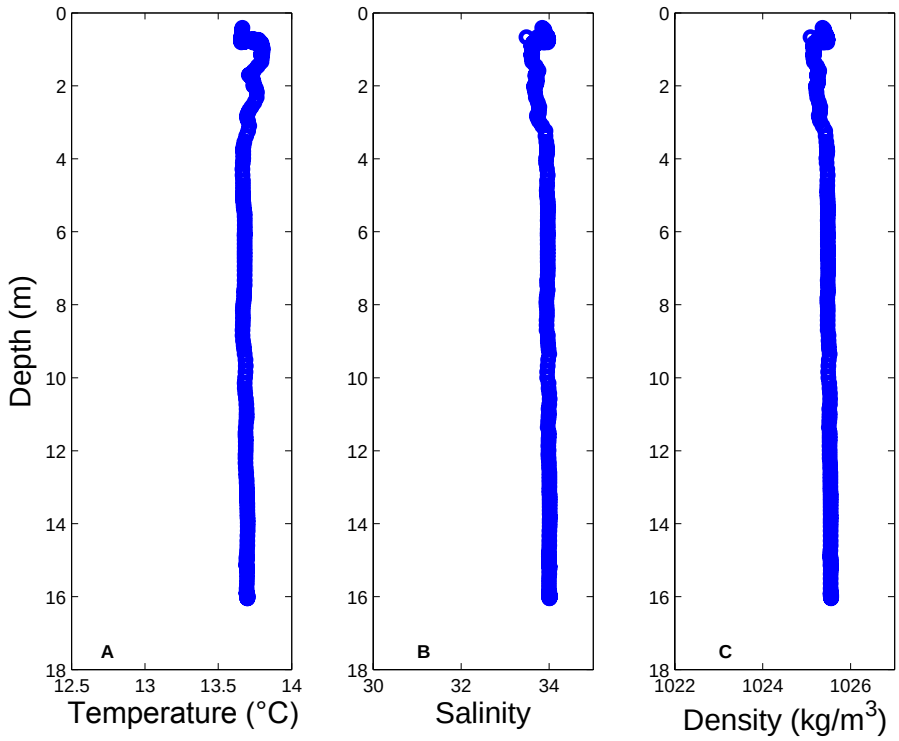

Figure 5.21 A: temperature, B: salinity, and C: density profiles at location B3 circuit 1. No plume was present as this cast was taken as the rain event started at 8.30 am on 12 July 2014.

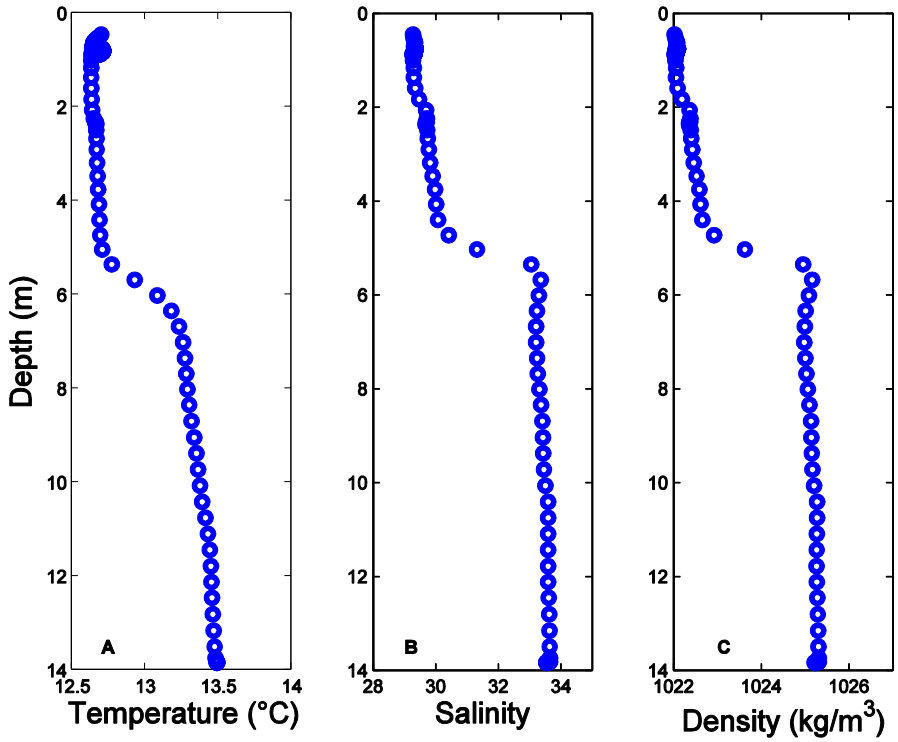

Figure 5.22 A: temperature, B: salinity, and C: density profiles at location B3 circuit 3. In plume at 1.40 pm on 12 July 2014.

5.4.2 Dry survey

Figure 5.23 shows the surface salinity measured with the CTD during the dry survey on 19th November 2013. The panels 1 to 7 correspond to the 7 circuits that were conducted over a 12 hour period. As it can be seen the surface salinity data, (obtained from the measured conductivity) the salinity is almost uniform over the course of the day. With the exception of some slight variations later in the day, especially panel 5 and 6.

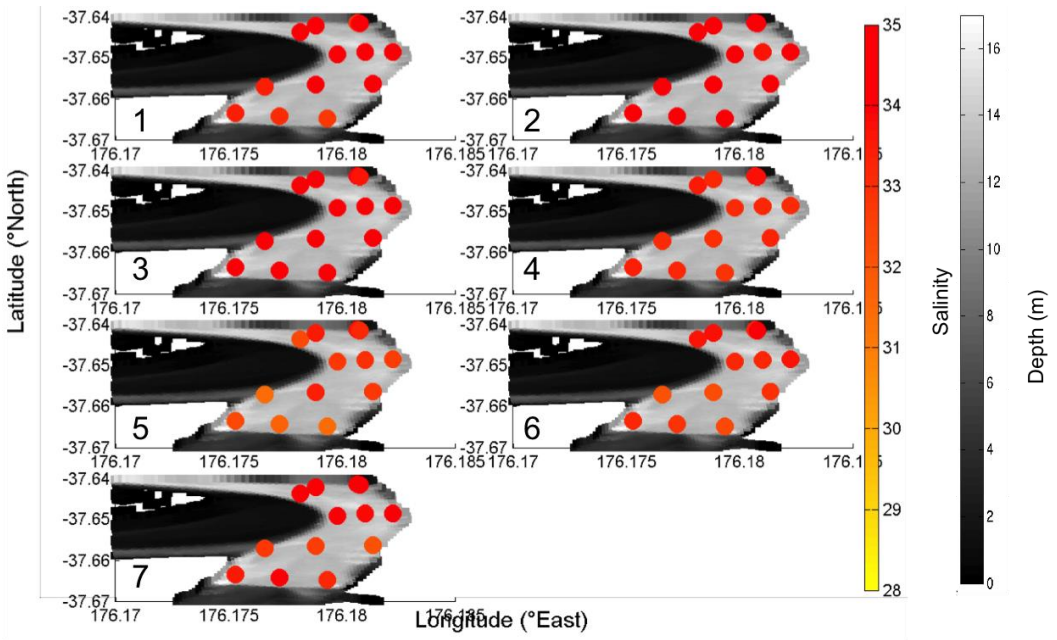

Figure 5.23: Surface salinities (psu). The panel numbers correspond to circuit number. The central time of each circuit was 8.10am, 10am, 12pm, 13.30pm, 4pm, 5.45pm, and 7pm. Note the colour scale for salinity has been chosen for ease of comparison with surveys conducted during rain events and so the values shown here tend to fall at the top (more saline) end of the scale.

The CTD profiles (Figure 5.24) from the same day show little variation in salinity with depth apart from panel 8 and 13. According to field observations those were the locations at which there was ship traffic just prior to the CTD casts and hence they show the influence of bilge water discharge from the container ships. The apparently fresh water on top of some of the profiles can be attributed to CTD handling. When the CTD was dropped too early and could not take a proper measurement of the surface conductivity it shows up as not a number (nan) in MATLAB and was plotted in black. In Figure 5.25 we see the surface backscatter data from the ADCP transects. The surface backscatter is calculated from the first

6 bins corresponding to the water column from 0.6 meters below the surface to two meters water depth. On careful examination and cross reference with Figure 5.24 it can be seen that the CTD profiles with stratification fall on locations where there is increased backscatter on the ADCP transect, indicating the influence of ship traffic. Figure 5.26 shows a section of the backscatter profiles for a non-plume event and Figure 5.27 shows the corresponding velocity profiles. High tide was at 8.45 am, just prior to when the profiles were taken. We can see a strong north current which is most likely the outgoing tide.

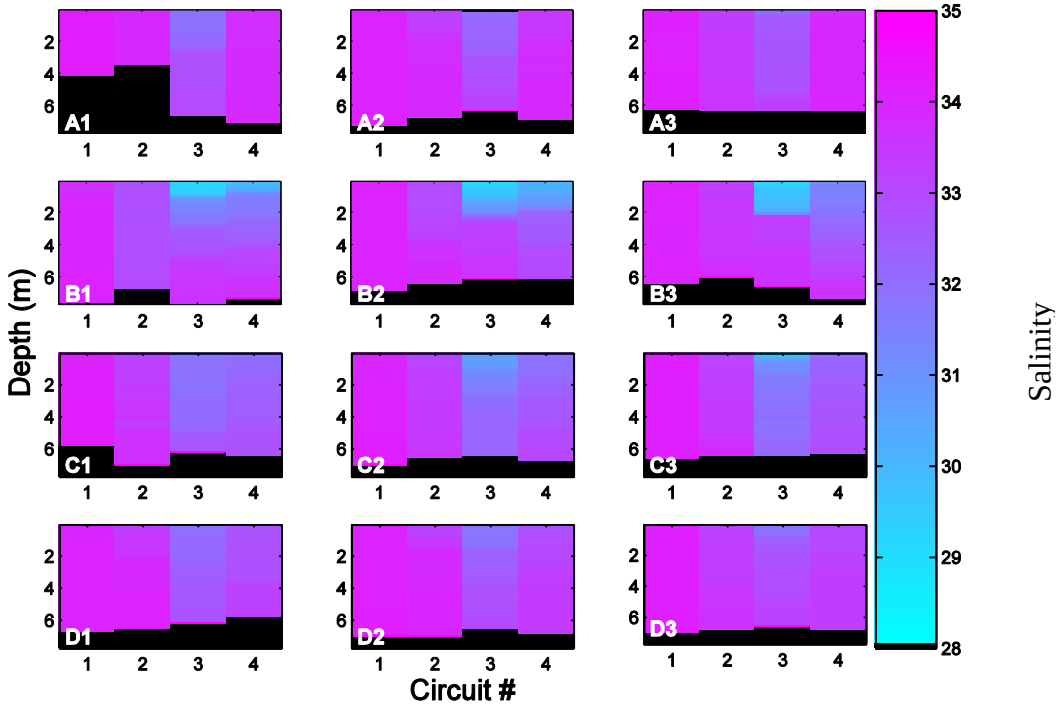

Figure 5.24: CTD profiles for dry survey. Panel numbers correspond to CTD cast locations from Figure 5.20. The different circuits/times are on x axis. The central time of each circuit was 8.10am, 10am, 12pm, 13.30pm, 4pm, 5.45pm, and 7pm. Salinity was calculated from conductivity. The black boxes at the bottom indicate ocean floor.

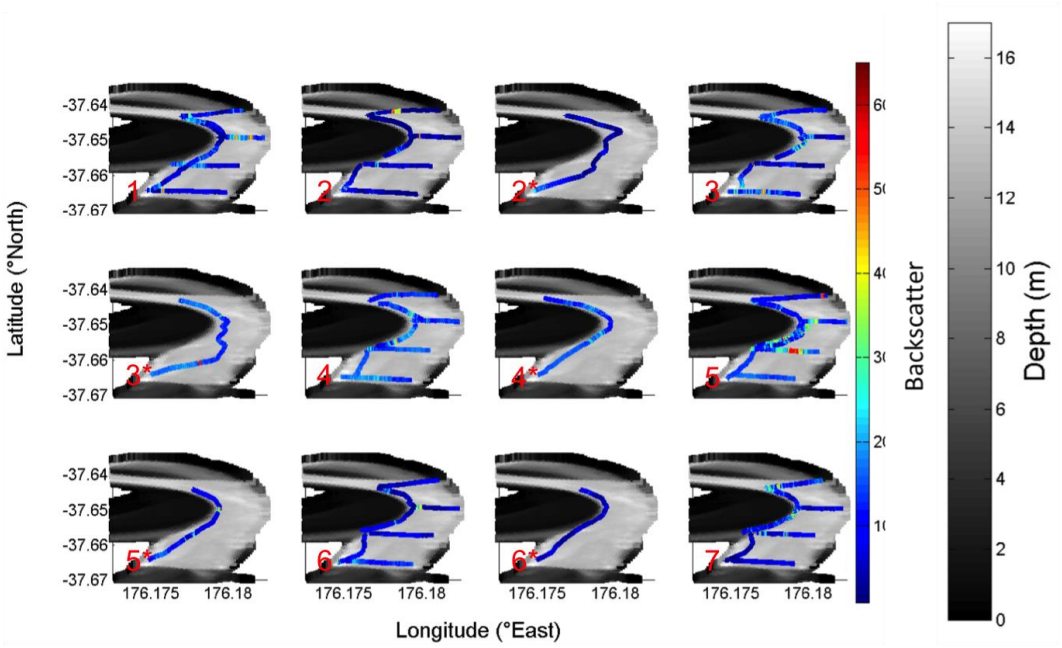

Figure 5.25: ADCP surface backscatter for dry survey. Blue corresponds to low backscatter, red is high backscatter. Panel numbers correspond to circuit number, with the asterisk '*' depicting the drive back to start a new circuit. The central time of each circuit was 8.10am, 10am, 12pm, 13.30pm, 4pm, 5.45pm, and 7pm.

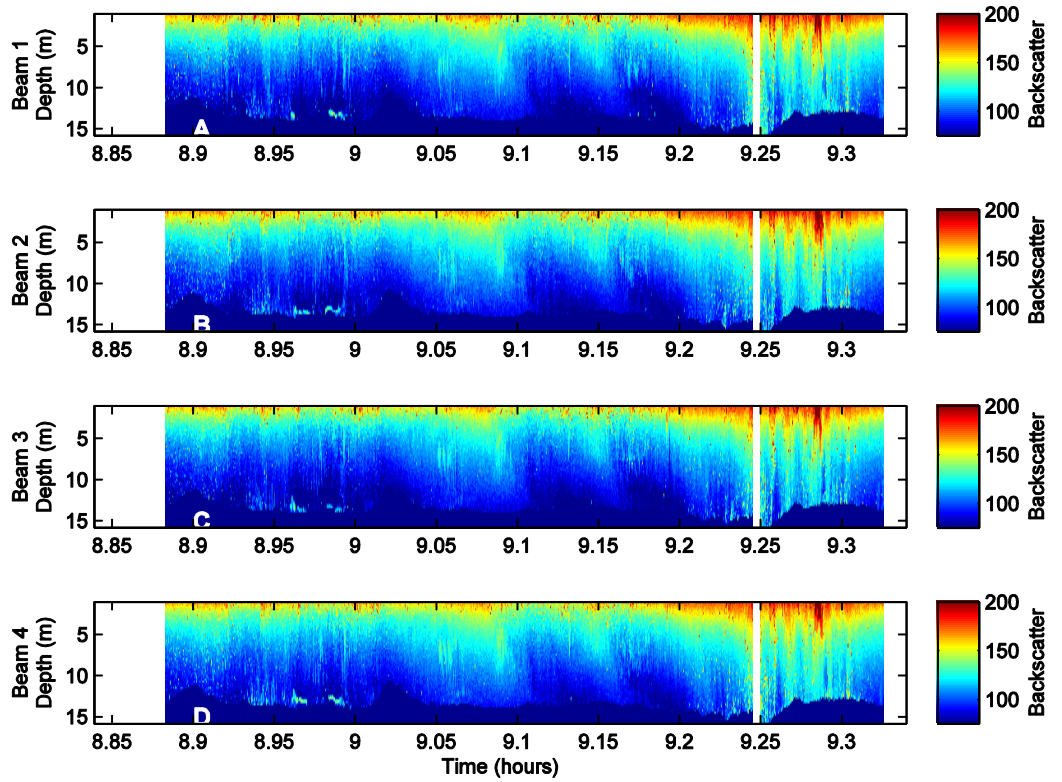

Figure 5.26: Backscatter profile on November 19th 2013 around 9 am going from West to East across Stella Passage. A: backscatter for beam one, B: backscatter for beam two, C: backscatter for beam three, D: backscatter for beam four.

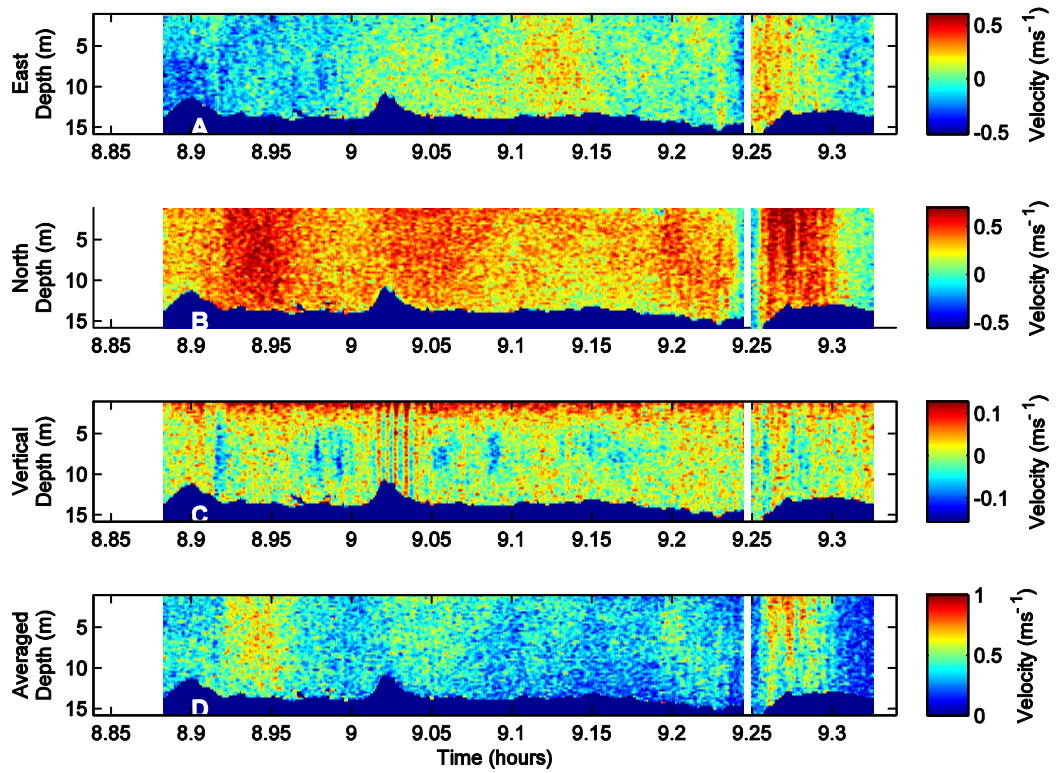

Figure 5.27: Velocity profiles from November19th 2013 around 9 am going from West to East across Stella Passage. A: east-west velocities, B: north-south velocities, C: vertical velocities, D: averaged velocities.

5.4.3 Wet survey 1

The first 'wet' survey was undertaken during a rain event on 17th April 2014. The rain started a day before on the 16th April.

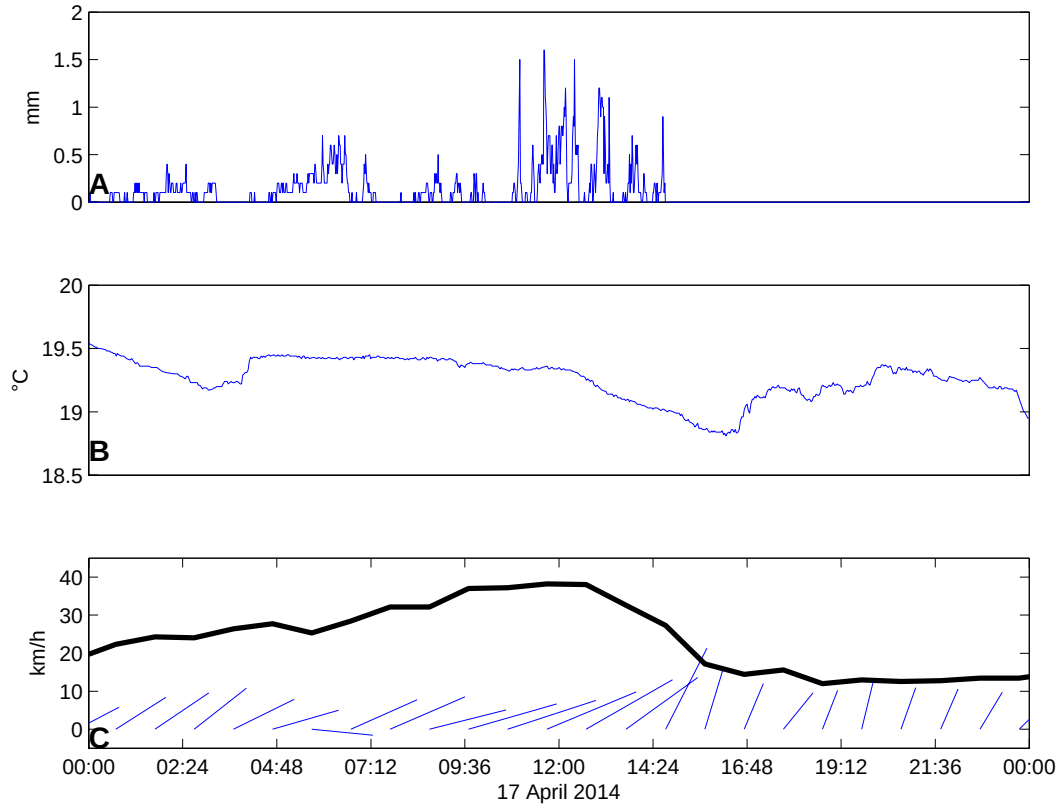

Figure 5.28 shows the weather data from the Port during the Survey. There were high hourly rainfalls of up to 1.5mm/h. The rainfall total for this event was 42mm.

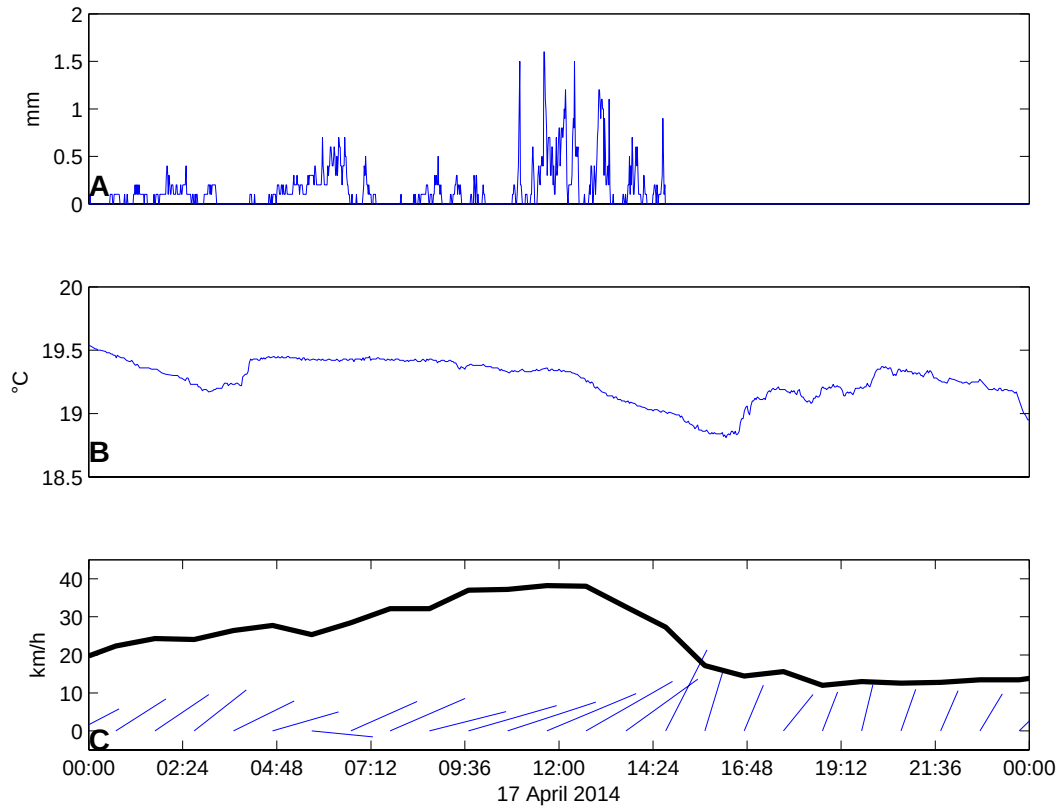

Figure 5.28: Weather data for April survey period. A: hourly rain (mm), B: temperature in Celsius, C: hourly wind speed and direction, thick black line is wind magnitude.

Figure 5.29 displays the surface salinities during the survey, which consisted of six circuits (and note that the along-channel sections were this time conducted on the Eastern side of Stella Passage next to the stormwater outlet pipes). During the first two circuits, the surface salinity remained approximately uniform. However, during the third circuit, a decrease in salinity can be observed in location B2. As the rain continued, the salinity of the surface water decreased throughout the harbour (panels 4, 5, and 6), although there was not a significantly different response adjacent to the run off pipes than elsewhere. This result likely indicates that the runoff plume was confined very close to the surface. Correct operation of the CTD requires submergence of the unit and hence the closest measurements to the surface were at a depth of approximately 1 m and so we can conclude that the plume was less than 1m thick.

The rain stopped between circuit 4 and circuit 5 and after a short delay we see the surface salinities rise again (panel 6). Comparing this to Figure 5.30 shows that the salinities rise for the complete water column.

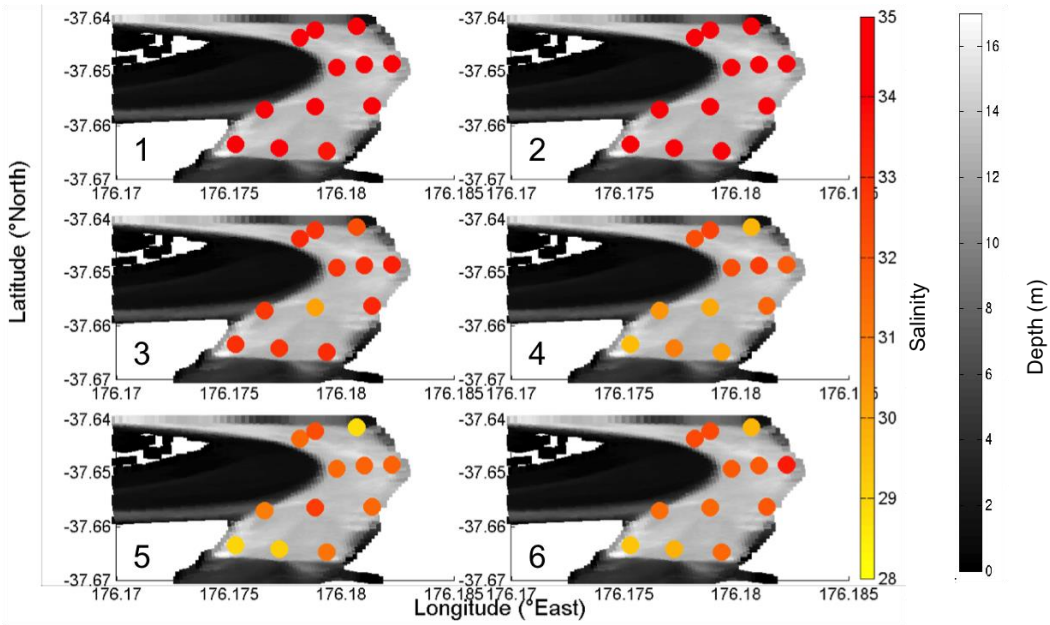

Figure 5.29: Surface salinities (psu). The panel numbers correspond to circuit number. The central time of each circuit was 9am, 11am, 1pm, 2.30pm, 4pm, 5.15pm, and 8pm. This is a rain event.

The CTD profiles in Figure 5.30 show that the surface changes observed in Figure 5.29 are qualitatively mirrored lower down in the water column. There was no change in salinity for the first two circuits (panel 1 and 2 in Figure 5.29 and columns 1 and 2 in each panel in Figure). The fact that there was no change during the first two circuits can be attributed to the rain just having started as we started the survey and as previously described it takes some time for the wharf to produce a runoff plume due to wetting. The plume can be measured halfway across the channel, about 170 meters. During circuits 3 and 4, there are salinity decreases. The salinity decreases the most at the top, and the decreases are strongest during circuit 4. After circuit 4 water column salinity starts to increase again. As mentioned above these salinity changes would be due to the rain stopping between circuit 4 and circuit 5. In Figure 5.31 we can basically observe the same thing. We see enhanced backscatter during circuits with the heaviest rain. Also, surface backscatter is averaged over the first two meter of water and we see the same variability. It is not quite as obvious in panel 1 and panel 2 as there was some ship traffic on the northern side of the channel and this shows up as increased backscatter on the ADCP transects. But the increased backscatter in panels 4 to 6 can be attributed to freshwater and debris/particulate matter as field observation confirms that at these points we were driving through the plume. Figure 5.32 shows the plume backscatter for the corresponding time and it is clear that the backscatter is increased to a water depth of about 5 meters. The decrease in backscatter in panels 8 to 10 is likely due to the rain and plume dispersal and mixing. By the time the transect in panel 10 was taken the plume was no longer visible.

Looking at Figure 5.32 we see the increased backscatter when driving through the plume at 10.9 am and out of the plume at 11.02 am. Comparing the velocities of those times to the backscatter indicates that there is not much difference in velocities (Figure 5.33) between plume water and non-plume water.

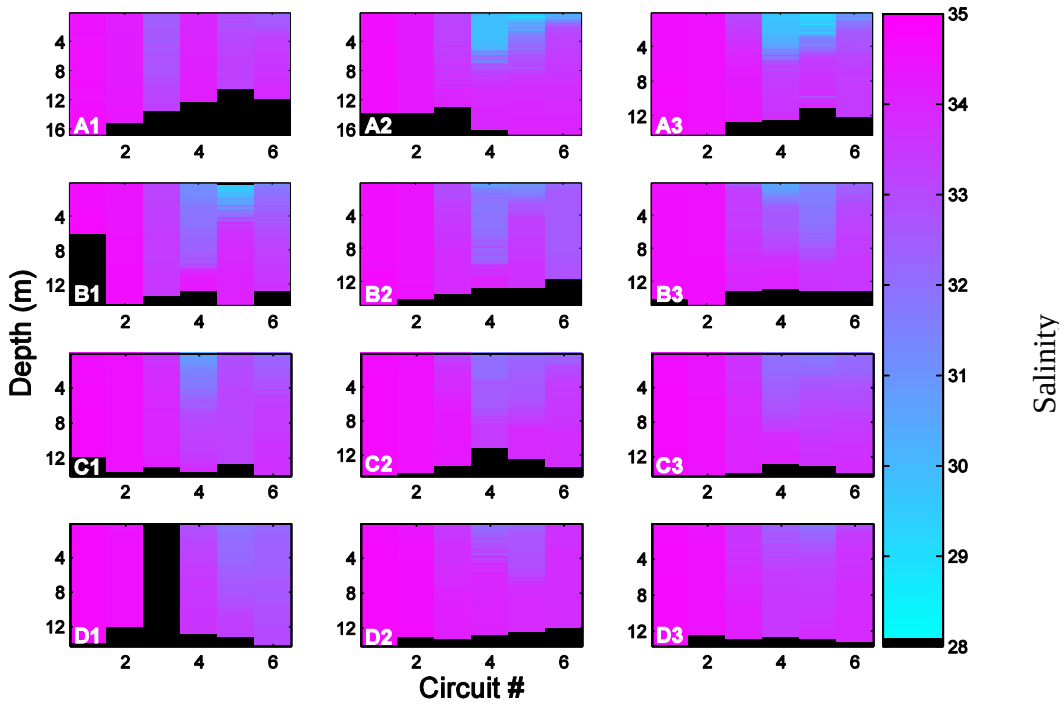

Figure 5.30: CTD profiles for wet survey on April 17 2014. Panel numbers correspond to CTD cast locations from **Figure 5.20**. The central time of each circuit was 9am, 11am, 1pm, 2.30pm, 4pm, 5.15pm, and 8pm. The black boxes at the bottom indicate ocean floor.

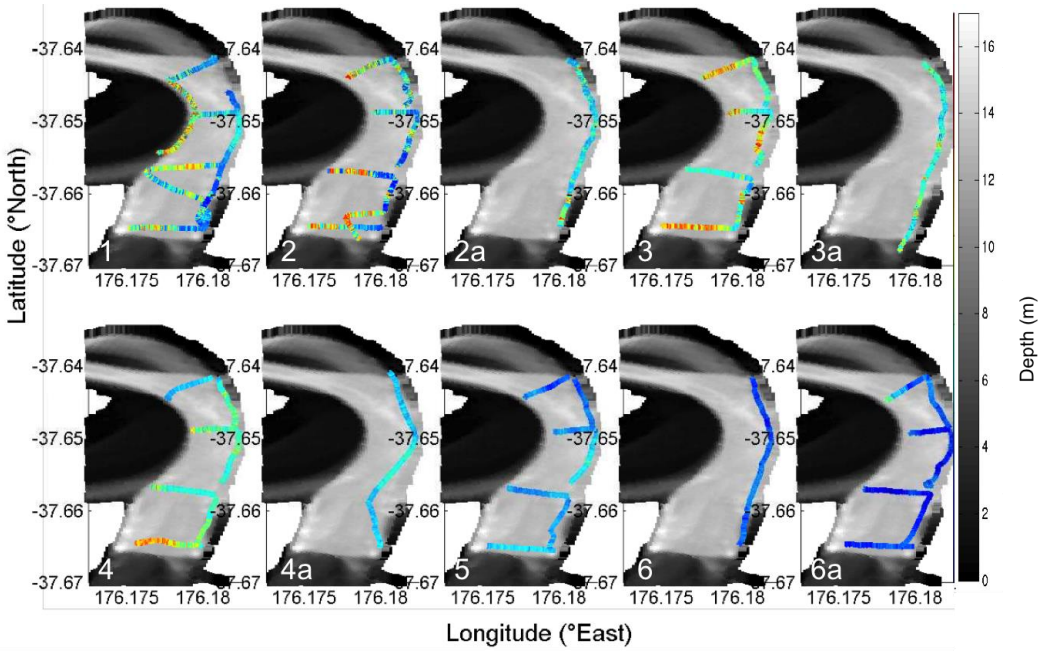

Figure 5.31: ADCP surface backscatter plots for wet survey from April 17 2014. Panel numbers correspond to circuit numbers, panel numbers with the letter 'a' show the drive back to the start of the circuit. The central time of each circuit was 9am, 11am, 1pm, 2.30pm, 4pm, 5.15pm, and 8pm.

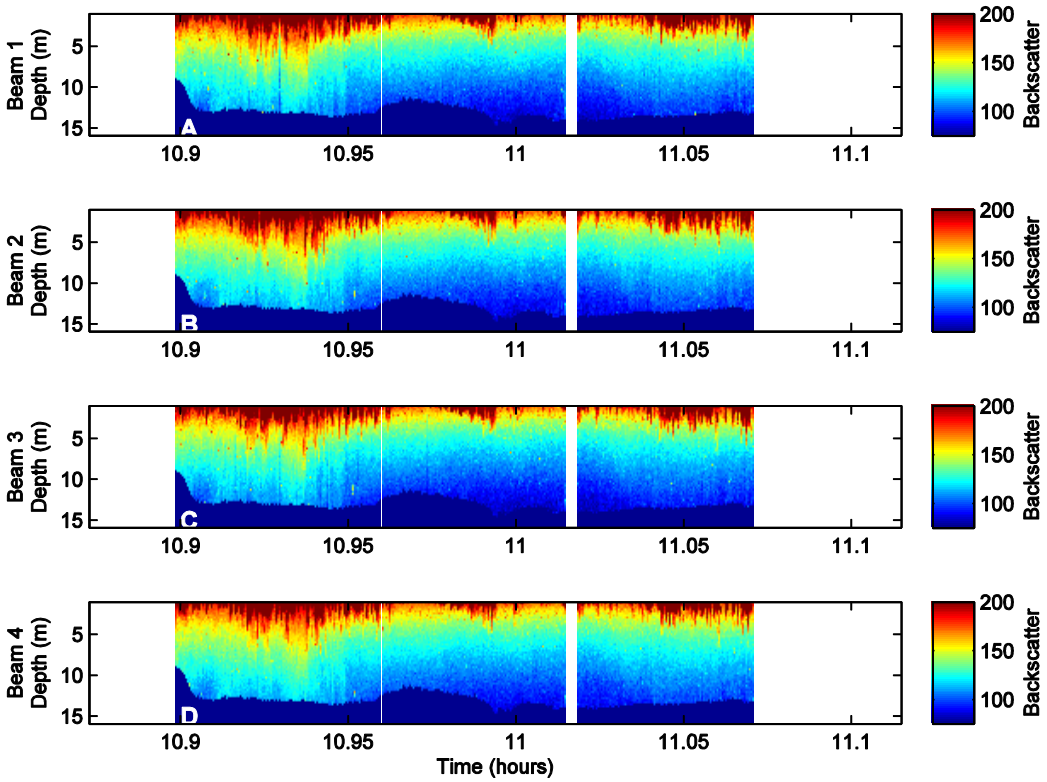

Figure 5.32: ADCP backscatter profiles on April 17th 2014 around 11am, driving through a visually observed surface plume. The transect from 10.9 to 10.96 is through the visually observed plume at Butters wharf, the transect from 10.96 to 11.02 was along the wharf, and the transect from 11.02 to 11.07 was east-west across Stella Passage. A: backscatter for beam one, B: backscatter for beam two, C: backscatter for beam three, D: backscatter for beam four.

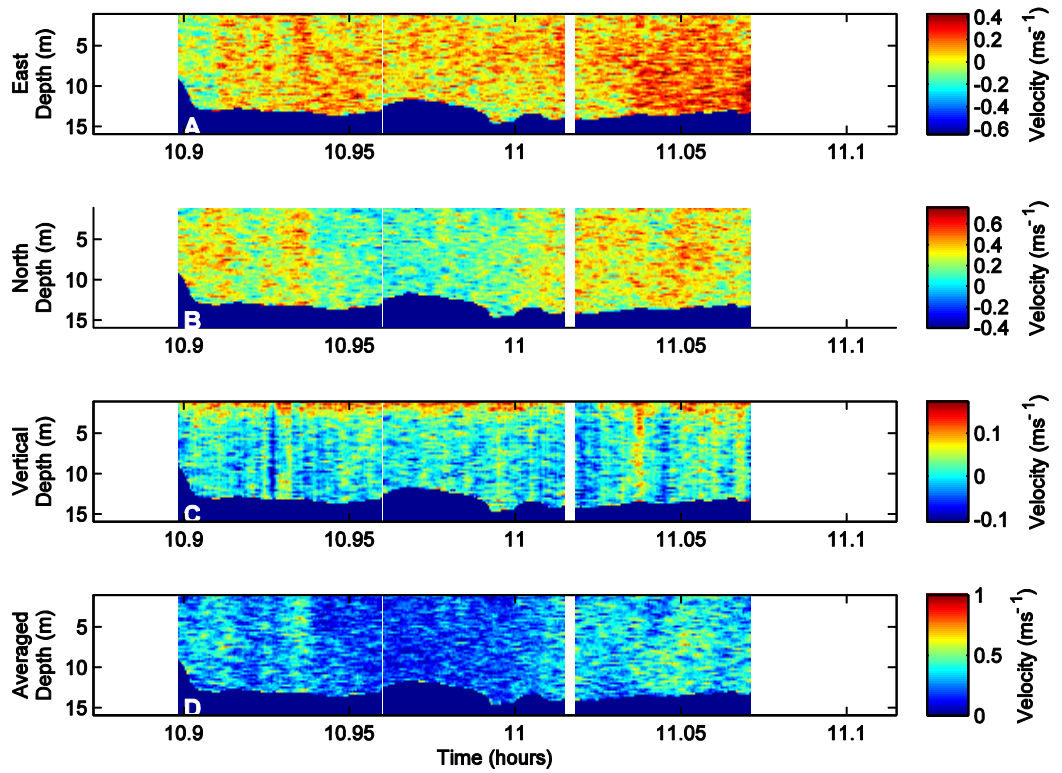

Figure 5.33: ADCP velocity profiles on April 17th 2014 around 11am, driving through a visually observed surface plume. The transect from 10.9 to 10.96 is through the visually observed plume at Butters wharf, the transect from 10.96 to 11.02 was along the wharf, and the transect from 11.02 to 11.07 was east-west across Stella Passage. A: east-west velocities, B: north-south velocities, C: vertical velocities, D: averaged velocities.

5.4.4 Wet survey 2

Figure 5.34 shows the weather data for the survey period. Rain was sparse in the morning, although the wind was moderate (20 km/h), the waves were relatively large for inside the harbour for the first two circuits. Rainfall increased at 12 pm and a further two circuits were conducted between 12.30 pm and 4 pm.

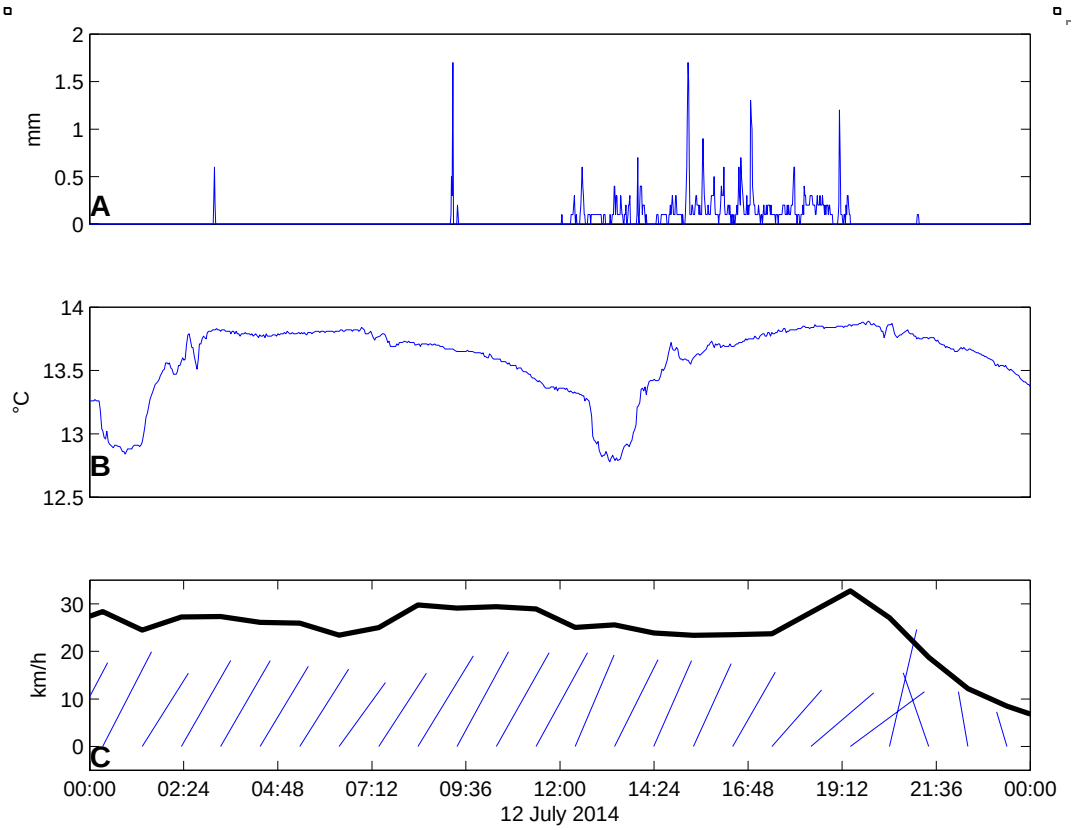

Figure 5.34: Weather data for July survey period. A: hourly rain (mm), B: temperature in Celsius, C: hourly wind speed and direction, thick black line is wind magnitude.

The surface salinities during the latter two surveys are shown in panels 3 and 4 (Figure 5.35). There is a clear drop in surface salinity in several places during both circuits. It is most obvious in circuit 3 (panel 3), location B2 (in the centre of the channel) has a significantly lower surface salinity during circuit 3 compared to circuit 1 and circuit 2, dropping from 35 to 28. According to field notes this CTD cast was taken in the runoff plume as assessed visually by significant discoloration of the surface waters.

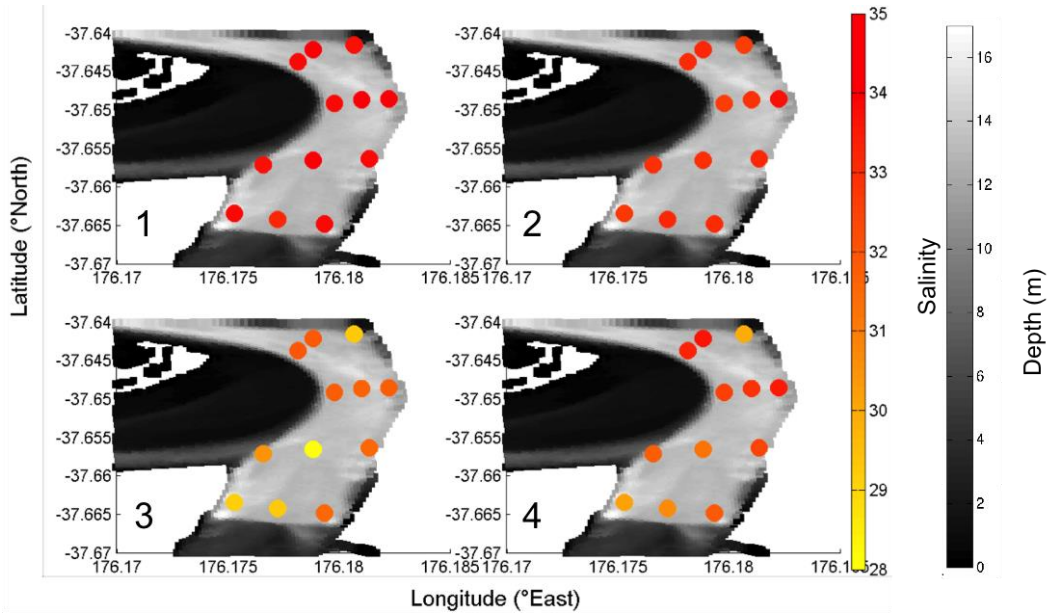

Figure 5.35 Surface salinities (psu). The panel numbers correspond to circuit number. The central time of each circuit was 8.10am, 10.30 am, 1.30pm, and 3.30pm.

The CTD profiles partly support the CTD surface salinity changes. Figure 5.36 shows that the salinity during circuit 1 was uniform.

Figure 5.37 shows the plume in panel 3 and panel 4. Unfortunately we miss the connecting transect between transects A and B along the wharf in panel 3. We also did not measure transects from end of transect 4 to the start of transect A as the weather was too rough. According to field observation the missing connecting transect went right through the plume. There was also a plume observed in the connecting transect between B and C (panel 3) which can be seen in the increased backscatter.

Figure 5.38 shows the backscatter profile from the connecting transect and it seems the plume was about 3 meters deep at that time and point. Looking at the velocity profiles (Figure 5.39) there is nothing remarkable apart from the velocities increasing due to ebb tidal flows getting stronger.

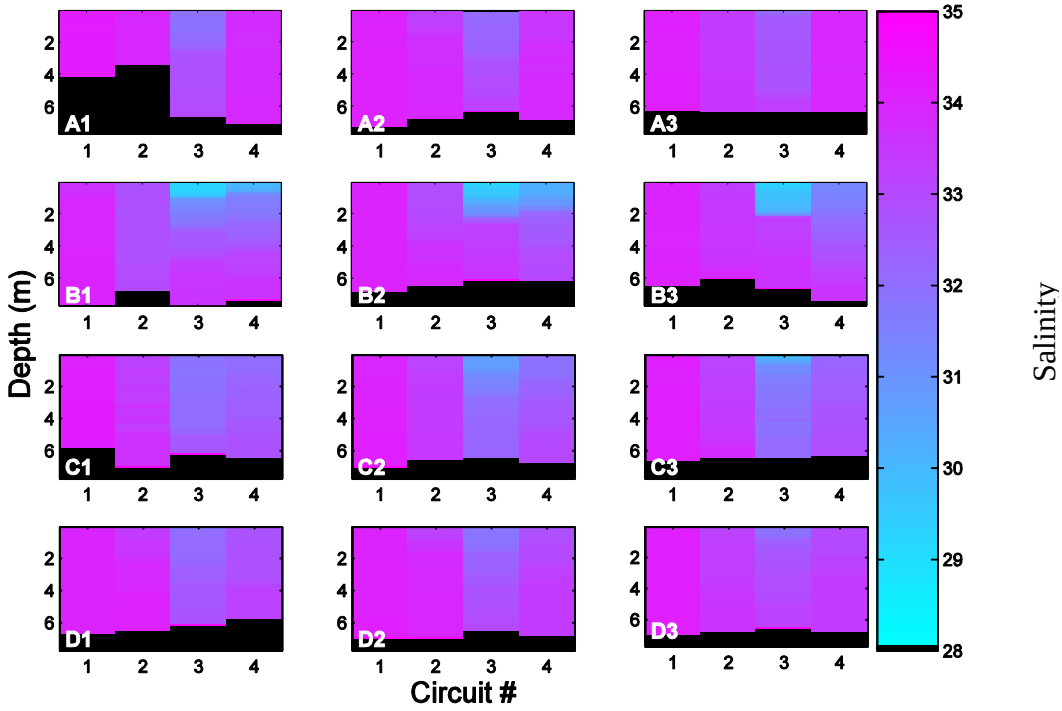

Figure 5.36: CTD profiles for wet survey July 12 2014. Panel numbers correspond to CTD drop location from Figure 5.20. The central time of each circuit was 8.10am, 10.30 am, 1.30pm, and 3.30pm. The black boxes at the bottom indicate ocean floor.

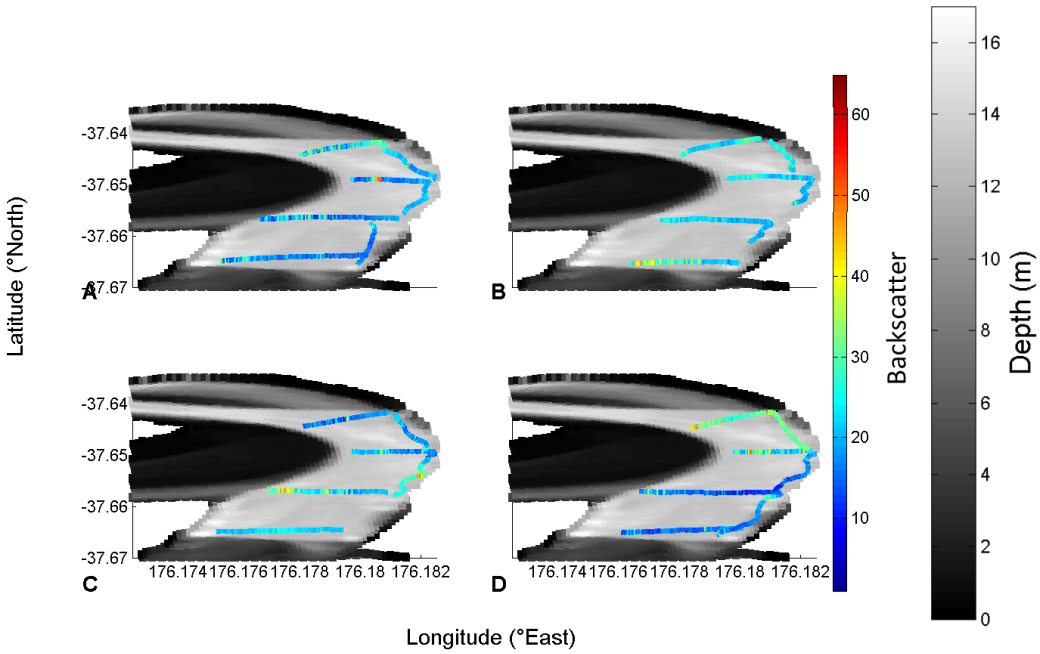

Figure 5.37: ADCP surface backscatter from wet survey July 12th 2014. Panel numbers correspond to circuit numbers. The central time of each circuit was 8.10am, 10.30 am, 1.30pm, and 3.30pm.

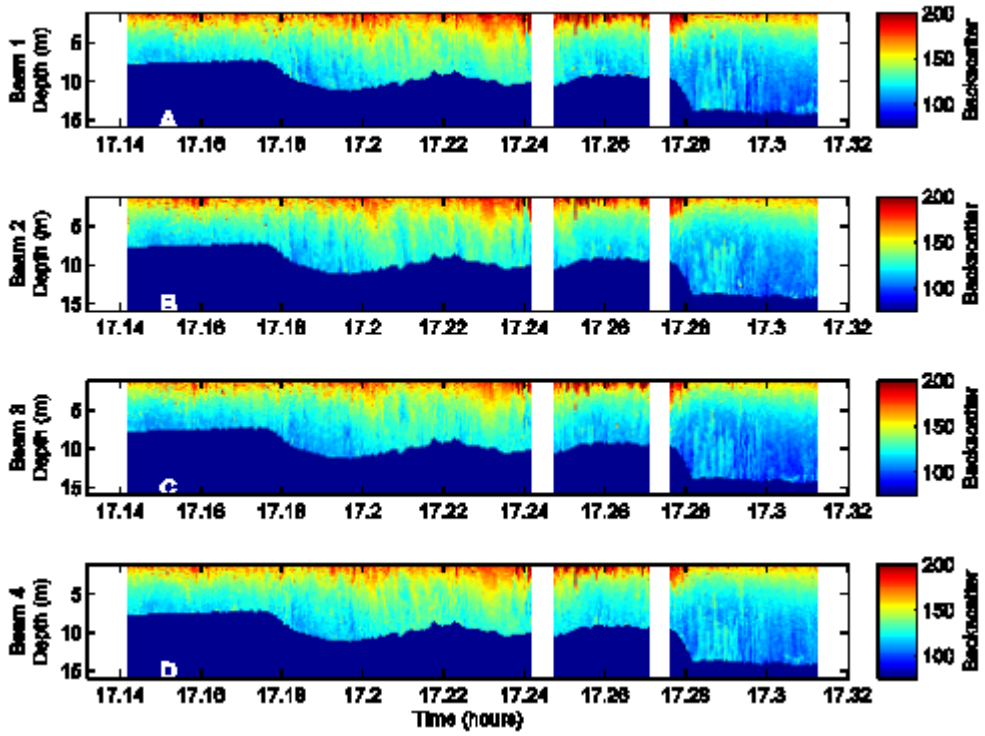

Figure 5.38: ADCP backscatter profiles from July 12th 2014 at 5 pm, driving through the visually observed plume. The transect starting at 17.14 to 17.24 was taken along the wharf (south to north), the transect from 17.24 to 17.28 was east-west across Stella Passage, and the transect from 17.28 to 17.31 is along the channel, extremely heavy rain was observed at the beginning of this specific transect. A: backscatter for beam one, B: backscatter for beam two, C: backscatter for beam three, D: backscatter for beam four.

During the first two transects shown on Figure 5.38 and Figure 5.39 there was an incoming tide, and on the third transect the tide was turning to slack water at high tide. Therefor the plume was pushed up into the estuary. As the currents are weak, especially at the surface, in the region of the plume, this effect is not very strong.

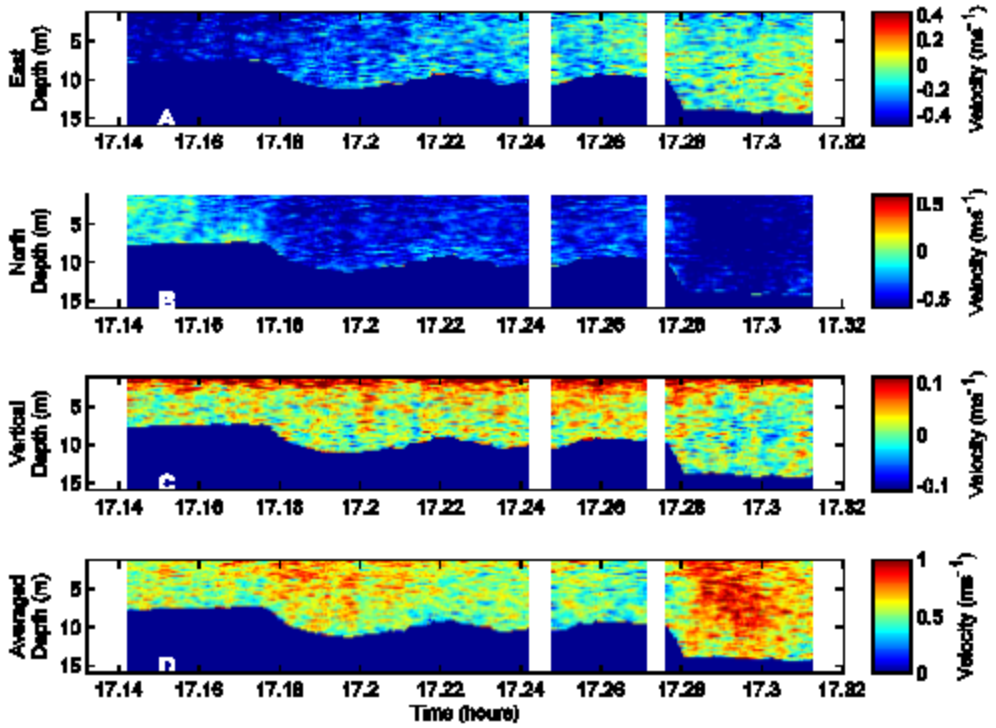

Figure 5.39: ADCP velocity profiles from July 12th 2014 at 5 pm, driving through the visually observed plume. The transect starting at 17.14 to 17.24 was taken along the wharf (south to north), the transect from 17.24 to 17.28 was east-west across Stella Passage, and the transect from 17.28 to 17.31 is along the channel, extremely heavy rain was observed at the beginning of this specific transect. A: east-west velocities, B: north-south velocities, C: vertical velocities, D: averaged velocities.

5.5 Plume parameter calculations

5.5.1 Overall Richardson number

To calculate the overall Richardson number for the plume on the 12th July 2014 in location B3 the following equations were used from (Turner, 1979).

The overall Richardson number Ri (Equation 5.1) is calculated using

$$Ri = g/\rho_0 + \Delta\rho * h/v \qquad \text{Equation 5.1}$$

where g is the gravitational acceleration (9.81 m/s^2), ρ_o is the ambient density (1025 kg/m^3), $\Delta\rho$ is the density difference between plume water and ambient water, h is the plume depth (in meters), and v is the ambient current speed (in m/s). The calculated numbers with a range can be found in Table 5.2. The Richardson number for plume source condition was calculated to be Ri = 0.75, and for far

field (shallow to no plume) conditions Ri = 0.12, indicating a reduction in stability as the plume propagates and is advected away from its source location.

5.5.2 Length scales

The length scales were calculated using the equations from (Jones *et al.*, 2007) for discharge flux Q_0 (Equation 5.2), momentum flux M_0 (Equation 5.3), and buoyancy J_0 (Equation 5.4). To calculate these numbers the ambient water current velocity U_a, discharge channel cross-sectional area a_0, and reduced gravity g'_0, which is the discharge buoyant acceleration are needed. The reduced gravity can be estimated from the density measurements that were taken in the plume and should therefore be reasonably accurate. The ambient water current velocities were extracted from ADCP measurements and should be adequate. The discharge channel cross-sectional area has to be estimated, as we do not have the means to calculate it precisely. To do that it would require knowing what part of the discharge pipe is covered in water during discharges. Thus we are only able to estimate discharge flux, momentum flux, and buoyancy.

$$Q_0 = U_a a_0 Q_0 = U_a a_0 \qquad \text{Equation 5.2}$$

$$M_0 = Q_0 U_0 M_0 = Q_0 U_0 \qquad \text{Equation 5.3}$$

$$J_0 = Q_0 g'_0 J_0 = Q_0 g'_0 \qquad \text{Equation 5.4}$$

With these initial numbers the length scales can be calculated. The discharge length scale L_Q (Equation 5.5) measures the region where the flow characteristics are strongly influenced by the discharge channel geometry (flow establishment). This is usually an important measure for surface jets.

$$L_Q = Q_0/M_0^{1/2} L_Q = Q_0 / M_0^{1/2} \qquad \text{Equation 5.5}$$

The transitional region from jet-like mixing to buoyant lateral spreading is the jet-to-plume length L_M (Equation 5.6).

$$L_M = M_0^{3/4}/J_o^{1/2} L_M = M_0^{3/4} / J_0^{1/2} \qquad \text{Equation 5.6}$$

The jet-to-crossflow length scale L_m (Equation 5.7), marks the point at which the flow is strongly deflected by the ambient cross flow.

$$L_m = M_0^{1/2}/u_a L_m = M_0^{1/2}/u_a \qquad \text{Equation 5.7}$$

To measure how far a strongly buoyant discharge can intrude against an ambient flow is called the plume-to-crossflow L_b (Equation 5.8).

$$L_b = J_0/u_a^3 L_b = J_0/u_a^3 \qquad \text{Equation 5.8}$$

All variables and length scales are given in Table 5.2. They were calculated for several different initial conditions. The calculated discharge length scales range between 0.82 m to 1.06 m, which means the discharge channel geometry does not influence the plume very far. Looking at the jet-to-plume length scale we see a range between 75 m and 118 m. Therefore we can conclude that the transition from jet-like mixing to buoyant lateral spreading is about a quarter of the channel width. It seems that the flow is most strongly affected by the ambient current at around 50 meters, with ranges between 36.7 m to 84.6 m. The plume-to-crossflow length scale is comparatively small with a range between 4.5 m and 43 m. This shows that the plume can intrude against the ambient flow but it strongly depends on the conditions, only really works when Q_0 is high, large discharge.

With these length scales the discharge plume can be classified using one of two classification systems (Jones *et al.*, 2007). According to the earlier system (Figure 5.40) our plume falls under the category of free buoyant jets except under one condition where it was a shoreline attached jet. Under the newer system (Figure 1.2 and Figure 5.41) all conditions calculated resulted in describing the plume as an upstream intruding plume that is mostly shore-hugging.

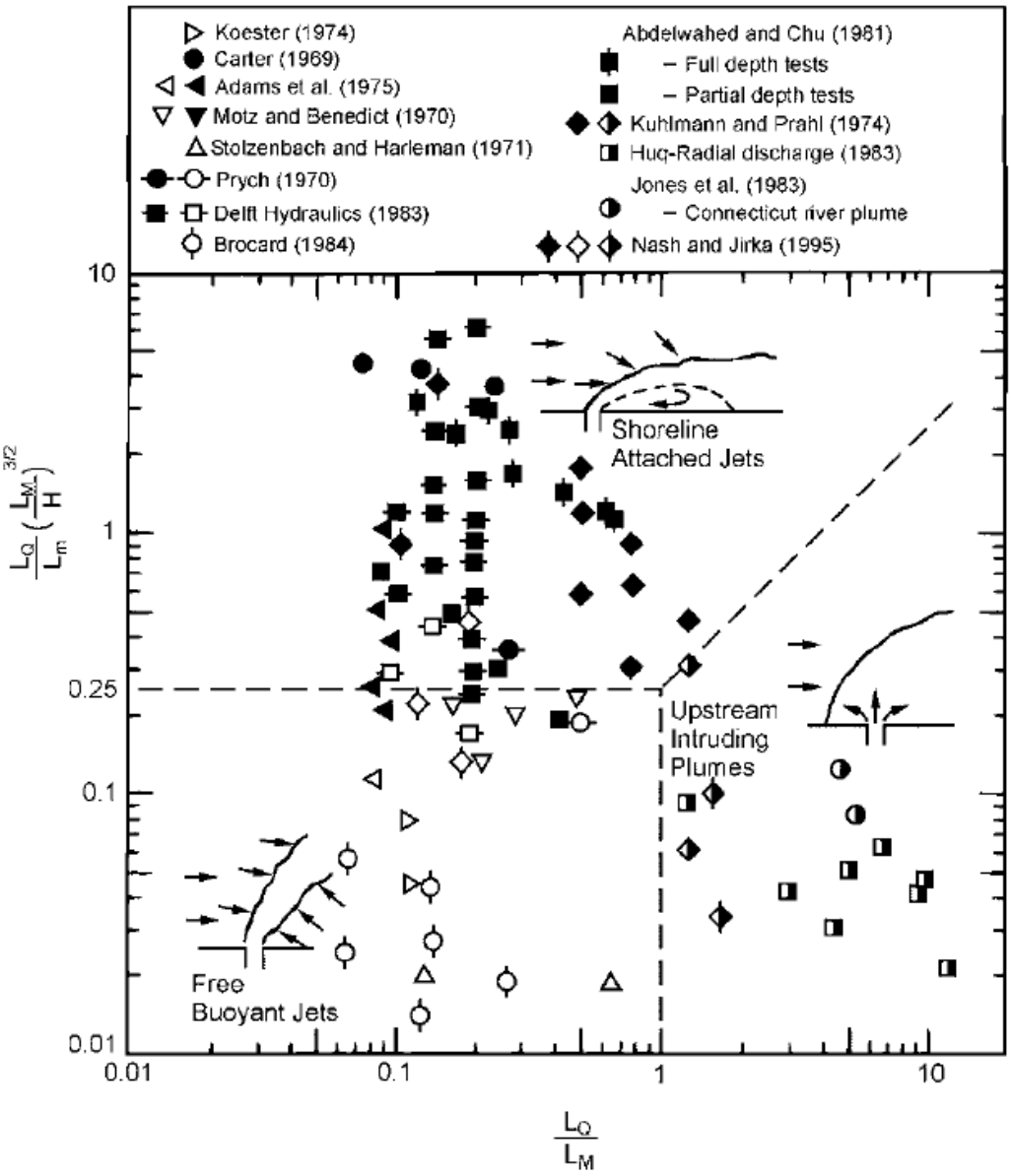

Figure 5.40: Diagram of buoyant surface discharge classifications with three flow categories: free jet (open symbols), upstream intruding plumes (half-closed symbols), and shoreline-attached jets (closed symbols). Source: (Jones *et al.*, 2007).

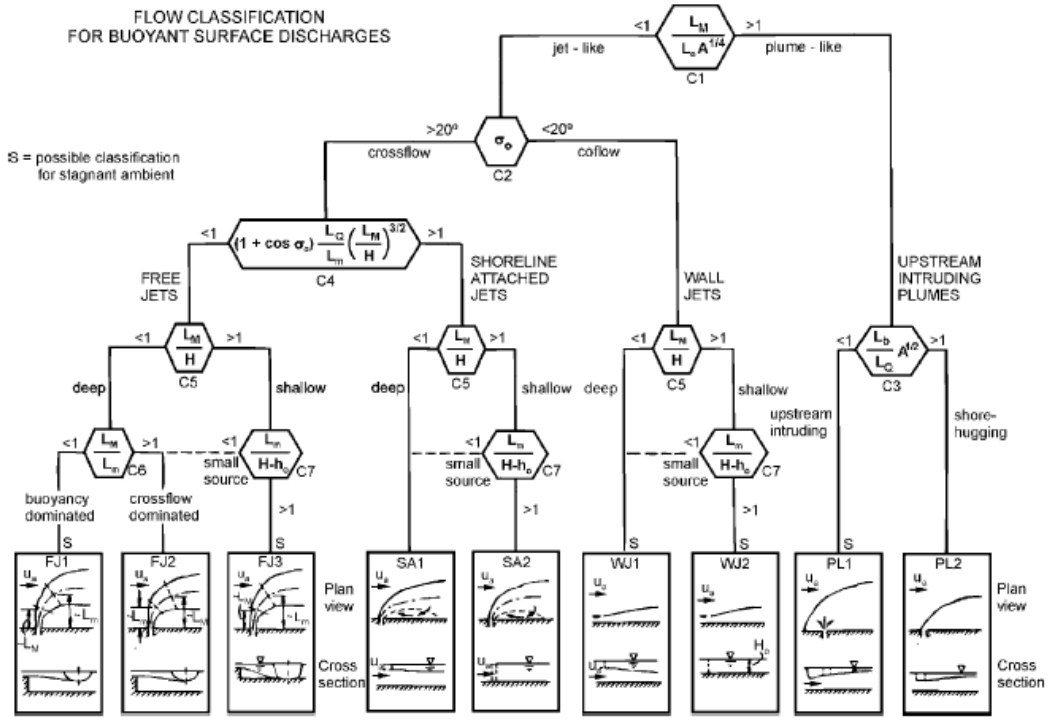

Figure 5.41: A detailed classification system for buoyant surface discharges. The four major flow categories are: free jets, shoreline-attached jets, wall jets, and upstream intruding plumes. Source: (Jones *et al.*, 2007).

Table 5.2: Length scale and Richardson number calculations and required variables for different plume depth, density differences, discharge velocities, ambient water velocities, aspect ratios, discharge channel width and depth. Scen1 to scen8 indicate different conditions.

	scen1	scen2	scen3	scen4	scen5	scen6	scen7	scen8	min	max	range
density difference	5.00	5.00	3.00	3.00	3.00	2.00	2.00	4.00	2.00	5.00	3.00
G0 reduced gravity	0.05	0.05	0.03	0.03	0.03	0.02	0.02	0.04	0.02	0.05	0.03
A0 discharge area	1.13	1.13	1.13	1.13	0.68	0.68	1.13	1.13	0.68	1.13	0.45
U0 discharge velocity	15.92	17.26	15.92	17.26	15.92	17.26	15.92	15.92	15.92	17.26	1.34
Q0 volume flux	18.00	19.52	18.00	19.52	10.80	11.71	18.00	18.00	10.80	19.52	8.72
M0 momentum flux	286.48	336.86	286.48	336.86	171.89	202.12	286.48	286.48	171.89	336.86	164.98
J0 buoyancy flux	0.86	0.93	0.52	0.56	0.31	0.22	0.34	0.69	0.22	0.93	0.71
ua ambient velocity	0.32	0.32	0.32	0.50	0.32	0.32	0.20	0.32	0.20	0.50	0.30
H water depth	16.00	16.00	16.00	16.00	16.00	16.00	16.00	16.00	16.00	16.00	0.00
h0 discharge channel depth	1.00	1.20	0.80	0.20	0.50	1.00	0.50	0.30	0.20	1.20	1.00
b0 discharge channel width	1.20	1.20	1.20	1.20	1.20	1.20	1.20	1.20	1.20	1.20	0.00
A aspect ratio h0/b0	0.83	1.00	0.67	0.17	0.42	0.83	0.42	0.25	0.17	1.00	0.83
LQ discharge length	1.06	1.06	1.06	1.06	0.82	0.82	1.06	1.06	0.82	1.06	0.24
LM jet-to-plume length	75.03	81.36	96.86	105.04	85.25	113.22	118.63	83.89	75.03	118.63	43.60
Lm jet-to-crossflow length	52.89	57.36	52.89	36.71	40.97	44.43	84.63	52.89	36.71	84.63	47.92
Lb plume-to-crossflow length	26.29	28.50	15.77	4.48	9.46	6.84	43.07	21.03	4.48	43.07	38.58
LQ/LM	0.01	0.01	0.01	0.01	0.01	0.01	0.01	0.01	0.01	0.01	0.01
LQ/Lm*(LM/H)^(3/2)	0.20	0.21	0.30	0.49	0.25	0.35	0.25	0.24	0.20	0.49	0.28
LM/(LQ*A^(1/4))	73.84	76.51	100.80	154.58	128.81	143.85	138.85	111.55	73.84	154.58	80.74
Lb/LQ*A^(1/2)	22.56	26.80	12.11	1.72	7.42	7.58	26.14	9.89	1.72	26.80	25.08
h plume depth	1	5	1	2	5	2	5	5	1.00	5.00	4.00
Ri overall Richardson number	0.15	0.75	0.09	0.12	0.45	0.12	0.48	0.6	0.09	0.75	0.66

5.6 Summary

- During rain events, the effect of the freshwater input could be detected on all our survey instrumentation as well as the CT sensors.
- However, it is often difficult to discern a clear signal of the run off plume even at the fixed sensors nearby – as all sensors show similar measurements, even those placed far away from the plume in regions which the plume was not observed to reach.
- The CT sensor under the wharf at 2 meters water depth appeared to pick up the freshwater plume as it is located in front of the outfall and showed a short-lived sharp decrease in salinity.
- Generally, the fact that the lower salinity signal on all sensors takes days to disappear would indicate changes are dominated by the surface rain..
- The CTD profiles which were observed to be definitely taken in the plume as observed by the surface discoloration show a plume depth of about 5 meters and a salinity difference of about 6 psu.
- Due to how the CTD profiles were calculated it seems obvious that the plume signal was detected. The CTD profiles suggest a plume depth of up to 5 meters but mostly closer to about 2-3 meters.
- Even the ADCP surface backscatter, taking into account that the surface backscatter is averaged over that top 2 meters of the water column, shows a clear plume signal.
- The ADCP backscatter profiles indicate plume thickness of up to 5 meters.
- According to the CT sensor deployments the rain detection delay is up to 24 hours whereas the survey detection delay was a few (around 4) hours.
- The dispersion time for the surface rain measured by the CT sensors was up to 4 days. On wet survey 1 (17 April) the dispersion time was about 3 hours.
- Figure 5.10 shows clearly that the background velocities (in the aquadopp) do not change during rain events.
- Comparing the dry survey with the wet survey data there seems to be no influence on the currents by the plume which would indicate that the

plume is very shallow and was not measured by the fixed instruments. The fact that the two profilers (ADP and aquadopp) were not able to measure the complete water column due to depth/bin size restriction comes into play here.

- Richardson numbers indicated the plume stability decreased as the plume spread (to less that the canonical critical value of 0.25).
- The length scales mainly depend on volume flux which is influenced by discharge velocity and area.
- The plumes can all be classified as free buoyant jets or upstream intruding plumes, depending on which classification system is used.

Chapter Six

Discussion

6.1 Overview

The main goal of this thesis was to investigate the dynamics of the stormwater runoff plume from the timber export area of the Port of Tauranga. The purpose was to provide the Port with plume parameters such as mixing timescales, mixing length, and dispersion characteristics. This chapter summarises the results, compares the results to previous work, describes how the objectives were achieved, how this work ties in with the toxicology assessment done by David Culliford, explains a few shortcomings of the field work, and points out areas for future work.

6.2 Summary of Results

The dry survey and the long-term deployment showed that the study area does not exhibit water column stratification when there is no rain (uniform backscatter and velocity profiles during the dry deployment period).

Rain events result in partial stratification, which was measured by most instruments. We cannot say with confidence that the change in salinity measured by the surface deployed CT sensors is the plume; it is more likely to be surface rain as the sensors were only at 20 cm depth and all sensors, even those known to not be in the plume measured so decrease in salinity during strong rain events. However, the plume was definitely detected by the CT sensor deployed at depth in front of the outlet and these signals manifested as short-lived decreases.

From the CTD salinity profiles we can deduce with some confidence, that the plume is about 2 to 4 meters deep. The ADCP survey surface data (top 2 meters) support this result. The ADCP survey profiles (not shown) also indicate the presence of the plume (high backscatter where plume was observed visually).

The estimated plume intrusion of about half-way across the channel (170 meters) lines up with the calculated length scales. The difference would come from either

a slight overestimation or errors in the calculations. As the calculations are based on a few assumptions of the initial conditions they should be used to provide estimates only and do not give exact lengthscales

6.3 Comparison to previous work

As in the modelling results from Tay *et al.* (2013) we found no significant stratification of the water column in the study area.

If we compare our data to the modelled plumes in Tian (1997) we see that his plume depth predictions correspond well to those observed in the field. We found similar salinity gradients over the same water depths that he described. On the strongest rain event of 17th April 2014 we had a salinity gradient in the top 3 meters of the water column of 7 psu while Tian (1997) modelled and found salinity gradients in the top 4 meters to be up to 6 psu during strong rain events.

The study of Tian (1997) has a limited sampling regime compared to what was done here. This limited sampling resulted in a limited resolution of the plume. We were able to do a better job as the instruments have improved considerably over the last decade or so, since Tian (1997) did his study. The better instrumentation allowed us to achieve a greater spatial coverage of the plume. We achieved to do consistent, relatively high resolution surveys of the plume, relative to the work done by Tian (1997). We also undertook longer duration surveys

6.4 Comparing to other plume studies

The method used in this study provides a good framework of a freshwater plume. It indicates horizontal as well as vertical spreading extent. Using salinity as a proxy to density worked in this case as the water temperature was approximately the same for both water bodies. Therefore the plume dynamics are controlled by the salinity variations. In cases where the water temperature differs between the water bodies this approximation will not work and actual density might have to be calculated. In the case of the stormwater runoff plume in Tauranga Harbour, where there is no background stratification the plume dynamics are simpler than if there was a background stratification. A background stratification would have an impact on the plume dynamics such as mixing and spreading behaviour,

especially vertical mixing, which would be suppressed. In these cases then it would be a good approach to follow the method proposed by O'Donnell (1997) to measure the horizontal spread of the plume.

Other plume work has been done using satellite imagery (Lahet & Stramski, 2010; Reifel *et al.*, 2009) and aerial photographs coupled with concurrent bacterial sampling (Svejkovsky *et al.*, 2010). However, these measurements are restricted to horizontal spreading and provide no information about the mixing rates at the base of the plume and if the vertical plume extent affects the basin floor or is affected by local currents. Using satellite imagery only worked for that study because the weather conditions in their study area are such that after a storm event the winds are strong enough to almost immediately disperse with any cloud cover. In our study area the cloud cover usually persists for long periods of time after the rain stopped, making it near impossible to use satellite imagery. Aerial photography would still work and could be incorporated into future studies.

6.5 Link to toxicology work

The student carrying out the related toxicology study, David Culliford, should be able to use our results to see if his mussel cages were likely to have been in the plume water and to estimate the frequency and duration of exposure to plume water.

6.6 Problems

Doing this work we encountered several problems, some of which I will mention here. First we had to find out if we could actually detect the plume with the instrumentation that we were planning on using, mainly ADCP and CTD. Fortunately we thought we could after a preliminary survey (data not included). However, the Seabird CTD used here is not an ideal choice of instrument for measuring close to the top of the water column; an alternative instrument without pump sampling system would be preferable.

The main problem or limitation we encountered was the unpredictability of the weather. It was difficult to assemble the gear and man-power on short notice when

we found out that we might have enough rain for a plume to occur, hence only two wet surveys.

Another limitation was the CT sensors. We did not have as many as we would have liked to produce a sensor array deployment. It would have been good to deploy the CT sensors at different depths and in an arc around the outlet to possibly capture early plume behaviour in particular to allow for robust estimation of volume and momentum fluxes close to the source. As we didn't have enough sensors or time to do this we don't know much about early plume behaviour and calculating plume parameters was difficult.

The next problem was that there were not that many big rain events to begin with in 2014, see weather data. Most rain events that occurred did not predict to yield enough rain for a plume to develop so we did not go out.

Another problem that I will mention here was the CTD limitations. After analysing an undiluted sample of runoff water we found that the runoff water is very acidic. One of the CTD's we used had a pH sensor which we had on recording for a few casts and we actually measured a plume signal. Unfortunately we did not always manage to acquire the CTD with the pH sensor and the sensor also broke down for one of the surveys. Therefor we were not able to use the pH information to detect the plume.

Lastly, plume spreading could not be measured accurately as the plume behaviour would have been influenced by the berthed ships. As the outlet pipes are under the wharf and most of the time there are ships berthed, the plume is forced to go around the ships.

6.7 Future Work

Using the new data from this study together with the data from Tian (1997) a new model should be developed to map the plume. A model plume prediction would be ideal to assess if the plume poses a threat to the kai moana on Centre Bank (with or without toxicology results).

Another point would be that one could basically repeat this work doing a better job at measuring the plume. It would be good to get pH profiles through the plume to compare to the salinity profiles. As there are not that many other ways to

measure the plume it would at least be a good idea to have a dense CT sensor array around at least one outlet on a future study.

The fixed instruments can also be used in future studies for calibration of numerical models under recent harbour conditions (i.e. after recent dredging).

Another useful experiment to undertake could be to map the plume extent with fluorescent dye.

6.8 Summary

We achieved the goals of this study.

- The detected plume is thin and disperses quickly, owing to strong tidal currents in this region.
- The salinity gradient in the top 5 meters of the water column is significantly bigger during rain events compared to dry days.
- It would have been good to have instrument arrays with a good resolution over a short distance similar to what O'Donnell (1997) used for the vertical and horizontal resolution.
- Satellite or aerial imagery could have provided better data about horizontal spread and persistence.
- The study would have benefitted from a working pH meter on the CTD casts due to the runoff water being very acidic.
- The length scale calculations indicate that the plume can intrude upstream for up to 43 meters. They also show that the plume can easily reach at least halfway across Stella Passage before being affected by ambient crosscurrents.

References

Ahn, J. H. (2012). Size distribution and settling velocities of suspended particles in a tidal embayment. *Water Research, 46*(10), 3219-3228.

Borga, P., Elowson, T., & Liukko, K. (1996a). Environmental loads from water-sprinkled softwood timber: 2. Influence of tree species and water characteristics on wastewater discharges. *Environmental Toxicology and Chemistry, 15*(9), 1445-1454.

Borga, P., Elowson, T., & Liukko, K. A. (1996b). Environmental loads from water-sprinkled softwood timber. 1. Characteristics of an open and a recycling watering system. *Environmental Toxicology and Chemistry, 15*(6), 856-867.

Boulay, S. O. (2012). *Analysis of multibeam sonar data for benthic habitat characterization of the Port of Tauranga, New Zealand.* University of Waikato.

Brannigan, A. M. (2009). *Change in Geomorphology, hydrodynamics and surficial sediment of the Tauranga entrance tidal delta system.* The University of Waikato.

Cole, R. G., Hull, P. J., & Healy, T. R. (2000). Assemblage structure, spatial patterns, recruitment, and post‐settlement mortality of subtidal bivalve molluscs in a large harbour in north‐eastern New Zealand. *New Zealand Journal of Marine and Freshwater Research, 34*(2), 317-329.

Davies-Colley, R. J. (1976). *Sediment dynamics of Tauranga Harbour and the Tauranga inlet.* University of Waikato.

Davies-Colley, R. J., & Healy, T. R. (1978a). Sediment and hydrodynamics of the Tauranga entrance to Tauranga harbour. *New Zealand Journal of Marine and Freshwater Research, 12*(3), 225-236.

Davies-Colley, R. J., & Healy, T. R. (1978b). Sediment transport near the Tauranga entrance to Tauranga Harbour. *New Zealand Journal of Marine and Freshwater Research, 12*(3), 237-243.

Davis, R. A., & Healy, T. R. (1993). Holocene coastal depositional sequences on a tectonically active setting: southeastern Tauranga Harbour, New Zealand. *Sedimentary Geology, 84*(1), 57-69.

de Lange, W. (1988). *Wave Climate and Sediment Transport within Tauranga Harbour, in the Vicinity of Pilot Bay. Hamilton, New Zealand: University of Waikato.* Ph. D. thesis, 189p.

de Lange, W., & Gibb, J. G. (2000). Seasonal, interannual, and decadal variability of storm surges at Tauranga, New Zealand. *New Zealand Journal of Marine and Freshwater Research, 34*(3), 419-434.

de Lange, W., & Healy, T. (1990). Wave spectra for a shallow meso-tidal estuarine lagoon: Bay of Plenty, New Zealand. *Journal of Coastal Research*, 189-199.

Fåhræus-Van Ree, G. E., & Payne, J. F. (1999). Enzyme Cytochemical Responses of Mussels (Mytilus edulis) to Resin Acid Constituents of Pulp Mill Effluents. *Bulletin of Environmental Contamination and Toxicology, 63*(4), 430-437.

Healy, T. R., Wilkins, A. L., & Leipe, T. (1997). Extractives from a Coniferous Bark Dump in Coastal Estuarine Sediments. *Journal of Coastal Research, 13*(2), 293-296.

Heath, R. A. (1976). Broad classification of New Zealand inlets with emphasis on residence times. *New Zealand Journal of Marine and Freshwater Research, 10*(3), 429-444.

Inglis, G., Gust, N., Fitridge, I., Floerl, O., Woods, C., Kospartov, M., . . . Fenwick, G. (2008). Port of Tauranga: Second baseline survey for non-indigenous marine species (pp. 125): Ministry of Agriculture and Forestry.

Jones, G. R., Nash, J. D., Doneker, R. L., & Jirka, G. H. (2007). Bouyant Surface Discharges into Water Bodies. I: Flow Classification and Prediction Methodology. *Journal of Hydraulic Engineering*, 1010-1020.

Kanber, S. A., Langdon, A. G., & Wilkins, A. L. (2006). Speciation of Particle-Associated Resin Acids and Chromophoric Compounds in Water Samples from the Biological Treatment System of Two New Zealand Pulp Mills. *Bulletin of Environmental Contamination and Toxicology, 76*(3), 450-457.

Kanber, S. A., Langdon, A. G., & Wilkins, A. L. (2008). Studies of Transformation and Particle-Binding of Resin Acids During Oxidative Treatment of Effluent from Two New Zealand Pulp Mills. *Bulletin of Environmental Contamination and Toxicology, 80*(2), 167-172.

Kwoll, E. (2010). *Evaluation of the Tauranga Harbour numerical model.* MSc Thesis, University of Bremen.

Lahet, F., & Stramski, D. (2010). MODIS imagery of turbid plumes in San Diego coastal waters during rainstorm events. *Remote Sensing of Environment, 114*(2), 332-344.

Lee, H., Swamikannu, X., Radulescu, D., Kim, S.-j., & Stenstrom, M. K. (2007). Design of stormwater monitoring programs. *Water Research, 41*(18), 4186-4196.

Lee, S. B., Birch, G. F., & Lemckert, C. J. (2011). Field and modelling investigations of fresh-water plume behaviour in response to infrequent high-precipitation events, Sydney Estuary, Australia. *Estuarine, Coastal and Shelf Science, 92*(3), 389-402.

Mathew, J. (1997). *Morphologic changes of tidal deltas and an inner shelf dump ground from large scale dredging and dumping, Tauranga, New Zealand.* University of Waikato.

Matranga, V., & Yokota, Y. (2008). Responses of marine organisms to physical and chemical impacts. *Cell Biology and Toxicology, 24*(6), 471-474.

Michels, K. H., & Healy, T. R. (1999). Evaluation of an Inner Shelf Site off Tauranga Harbour, New Zealand, for Disposal of Muddy-Sandy Dredged Sediments. *Journal of Coastal Research, 15*(3), 830-838.

Miller, G., & Spoolman, S. (2011). *Living in the environment: principles, connections, and solutions*: Cengage Learning.

Nash, J. D., & Jirka, G. H. (1996). Bouyant surface discharges into unsteady ambient flows. *Dynamics of Atmospheres and Oceans, 24*, 75-84.

O'Donnell, J. (1997). Observations of near-surface currents and hydrography in the Connecticut River plume with the surface current and density array. *Journal of Geophysical Research: Oceans, 102*(C11), 25021-25033.

Odyssey. (*Odyssey Conductivity & Temperature Logger.* D. S. P. Ltd (Ed.) *User Guide*

Park, S. G., & Donald, R. (1994). Environment B.O.P Tauranga Harbour Regional plan environmental investigations; Ecology of Tauranga Harbour: Environment B. O. P.

Pawlowicz, R., Beardsley, B., & Lentz, S. (2002). Classical tidal harminic analysis including error estimates in MATLAB using T_TIDE. *Computers and Geosciences, 28,* 929-937.

Phleger, F. B., Castanares, A. A., & Phleger, F. B. (1969). *"Coastal Lagoons"* (Vol. null).

Price, W. A. (1968). Tidal deltas. Pp. 1151-2. In R. W. Fairbridge (Ed.), *Encyclopedia of Geomorphology* (pp. 1295). New York: Reinhold.

Reifel, K. M., Johnson, S. C., DiGiacomo, P. M., Mengel, M. J., Nezlin, N. P., Warrick, J. A., & Jones, B. H. (2009). Impacts of stormwater runoff in the Southern California Bight: Relationships among plume constituents. *Continental Shelf Research, 29*(15), 1821-1835.

Simpson, J. E. (1997). *Gravity currents in the environment and the laboratory* (2nd ed.). Cambridge, UK: Cambridge University Press.

Spiers, K. C., & Healy, T. R. (2009). Wave Focusing in Response to a Dredged Sediment Mound. *Journal of Coastal Research*(ArticleType: research-article / Issue Title: Special Issue No. 56. Proceedings of the 10th International Coastal Symposium ICS 2009, Vol. II / Full publication date: 2009 / Copyright © 2009 Coastal Education & Research Foundation, Inc.), 1070-1074.

Spiers, K. C., Healy, T. R., & Winter, C. (2009). Ebb-Jet Dynamics and Transient Eddy Formation at Tauranga Harbour: Implications for Entrance Channel Shoaling. *Journal of Coastal Research, 25*(1), 234-247.

Svejkovsky, J., Nezlin, N. P., Mustain, N. M., & Kum, J. B. (2010). Tracking stormwater discharge plumes and water quality of the Tijuana River with multispectral aerial imagery. *Estuarine, Coastal and Shelf Science, 87*(3), 387-398.

Tay, H. W., Bryan, K. R., de Lange, W. P., & Pilditch, C. A. (2013). The hydrodynamics of the southern basin of Tauranga Harbour. *New Zealand Journal of Marine and Freshwater Research, 47*(2), 249-274.

Tian, F. (1993). *Aspects of Hopper Washings Disposal and Storm Runoff Water Quality from the Log Handling Areas at the Port of Tauranga.* (Masters of Philosophy in Earth Sciences), University of Waikato, Hamilton. (ES213)

Tian, F. (1997). *Environmental Aspects of Storm Runoff Discharge from a Timber Port, Tauranga, New Zealand.* (Doctor of Philosophy), University of Waikato, Hamilton. (ES319)

Tian, F., Healy, T. R., & Davies-Colley, R. J. (1994). Light Absorption by Yellow Substance in Storm Runoff from Log Handling Areas at a Timber Export Port, Tauranga, New Zealand. *Journal of Coastal Research, 10*(4), 803-808.

Tian, F., Wilkins, A. L., & Healy, T. R. (1998). Accumulation of Resin Acids in Sediments Adjacent to a Log Handling Area, Tauranga Harbour, New Zealand. *Bulletin of Environmental Contamination and Toxicology, 60*, 441-447.

Turner, J. S. (1979). *Buoyancy effects in fluids*: Cambridge University Press.

Washburn, L., McClure, K. A., Jones, B. H., & Bay, S. M. (2003). Spatial scales and evolution of stormwater plumes in Santa Monica Bay. *Marine Environmental Research, 56*(1–2), 103-125.

Wu, Y., Washburn, L., & Jones, B. H. (1994). Buoyant plume dispersion in a coastal environment: evolving plume structure and dynamics. *Continental Shelf Research, 14*(9), 1001-1023.

Yapp, W. B., & Yapp, B. (1972). *Production, pollution, protection* (Vol. 19): Wykeham London.

Appendix A

This Appendix shows the results of the plume sample analysis undertaken by Hill Laboratories.

Hill Laboratories
BETTER TESTING BETTER RESULTS

R J Hill Laboratories Limited
1 Clyde Street
Private Bag 3205
Hamilton 3240, New Zealand

Tel +64 7 858 2000
Fax +64 7 858 2001
Email mail@hill-labs.co.nz
Web www.hill-labs.co.nz

ANALYSIS REPORT

Client:	Port of Tauranga Ltd	**Lab No:**	1200080	SPv1
Contact:	Grant Sedgwick	**Date Registered:**	06-Nov-2013	
	C/- Port of Tauranga Ltd	**Date Reported:**	14-Nov-2013	
	Private Bag 12504	**Quote No:**	56846	
	Tauranga Mail Centre	**Order No:**		
	TAURANGA 3143	**Client Reference:**	Stormwater	
		Submitted By:	Grant Sedgwick	

Sample Type: Aqueous

Sample Name:		Log Yard 06-Nov-2013 8:50 am				
Lab Number:		1200080.1				
Individual Tests						
pH	pH Units	4.4	-	-	-	-
Total Suspended Solids	g/m³	117	-	-	-	-
Total Aluminium	g/m³	3.6	-	-	-	-
Total Boron	g/m³	0.035	-	-	-	-
Hexavalent Chromium	g/m³	< 0.0010	-	-	-	-
Total Cobalt	g/m³	0.00193	-	-	-	-
Total Manganese	g/m³	0.29	-	-	-	-
Total Mercury	g/m³	< 0.00008	-	-	-	-
Total Ammoniacal-N	g/m³	0.022	-	-	-	-
Nitrite-N	g/m³	0.003 #1	-	-	-	-
Nitrate-N	g/m³	< 0.002	-	-	-	-
Nitrate-N + Nitrite-N	g/m³	< 0.002 #1	-	-	-	-
Chemical Oxygen Demand (COD)	g O_2/m³	840	-	-	-	-
Escherichia coli	cfu / 100mL	2,800	-	-	-	-
Heavy metals, totals, trace As,Cd,Cr,Cu,Ni,Pb,Zn						
Total Arsenic	g/m³	0.0011	-	-	-	-
Total Cadmium	g/m³	0.000055	-	-	-	-
Total Chromium	g/m³	0.0025	-	-	-	-
Total Copper	g/m³	0.0067	-	-	-	-
Total Lead	g/m³	0.00185	-	-	-	-
Total Nickel	g/m³	0.0021	-	-	-	-
Total Zinc	g/m³	0.104	-	-	-	-
Polycyclic Aromatic Hydrocarbons Screening in Water, By Liq/Liq						
Acenaphthene	g/m³	< 0.00010	-	-	-	-
Acenaphthylene	g/m³	< 0.00010	-	-	-	-
Anthracene	g/m³	< 0.00010	-	-	-	-
Benzo[a]anthracene	g/m³	< 0.00010	-	-	-	-
Benzo[a]pyrene (BAP)	g/m³	< 0.00010	-	-	-	-
Benzo[b]fluoranthene + Benzo[j] fluoranthene	g/m³	< 0.00010	-	-	-	-
Benzo[g,h,i]perylene	g/m³	< 0.00010	-	-	-	-
Benzo[k]fluoranthene	g/m³	< 0.00010	-	-	-	-
Chrysene	g/m³	< 0.00010	-	-	-	-
Dibenzo[a,h]anthracene	g/m³	< 0.00010	-	-	-	-
Fluoranthene	g/m³	< 0.00010	-	-	-	-
Fluorene	g/m³	< 0.0002	-	-	-	-
Indeno(1,2,3-c,d)pyrene	g/m³	< 0.00010	-	-	-	-

Sample Type: Aqueous						
Sample Name:		Log Yard 06-Nov-2013 8:50 am				
Lab Number:		1200080.1				
Polycyclic Aromatic Hydrocarbons Screening in Water, By Liq/Liq						
Naphthalene	g/m³	< 0.0005	-	-	-	-
Phenanthrene	g/m³	< 0.0004	-	-	-	-
Pyrene	g/m³	0.0005	-	-	-	-
Total Petroleum Hydrocarbons in Water						
C7 - C9	g/m³	< 0.10	-	-	-	-
C10 - C14	g/m³	< 0.2	-	-	-	-
C15 - C36	g/m³	< 0.4	-	-	-	-
Total hydrocarbons (C7 - C36)	g/m³	< 0.7	-	-	-	-

Analyst's Comments

Please interpret these microbiological results with caution as the sample temperature was > 8 °C on receipt in the lab. Samples are required to be less than 8 °C (but not frozen).

#1 It has been noted that the result for Nitrite-N was greater than that for Nitrate-N + Nitrite-N, but within the analytical variation of these methods.

SUMMARY OF METHODS

The following table(s) gives a brief description of the methods used to conduct the analyses for this job. The detection limits given below are those attainable in a relatively clean matrix. Detection limits may be higher for individual samples should insufficient sample be available, or if the matrix requires that dilutions be performed during analysis.

Sample Type: Aqueous			
Test	**Method Description**	**Default Detection Limit**	**Samples**
Heavy metals, totals, trace As,Cd,Cr,Cu,Ni,Pb,Zn	Nitric acid digestion, ICP-MS, trace level	-	1
Polycyclic Aromatic Hydrocarbons Screening in Water, By Liq/Liq	Liquid / liquid extraction, SPE (if required), GC-MS SIM analysis [KBIs:4736,2695]	-	1
Total Petroleum Hydrocarbons in Water	Hexane extraction, GC-FID analysis US EPA 8015B/MfE Petroleum Industry Guidelines [KBIs:2803,10734]	-	1
Filtration, Unpreserved	Sample filtration through 0.45µm membrane filter.	-	1
Total Digestion	Boiling nitric acid digestion. APHA 3030 E 22nd ed. 2012 (modified).	-	1
pH	pH meter. APHA 4500-H^+ B 22nd ed. 2012.	0.1 pH Units	1
Total Suspended Solids	Filtration using Whatman 934 AH, Advantec GC-50 or equivalent filters (nominal pore size 1.2 - 1.5µm), gravimetric determination. APHA 2540 D 22nd ed. 2012.	3 g/m³	1
Total Aluminium	Nitric acid digestion, ICP-MS, trace level. APHA 3125 B 22nd ed. 2012 / US EPA 200.8.	0.0032 g/m³	1
Total Boron	Nitric acid digestion, ICP-MS, trace level. APHA 3125 B 22nd ed. 2012.	0.0053 g/m³	1
Hexavalent Chromium	Diphenylcarbazide colorimetry. Discrete Analyser. APHA 3500 Cr B (modified from manual analysis) 22nd ed. 2012.	0.0010 g/m³	1
Total Cobalt	Nitric acid digestion, ICP-MS, trace level. APHA 3125 B 22nd ed. 2012 / US EPA 200.8.	0.00021 g/m³	1
Total Manganese	Nitric acid digestion, ICP-MS, trace level. APHA 3125 B 22nd ed. 2012 / US EPA 200.8.	0.00053 g/m³	1
Total Mercury	Bromine Oxidation followed by Atomic Fluorescence. US EPA Method 245.7, Feb 2005.	0.00008 g/m³	1
Total Ammoniacal-N	Filtered sample. Phenol/hypochlorite colorimetry. Discrete Analyser. (NH_4-N = NH_4+-N + NH_3-N). APHA 4500-NH_3 F (modified from manual analysis) 22nd ed. 2012.	0.010 g/m³	1
Nitrite-N	Automated Azo dye colorimetry, Flow injection analyser. APHA 4500-NO_3^- I 22nd ed. 2012.	0.002 g/m³	1
Nitrate-N	Calculation: (Nitrate-N + Nitrite-N) - NO2N.	0.0010 g/m³	1
Nitrate-N + Nitrite-N	Total oxidised nitrogen. Automated cadmium reduction, flow injection analyser. APHA 4500-NO_3^- I 22nd ed. 2012.	0.002 g/m³	1
Chemical Oxygen Demand (COD), trace level	Dichromate/sulphuric acid digestion in Hach tubes, colorimetry. Trace Level method. APHA 5220 D 22nd ed. 2012.	6 g O_2/m³	1
Escherichia coli	Membrane filtration, Count on mFC agar, Incubated at 44.5°C for 22 hours, MUG Confirmation. Analysed at Hill Laboratories - Microbiology; 1 Clow Place, Hamilton. APHA 9222 G, 22nd ed. 2012.	1 cfu / 100mL	1

These samples were collected by yourselves (or your agent) and analysed as received at the laboratory.

Samples are held at the laboratory after reporting for a length of time depending on the preservation used and the stability of the analytes being tested. Once the storage period is completed the samples are discarded unless otherwise advised by the client.

This report must not be reproduced, except in full, without the written consent of the signatory.

Ara Heron BSc (Tech)
Client Services Manager - Environmental Division